

# Research and Development on Critical (Sonic) Flow of Multiphase Fluids through Wellbores in Support of Worst-Case-Discharge Analysis for Offshore Wells



Mewbourne School of Petroleum and Geological Engineering  
The University of Oklahoma, Norman  
100 E Boyd St. Norman, OK-73019



February 16, 2018

*This page intentionally left blank.*

# Research and Development on Critical (Sonic) Flow of Multiphase Fluids through Wellbores in Support of Worst-Case-Discharge Analysis for Offshore Wells

## Authors:

Saeed Salehi, Principal Investigator  
Ramadan Ahmed, Co- Principal Investigator  
Rida Elgaddafi, Postdoctoral Associate  
Raj Kiran, Research Assistant

Report Prepared under Contract Award M16PS00059  
By: Mewbourne School of Petroleum and Geological Engineering  
The University of Oklahoma, Norman



For: The US Department of the Interior  
Bureau of Ocean Energy Management Gulf  
of Mexico OCS Region



*This page intentionally left blank.*

## **DISCLAIMER**

Study concept, oversight, and funding were provided by the US Department of the Interior, Bureau of Ocean Energy Management (BOEM), Environmental Studies Program, Washington, DC, under Contract Number M16PS00059. This report has been technically reviewed by BOEM, and it has been approved for publication. The views and conclusions contained in this document are those of the authors and should not be interpreted as representing the opinions or policies of the US Government, nor does mention of trade names or commercial products constitute endorsement or recommendation for use.

## Table of Contents

Table of Contents .....	vi
List of Figures.....	viii
List of Tables .....	xii
Nomenclature .....	xiii
Executive Summary.....	xix
1. Introduction .....	1
1.1 Background.....	1
1.2 Problem Statement.....	2
1.3 Objectives .....	3
2. Literature Review .....	5
2.1. Past Incidents of Blowouts .....	5
2.2. Worst Case Discharge.....	6
3. Mathematical Modeling of WCD.....	9
3.1. Multiphase Flow .....	9
3.2. Nodal Analysis.....	16
3.3. Multiphase Flow Modeling.....	19
3.3.1. Empirical Models .....	19
3.3.2. Analytical Models .....	21
3.3.3. Mechanistic Model.....	25
3.3.4. Numerical Models.....	34
3.4. Current WCD Modeling .....	36
4. Experimental Study .....	40
4.1 Field Case Study .....	40
4.2 Two-phase flow in large pipe diameter (ID> 6 in).....	41
4.3 Two-phase flow in small pipe diameter (ID< 6 in) .....	49
4.4 Two-phase flow in annulus.....	64
5. Subsonic and Supersonic Multiphase Flow.....	67
5.1 Subsonic/Supersonic Flow.....	67
5.2 Experimental Studies .....	69

5.3 Mathematical Modeling.....	81
5.4 Subsonic/Supersonic Discharge Conditions .....	86
6. Conclusions and Recommendations.....	100
6.1 Conclusions.....	101
6.2 Recommendations.....	101
References .....	102

## List of Figures

Figure 1.1 Open questions on fluid dynamics implications in WCD scenarios .....	1
Figure 2.1 Key Blowout Events .....	6
Figure 3.1 Typical flow pattern of in vertical pipeline: a) bubbly flow, b) dispersed bubbly, c) plug/slug flow, d) churn flow, e) annular flow, and f) mist flow (After Image by MIT-OCW) .....	10
Figure 3.2 Flow Patterns in Annular Geometry (Caetano et al., 1992a) .....	11
Figure 3.3 Flow pattern map for air and water in vertical up flow (Griffith, 1984).....	13
Figure 3.4 Experimental flow regime map (After Waltrich et al., 2015).....	14
Figure 3.5 Flow pattern map for air-water mixture in concentric annulus (Caetano et al., 1992a) .....	15
Figure 3.6 Flow pattern map for air-kerosene in concentric annulus (Caetano et al., 1992a)....	15
Figure 3.7 Flow across the Operation system .....	17
Figure 3.8 Effect of rate of liquid on the accuracy of different flow correlations (Aggour et al., 1996).....	34
Figure 3.9 Effect of tubing size on the accuracy of different flow correlations (Aggour et al., 1996).....	34
Figure 4.1 Schematic of the experimental flow loop (Shen et al. 2010).....	41
Figure 4.2 Dominant flow regimes: (a) bubbly flow, (b) churn flow, and (c) slug flow (Shen et al. 2010).....	42
Figure 4.3 Test setup: (a) gas-liquid flow loop; and (b) plexiglas pipe configuration (Schoppa et al., 2013).....	43
Figure 4.4 Liquid removal rate with rate of gas injection (After Schoppa et al., 2013).....	43
Figure 4.5 Pressure variation and gas injection rate with time (After Schoppa et al., 2013).....	43
Figure 4.6 Variation of pressure gradient with superficial gas velocity (After Schoppa et al., 2013).....	44
Figure 4.7 Schematic diagram of test setup ((Waltrich et al. 2015, LSU report).....	44
Figure 4.8 Flow regime map for large ID pipes (Waltrich et al. 2015, LSU report).....	45
Figure 4.9 Measured liquid holdup versus gas velocity at various liquid velocities and pipe sizes: a) 2 in; b) 4 in; c) 8 in; and d) 12 in (Waltrich et al. 2015, LSU report; Waltrich et al. 2013).....	46

Figure 4.10 Measured pressure gradient vs. gas velocity at various liquid velocities and pipe sizes: a) 2 in; b) 4 in; c) 8 in; and d) 12 in (Waltrich et al. 2015, LSU report; Waltrich et al. 2013).....	47
Figure 4.11 Comparison of pressure gradient data from previous studies and LSU report .....	48
Figure 4.12 Comparison of liquid holdup data from previous studies and LSU report .....	48
Figure 4.13 Large-scale closed flow loop (Zangana et al. 2010) .....	49
Figure 4.14 Pressure drop versus gas superficial velocity: a) total pressure drop, and b) frictional pressure drop (Zangana et al., 2010) .....	50
Figure 4.15 Schematic of test section (Tang et al. 2013) .....	50
Figure 4.16 Schematic of experimental setup (Tang et al. 2013).....	51
Figure 4.17 Variation of the test parameter measurements with superficial gas velocity for upward vertical two-phase flow: a) void fraction and b) friction pressure gradient (Tang et al. 2013) .....	51
Figure 4.18 Total pressure drop vs. gas superficial velocity at various $V_{SL}$ (Biria, 2013).....	52
Figure 4.19 Schematic of two-phase flow setup .....	53
Figure 4.20 Flow pattern inside a) 0.83 in; b) 1.85 in; and c) 3.74 in pipe (Zubir and Zainon 2011) .....	53
Figure 4.21 Comparison measured void fraction and prediction by Bestion correlation at various gas and liquid superficial velocities for different pipes: a) 0.83 in and b) 3.74 in (Zubir and Zainon 2011).....	54
Figure 4.22 Observed flow pattern at various gas and liquid superficial velocities (Perez, 2008) .....	54
Figure 4.23 Effect of pipe diameter on liquid holdup at different $V_{SL}$ : a) 0.2 m/s; and b) 0.7 m/s (Perez, 2008).....	55
Figure 4.24 Effect of pipe size on pressure gradient at different $V_{SL}$ : a) 0.2 m/s; and b) 0.7 m/s (Perez 2008).....	56
Figure 4.25 Schematic diagram of the two-phase flow loop (Waltrich et al. 2013) .....	56
Figure 4.26 Pressure Gradient versus dimensionless superficial gas velocity at $V_{sl} = 0.3$ m/s for different pressure drops: a) 20 psi, and b) 55 psi (Waltrich et al., 2013).....	57
Figure 4.27 Pressure gradient versus dimensionless superficial gas velocity at $V_{sl} = 0.019$ m/s for different pressure drops a) 20 psi, and b) 55 psi (Waltrich et al., 2013) .....	58

Figure 4.28 Schematic of two-phase flow test setup (Sultan 1999) .....	58
Figure 4.29 Gas-Liquid mixer (a) bubbly/slug/froth flow (b) annular flow (Sultan 1999).....	59
Figure 4.30 Void fraction measurements versus air flow rate at water flow rate range of 1.75 - 63 cm <sup>3</sup> /s (Sultan 1999) .....	60
Figure 4.31 Void fraction measurements versus air flow rate at water flow rate range of 7 - 189 cm <sup>3</sup> /s (Sultan 1999) .....	60
Figure 4.32 Pressure drop components for air-water mixture at water flow rate of 189 cm <sup>3</sup> /s (Sultan 1999) .....	61
Figure 4.33 Measured total pressure drop versus air flow rate at various liquid flow rates (Sultan 1999).....	61
Figure 4.34 Schematic diagram of two-phase annular flow test section (Caetano, 1985) .....	64
Figure 4.35 Flow patterns in upward vertical flow through a concentric annulus (Caetano, 1992a) .....	65
Figure 4.36 Schematic of experimental setup (Hasan and Kabir 1992).....	65
Figure 5.1 Variation of (a) adiabatic and (b) isothermal speed of sound in air-water mixture with gas void fraction and pressure (Kieffer, 1977).....	68
Figure 5.2 Schematic of experimental setup (Martindale and Smith 1980).....	69
Figure 5.3 Dimensionless sonic velocity and pressure drop versus gas fraction (Martindale and Smith 1980) .....	70
Figure 5.4 Dimensionless pressure drop versus quality at various superficial gas velocities (Martindale and Smith 1980).....	70
Figure 5.5 Experimental facility: a) schematic of test setup, and b) test apparatus (Luo et al. 2016) .....	71
Figure 5.6 Measured two-phase flow characteristics versus gas velocity at various liquid velocities: a) pressure drop, and b) liquid holdup (data from Luo et al., 2016).....	72
Figure 5.7 Measured liquid holdup versus superficial gas velocity from different previous studies .....	73
Figure 5.8 Schematic of two-phase tunnel (Eddington 1970).....	74
Figure 5.9 Upstream Mach number versus mixture velocity at various static pressures (Eddington 1970).....	75

Figure 5.10 Pressure ratio versus upstream Mach number for two different shocks: a) normal shock, and b) oblique shock (Eddington 1970) .....	76
Figure 5.11 Shock tube experiment for flow instabilities (Mariani et al., 2012) .....	77
Figure 5.12 Schematic of experimental set-up for mixing shock (Witte, 1969) .....	78
Figure 5.13 Relative resistance coefficient with Mach number (Fisenko and Sychikov 1977). .....	79
Figure 5.14 Sonic speed on volumetric ratio of streams (Fisenko et al. 2010) .....	80
Figure 5.15 Variation of absolute pressure along the distance from the inlet, $G$ represents the mass flux rate, $x$ is the vapor quality, $d_o$ is the pipe diameter, $\lambda$ is the coefficient of wall friction pressure drop, $\xi$ is the coefficient of interphase frictional pressure drop (Okazaki, 1980).....	81
Figure 5.16 Variation of gas and liquid velocity with the distance from the inlet at different reservoir pressure ( $P_o$ ); $U_G$ represents the gas velocity, $U_L$ is the velocity of the liquid phase, $x$ is the vapor quality, $d_o$ is the pipe diameter, $\lambda$ is the coefficient of wall friction pressure drop, $\xi$ is the coefficient of interphase frictional pressure drop (Okazaki, 1980). .....	82
Figure 5.17 Variation in speed of sound in multiphase mixture flow with void fraction (Venkateswaran et al., 2002) .....	85
Figure 5.18 Two-phase flow discharging through a variable duct (Prepared after Dobran, 1987) .....	87
Figure 5.19 Numerical results for flow characteristics and fluid properties, $U_G^*$ is dimensionless superficial gas velocity, $U_L^*$ is dimensionless superficial liquid velocity, $\alpha$ is the volumetric gas fraction, $x$ is quality (Modified after Dobran, 1987). .....	92
Figure 5.20 Flow regime profile for volcanic eruption (Dobran, 1992).....	93
Figure 5.21 Velocity distribution along the height for homogenous and non-homogenous model ( $u^*$ is dimensional velocity parameter) (Dobran, 1992).....	98
Figure 5.22 Multiphase flow during Volcanic Eruptions (Melnik, 1999).....	98

## List of Tables

Table 3.1 Summary of empirical correlations .....	21
Table 3.2 Summary of analytical models .....	23
Table 3.3 Statistical result of comparative study of models for annular flow (After Ansari et al. 1994).....	26
Table 3.4 Summary of mechanistic models .....	28
Table 3.5 Comparison of Industry software .....	39
Table 4.1 Well data used for modern validation (Asheim, 1986) .....	40
Table 4.2 Field data for multiphase flow (After Asheim, 1986).....	40
Table 4.3 Summary of flow pattern observations and test conditions .....	55
Table 4.4 Description of observed flow pattern .....	59
Table 4.5 Literature survey summary for two-phase flow in vertical pipe .....	63
Table 5.1 Two-phase tunnel dimensions and operating conditions .....	74
Table 5.2 Experimental data and calculated results for Fauske's experiment; $\lambda$ is the coefficient of wall friction, $\xi$ is coefficient of interphase friction (Okazaki, 1981).....	83
Table 5.3 Experimental data and calculated results for Sozzi et al. (1975) experiment; $\lambda$ is the coefficient of wall friction, $\xi$ is coefficient of interphase friction (Okazaki, 1981).....	83

# Nomenclature

## Abbreviations and Acronyms

$a$	Interfacial area per unit volume of the mixture
$A$	Flow cross-sectional area/Cross-sectional area of the tube
$A_{CL}$	Area of the casing film
$A_{TL}$	Area of the tubing film
$A_{core}$	Area of the mixture core
$a_{mix}$	Velocity of sound in the two-phase mixture
B1/B2	Coefficients
BOP	Blowout Preventer
BSEE	Bureau of Safety and Environmental Enforcement
BOEM	Bureau of Ocean Energy Management
$c$	speed of sound
$C_0$	Distribution coefficient
$C_D$	Drag coefficient
$C_{D_{1-\alpha}}$	Bubble drag coefficient
$C_{fi}$	Interfacial friction coefficient
$C_{f1}$	Interfacial friction coefficient
$C_p$	Specific heat at constant pressure
$c_{vmix}$	Specific heat steam-heat mixture
$D_{EP}$	Equi-periphery diameter (m)
$D_H$	Hydraulic diameter (m)
$d$	Pipe diameter
$d_b$	Bubble diameter
$d_d$	Gas/droplet diameter
$D$	Conduit diameter
$D_c$	Inner diameter of casing
$D_H$	Hydraulic diameter
$D_T$	Outer diameter of the tubing
$D_p$	Outer diameter of tubing (m)
$d_{pi}$	Inner diameter of tubing (m)
$f$	Fanning friction factor
$f_{LO}$	Single phase frictional coefficient for liquid phase only
$f_{GO}$	Single phase frictional coefficient for gas only
$f_{TP}$	Two-phase friction factor
$F$	Force due to frictional pressure loss
$F_e$	Entrained liquid fraction in the gas core
$f_f$	Fanning friction factor in the film
$f_{SL}$	Fanning friction factor for superficial liquid velocity

$f_w$	Fanning friction factor at the wall
$F_{wl}$	Frictional pressure drop
$F_{LG}$	Interfacial drag forces between the phases
$F_{wG}$	Friction force between wall and gas phase
$F_{LG}$	Interfacial drag force
$g$	Acceleration due to gravity ( $m/s^2$ )
$G$	Force due to gravity
$G_1$	Mass flux
$h$	Enthalpy
$G_{air}$	Gas constant
$GLR$	Gas liquid ratio
$GoM$	Gulf of Mexico
$\widetilde{h}_b$	Heat transfer coefficient for bubble regime
$\widetilde{h}_a$	Heat transfer coefficient for annular flow regime
$\widetilde{h}$	Interfacial heat transfer coefficient
$h_L$	Enthalpy of the liquid phase
$h_G$	Enthalpy of the gas phase
$h_{LG}$	Difference between the enthalpy of the liquid phase and gas phase
$H_L$	Liquid holdup
$H_{gLS}$	Liquid slug void fraction
$H_{LTB}$	Liquid Taylor bubble holdup
$H_{SU}$	Unit average liquid holdup
$H_{SL}$	Liquid holdup in liquid slug zone
$H_{LF}$	Liquid holdup in the liquid film
$H_{TL}$	In-situ liquid holdup in the tubing wall film
$H_{CL}$	In-situ liquid holdup in the casing wall film
$H_{L\_total}$	Liquid holdup in the annulus
$J$	Productivity index
$k_L$	Thermal conductivity of the liquid phase
$k_G$	Thermal conductivity of the gas phase
$K$	Casing-tubing diameter ratio
$K_1$	Tube inlet loss coefficient/Entrance loss coefficient
$K_c$	Thermal conductivity of cement sheath (W/m-C)
$K_p$	Thermal conductivity of tubing (W/m-C)
$L_1$	Tube length
$L$	Depth (m)
$L_{LS}$	Liquid slug length
$L_{SU}$	Unit slug length
$m$	Exponent in solubility law
$M$	Mach number

$M_f$	Mass flow rate
$M_G$	Total mass flow rate of the gas
$M_L$	Mass flow rate of the liquid phase
$M_1$	Upstream Mach number
$M_2$	Downstream Mach number
$N$	Bubble density
$Nu$	Nusselt number
$n$	Index number (considered to 0.5)
OCS	Outer Continental Shelf
$P_1$	Upstream pressure
$P_2$	Downstream pressure
$P_b$	Bubble Point Pressure
$P$	Pressure
$P_a$	Reference pressure
$Pr$	Prandtl number
$Pr_L$	Prandtl number for the liquid phase
$Pr_G$	Prandtl number for the gas phase
$\bar{P}$	Average reservoir pressure (psi)
$P_{wf}$	Bottom hole pressure (psi)
$\left(\frac{dp}{dl}\right)_f$	Pressure loss due to friction
$\left(\frac{dp}{dl}\right)_T$	Total pressure gradient
$\left(\frac{dp}{dl}\right)_{SC}$	Superficial friction pressure gradient in the core
$\left(\frac{dp}{dl}\right)_{SL}$	Superficial liquid friction pressure gradient
$\left(\frac{dp}{dl}\right)_C$	Pressure gradient in the core
$\left(\frac{dp}{dl}\right)_F$	Pressure gradient in the film
$\left(\frac{dp}{dl}\right)_{CL}$	Total pressure gradient for casing wall film
$\left(\frac{dp}{dl}\right)_{core}$	Total pressure gradient for gas core
$\left(\frac{dp}{dl}\right)_{TL}$	Total pressure gradient for tubing wall film
$\left(\frac{dP}{dz}\right)_{FLO}$	Pressure gradient due to liquid friction only
$\left(\frac{dP}{dz}\right)_{wall\ friction}$	Pressure gradient due to wall friction
$q$	Flow rate
$q_{max}$	Absolute open flow
$Q_a$	Fluid Injection rate ( $m^3/s$ )

$Q_f$	Formation fluid influx rate ( $m^3/s$ )
$Q_L$	Heat transfer rate from liquid
$R$	Gas constant
$R_l$	Richardson number
$Re$	Reynolds number
$Re_b$	Reynolds number
$Re_G$	Reynolds number for the gas phase
$Re_{Ga}$	Reynolds number for gas phase corresponding to annular flow regime
$R_0$	Universal Gas constant
$r_v$	Gas to liquid volume ratio
$r_m$	Gas to liquid mass ratio
$s$	solubility constant
$S$	Slip ratio
$S_c$	Solubility constant
$S_{CW}$	Wetted liquid perimeter on casing wall
$S_{CI}$	Wetted liquid perimeters on casing film-gas core interface
$S_{TW}$	Wetted liquid perimeter on tubing wall
$S_{TI}$	Wetted liquid perimeters on tubing film-gas core interface
$T$	Thickness ratio between casing and tubing liquid film
$T_L$	Temperature of liquid phase
$T_G$	Temperature of gas phase
$T_1$	Temperature
$t$	Time
$dU$	Internal Energy
$u$	Velocity in individual direction
$u_G$	Velocity of gas phase
$u_L$	Velocity of liquid phase
$V_{TB}$	Velocity of the Taylor bubble
$v$	Velocity
$V$	Mixture velocity
$V_{slip}$	Slip velocity (m/s)
$V_g$	Average gas velocity (m/s)
$V_l$	Average liquid phase velocity (m/s)
$V_m$	Mixture superficial velocity (m/s)
$V_{sg}$	Superficial gas velocity (m/s)
$V_{sl}$	Superficial liquid velocity (m/s)
$V_{TL}$	Tubing wall liquid film velocity
$V_{CL}$	Casing wall liquid film velocity
$V_{core}$	In-situ gas core velocity
$V$	In-situ average phase velocity

$V_{\text{mix}}$	Specific heat of the mixture
WCD	Worst Case Discharge
$\langle \text{WT}' \rangle$	Angle associated with the tubing wall and averaged over the whole annulus cross sectional area
X	Evolved gas mass fraction
$x_q$	Quality
$X_f$	Maximum evolved gas fraction
$X_M$	Modified Martinelli parameter
x	Position vector
Y	Gas mass fraction
$Y_f$	Maximum dissolved gas fraction
$Y_M$	Dimensionless group parameter
Z	Correlating factor for interfacial friction and film thickness
z	Distance from the inlet

### Greek Symbols

$\sigma$	Surface tension
$\beta^*$	Liquid holdup
$\beta$	Shock angle
$\eta$	Gas mass fraction
$\xi$	Resistivity coefficient
$\xi_r$	Relative resistivity coefficient
$\rho_l$	Liquid density ( $\text{kg}/\text{m}^3$ )
$\rho_G$	Density of gas ( $\text{kg}/\text{m}^3$ )
$\rho_m$	Density of the mixture ( $\text{kg}/\text{m}^3$ )
$\rho_{Lm}$	Density of the mixture ( $\text{kg}/\text{m}^3$ )
$\rho_{LA}$	Liquid density at reference pressure ( $\text{kg}/\text{m}^3$ )
$\rho_g$	Gas density ( $\text{kg}/\text{m}^3$ )
$\Gamma$	Gas dissolution rate from gaseous phase to liquid phase
$\alpha$	Gas fraction
$\alpha_{dm}$	Maximum particle density
$\alpha_l$	Gas volumetric fraction
$\alpha_l$	Liquid fraction
$\alpha_g$	Gas fraction
$\tilde{\delta}$	Dimensionless film thickness
$\lambda_L$	Non-slip liquid holdup
$\mu$	Viscosity
$\mu_m$	Viscosity of mixture phase
$\mu_l$	Viscosity of the liquid phase

$\mu_g$	Viscosity of the gas phase
$\lambda$	Viscosity
$\tau$	Shear stress
$\tau_w$	Shear stresses at the wall
$\tau_{TW}$	Shear stresses at tubing wall
$\tau_{TI}$	Shear stresses at tubing film-gas core interface
$\tau_{cw}$	Shear stresses at casing wall
$\gamma$	Adiabatic constant
$\tau_{CI}$	Shear stresses at casing film-gas core interface
$\Delta$	Virtual mass coefficient
$\eta$	Energy redistribution coefficient
$\xi$	Viscous drag coefficient
$\xi_{GG}$	Viscous drag coefficient for relative acceleration between the phases
$\Delta_{GG}$	Virtual Mass Coefficient
$\phi$	Two-phase frictional multiplier

## Executive Summary

The following report provides a literature survey including a critical review of past studies on a conceptual and theoretical understanding of worst case discharge (WCD) under BSEE/BOEM project no. M16PS00059. It highlights the key objectives tied to literature survey under i) multiphase flow theory and models; ii) experimental studies; and iii) subsonic/supersonic multiphase flow modeling and experiments. In the first section of this report, a brief outline of blowouts in the context of worst case discharge is provided. The second part deals with the concepts and modeling of multiphase flow and current modeling approaches. Next section presents the experimental studies on multiphase flow. The final part is devoted to high velocity flows including multiphase flow in subsonic and supersonic conditions.

Literature studies suggest that the multiphase flow shows dominant fluid acceleration phenomenon in the critical flow conditions, which has been so far not emphasized in the wellbore flow modeling efforts. The compressibility effect is vital for numerical modeling of subsonic and supersonic conditions. The effort also requires the incorporation of the effect of bubble point pressure, when the free gas is released from the liquid with the dissolved gas. The flow patterns exhibit different characteristics in case of different fluid types. The effect of geometry cannot be neglected. The flow pattern map shows significant deviation in case of flow in annulus when compared with the flow in the pipe.

The experimental study reveals that the trend of pressure drop changes at a higher velocity in comparison to the trend at lower velocities. In the multiphase flow, the speed of sound is different from that of single-phase flow. Subsonic/supersonic conditions lead to the generation of shock waves in the system, which was not the part of past studies. Though, the two-phase flow characteristics have been well studied for low velocities (Mach number  $<0.3$ ) in vertical pipes, it lacks significantly at the subsonic and supersonic front.

Keeping in mind all these two-phase flow concepts, the first step is to understand the flow parameters in the wellbore during worst case discharge. The old experiments and WCD models characterize the flow with less than 0.3 Mach number. These models need validation from the experimental data in the critical conditions. A multiphase flow computational fluid dynamics (CFD) analysis integrated with the experiments is highly recommended to carry forward the current experimental effort and develop models for high Mach number flows.

Overall, this report includes a critical review of existing theoretical understanding and experimental work relevant to the estimation of the WCD.

# 1. Introduction

## 1.1 Background

Complex systems for severe conditions require high reliability and greater confidence. The reliability and confidence in any system always come up with an in-depth understanding of problem/phenomenon, the efficient and accurate anticipation of the conditions, and protective measures. On the same line, the worst-case discharge as a result of offshore blowout has always been a concern for oil and gas industry in the US Gulf of Mexico (Bourgoyne et al., 1995; CSB report, 2016). Over the past decades, the technology has evolved and accompanied by several innovations and deeper understating on the very topic. However, the challenges have also been on the consistent upsurge. This upsurge is mainly attributed to increased activity in the entirely new realm of hydrocarbon zones. Looking at the blowouts, it becomes evident that the inaccurate prediction of volumetric discharge characteristics beforehand leads to insufficient fail-safe measures on the rigs, finally manifesting into a blowout. The unexplored issues prevailing on this front are depicted in **Figure 1.1**.

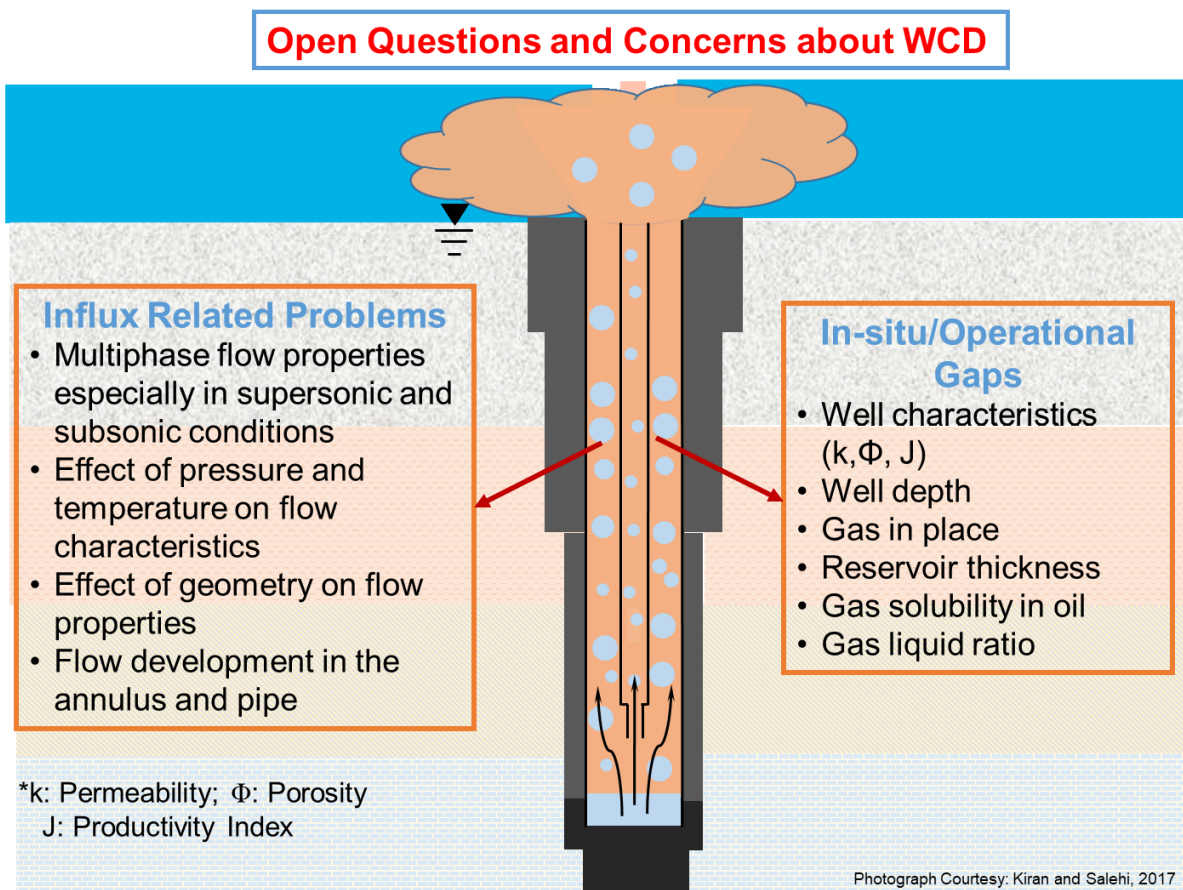


Figure 1.1 Open questions on fluid dynamics implications in WCD scenarios

With the anticipation of a blowout, the role of well control becomes imminent in any drilling operation. The well control equipment including BOP plays a crucial role in well control procedures. After the influx detection, blowout preventer (BOP) is closed to prevent the escape and discharge of the fluid to the nearby operational site. Only by addressing the influx related problems and in-situ/operational gaps, we can connect the dots and decipher the worst case discharge problem. One of the primary issues is regarding the pressure drop and velocity of the influx in subsonic and supersonic conditions. The influx behavior and its excessive discharge depend on several parameters such as multiphase flow characteristics, gas and liquid thermodynamic properties, temperature and pressure effects, depth and size, and reservoir characteristics.

In this post Macondo era, with the advent of the highly advanced system, numerous studies had been conducted to develop several models to predict fluid discharge characteristics (Pagan et al., 2016; Putcha and Ertekin, 2017; Shirdel and Sepehrnoori, 2011). These models include the pipe and annular flow models which are used to predict capacities of rig components to handle such catastrophic incidents.

The gas is soluble in crude oil. Hence, if the hydrocarbon migrates after the influx, the solubility of gas in the crude oil varies with the in-situ temperature and pressure in the annulus/pipe as it travels upward. In addition to this, if the pressure drops below the bubble point, the free gas comes out of the liquid phase and rapidly moves upward. The reduction in pressure paves the way for the expansion of gas, even more quickly, and can push the fluid to the surface vigorously. Apart from this, there are other factors such as flow pattern, liquid hold up, and frictional pressure loss, which also implicate the phenomenon. These factors make the prediction of design envelope even more complicated. There are different outflow models available to predict flow rate, pressure drop and liquid holdup. However, the validity of these models has never been verified for unique circumstances such as subsonic and supersonic flow conditions. Therefore, it is necessary to evaluate the performance of the existing models, determine their limitations in anticipating the conditions and develop suitable models for future predictions.

## **1.2 Problem Statement**

In the past decades, various studies (Hasan and Kabir, 2007; Hasan et al., 2007; Shirdel and Sepehrnoori, 2011, Vuong et al., 2017) had been focused on multiphase flow characteristics such as flow pattern, frictional pressure loss, and liquid holdup. The developed models combine reservoir flow model (inflow model) and tubing/annular flow model (outflow model). Due to high-pressure in the reservoir, solution gas often completely dissolves in oil under reservoir condition. However, as the fluid travels in the tubing/annulus, the pressure reduces significantly due to a reduction in the hydrostatic head. The reduction in pressure causes the solution gas to liberate once it reaches the bubble point pressure and eventually increases total volume flow rate and subsequently superficial velocities of the phases. As the fluid flows up in the tubing/annulus, more solution gas liberates. In addition, the gas present in the mixture expands very rapidly due to a reduction in pressure. As a result, extremely high fluid velocity occurs as the fluid approaches

the surface. In case of a blowout, the flow might reach sonic conditions at the surface while exiting. Depending on the reservoir pressure and temperature, the flow in the tubing/annulus can establish sonic state during its upward flow, which impacts the discharge rate. Bottom hole flowing pressure creates strong coupling between inflow and outflow. As a result, a minor change in outflow condition can have a substantial impact on worst cased discharge (WCD) rate. Hence, estimation of the outflow condition is significant to the accuracy of the WCD rate prediction. At present, different outflow models are available to predict flow patterns, pressure drop and liquid holdup, but not in the subsonic and supersonic conditions. Hence, it is highly recommended to develop models accounting for high Mach number two-phase flows and perform WCD calculations.

### **1.3 Objectives**

The main objective of this study is to develop a user-friendly computational tool to characterize the well control events by simulating the possible worst case discharge (WCD) scenarios under field conditions. The ideal tool can potentially integrate the reservoir (inflow) and wellbore two-phase (outflow) flow models. There is also a need for evaluation of the applicability of existing empirical, analytical, and mechanistic models to analyze reservoir and wellbore flow for WCD calculations. The role of experimental measurements and computational fluid dynamics (CFD) simulations in predicting pressure, temperature, flow patterns, superficial velocities, liquid holdup, and the gas-liquid ratio (GLR) will be highly desired for WCD calculation. A profound understanding of high Mach number (Ma 0.3 to 1+) two-phase flow can be established through the experimental and modeling studies. In addition, through several runs of the experiment, different flow rates and associated pressure drops, and superficial fluid velocities will be obtained and analyzed. This data will be used to formulate a robust two-phase flow computational tool.

As per the SPE Technical Report (Committee, 2015), the potential issue of sonic velocity flow limitations on WCD calculations will be investigated in this study. Experiments will be conducted in the pipe (3.25" ID) and annulus (3.25" × 1.33") at high velocities. Experimental results will be used to validate the numerical models developed in Computational Fluid Dynamics (CFD) software ANSYS (Fluent, 2014). Then, the CFD model will be extended to study gas-liquid flows for wide range of Mach number, flow geometry (6" to 22" ID), Gas Liquid Ratio (up to 100,000 scf/stb), well depth (30,000+ ft), temperature (up to 480°F), and pressure (up to 32,000 psi). Results obtained from these techniques will be combined to facilitate the upscaling of WCD calculation based on actual field conditions of offshore wells.

The specific project objectives are to:

1. Characterize two-phase flows through applicability analyses of existing models under different well flow conditions, specifically subsonic and supersonic discharge flow conditions.
2. Perform experimental studies to better understand the impact of high Mach number ( $0.3 - 1 + Ma$ ) on flow properties.
3. Develop numerical models that can simulate realistic scenarios under different operational conditions.
4. Develop a user-friendly computational tool to provide insights on real field scenario based on different inflow/outflow models considering various operational conditions.
5. Present experimental database for validating the proposed models.
6. Conduct statistical and sensitivity analyses based on proposed models over a wide range of operational parameters by considering various flow patterns, temperature, pressure, slip velocity, rheological properties, solubility, and GLR.

The primary outcome of this study is a robust model, which can predict WCD in various loss of well control incidents. The literature survey part of the study has following objectives:

- a) Provide an understanding of the theoretical models and investigate the limitations of these models.
- b) Thoroughly review the experimental studies for two-phase vertical flow in pipe/annulus.
- c) Investigate the past studies regarding the high velocity two-phase vertical flow.
- d) Present the conceptual understanding of the theoretical models and constitutive equations.
- e) Review subsonic/supersonic multiphase flows that are similar to the worst case discharge in other engineering applications.
- f) Establish the existing research gaps in the context of specific objectives of the project.

## 2. Literature Review

### 2.1. Past Incidents of Blowouts

Systemic limitations during deepwater horizon incident have ignited the discussion on the nuances in the operational and in-situ parameters. U.S. Chemical Safety Board (CSB), Volume 2 of its investigation report stated that the identification of safety-critical elements and tasks to ensure the safety barriers and controls are key in dealing with the complex systems (CSB report, 2014). Furthermore, a closer look at the theoretical and technical aspects revealed several loopholes in the understanding and limitations of the existing concepts, which are used without taking into considerations the actual flow conditions in the wellbore. Loss of well control (LOWC) incidents has existed in oil and gas operations since its inception. LOWC is defined as “the uncontrolled flow of formation or other fluids which may be to an exposed formation (underground blowout) or at the surface (surface blowout) or flow through a diverter or uncontrolled flow resulting from a failure of surface equipment or procedures” (Per Holland, 2017). The LOWC incidents are categorized into blowouts (surface and underground), well release, and diverted well release. Typical categorization of blowouts is presented in **Table 2.1**.

**Table 2.1: Blowouts Categorization**

Category	Subcategory	Examples
Blowout (Surface flow)	Totally uncontrolled flow from a deep zone	Uncontrolled incidents with surface/subsea flow
	Totally uncontrolled flow from a shallow zone	Diverter system fails
	Shallow gas “controlled” subsea release only	In riserless drilling well starts to flow
Blowout (Underground flow)	Underground flow only	Minor flow appears, and BOP is activated to shut the surface flow.
	Underground flow mainly, limited surface flow	

Some of the major catastrophic well control incidents leading to uncontrolled fluid discharge have been happening since past several decades. The oil and gas industry has been dealing with severe blowouts since 1964 on the Baker Drill Barge to the recent Macondo. **Figure 2.1** depicts the examples of blowouts occurred in past decades (Bourgoyne et al., 1995; CSB report, 2016). Even after the Macondo incident, several significant steps have been taken to contain the blowouts incidents, but these unfortunate events have not completely stopped. For instance, in the US GoM, 2013 Hercules 265 blowout, the BOP was not closed against the very high flow, and after 13 hours of the uncontrolled flow of natural gas, there was fire on the rig (Per Holland, 2017). These incidents only point out at the vulnerability of current theoretical understanding and technological limitations. Hence, it is highly desirable to improve the current system and the conceptual understanding of these catastrophic incidents to ensure a safe oil and gas operations in future.

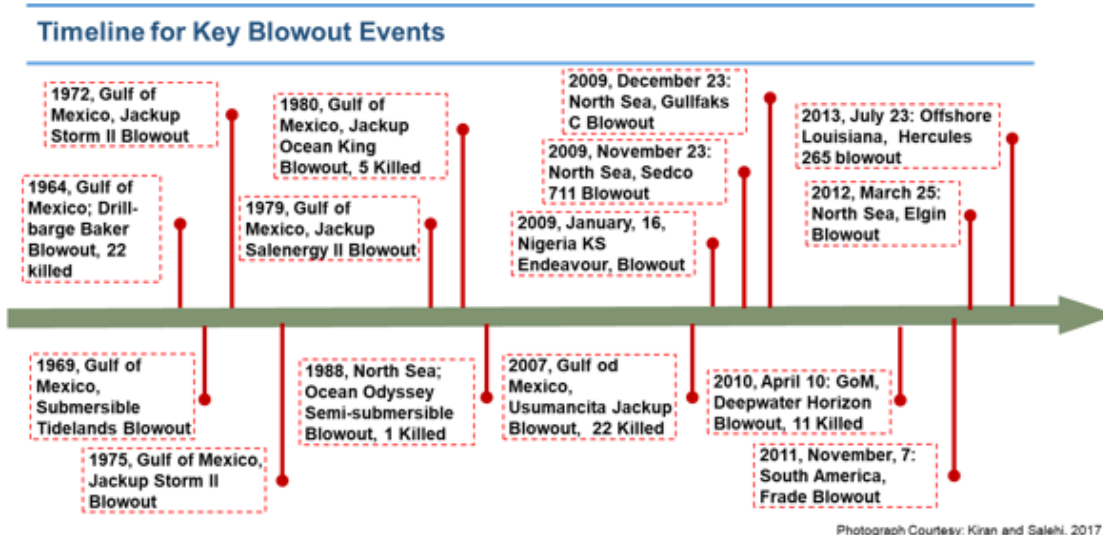


Figure 2.1 Key Blowout Events

## 2.2. Worst Case Discharge

Past blowout cases led to a considerable volume of crude oil accumulation in nearby affected zones and/or severe discharge of gas into the atmosphere. In the recent report prepared for BSEE, it was stated that 58 blowout incidents in the US Gulf of Mexico and 36 blowouts in the rest of the world have occurred from 2000 to 2015 (Per Holand, 2017). This fact only considers the officially reported incidents. Most of these blowouts are accompanied by the gas release and/or oil spill. Some of the significant oil and condensate spills due to blowouts are presented below (Per Holand, 2017):

- Montara, Australia (2009): 29000 bbls
- Macondo, USA (2010): 4250000 bbls
- Frade, Brazil (2011): 3700 bbls

These oil spills pose a serious question about the existing fail-safe system. One of the reasons behind the inadequacy of the system relies on the limitation of the current models and consequently insufficient design envelope of the onsite equipment. Eventually, lack of a proper model to estimate the worst-case discharge constrain the design as well as the regulatory work. In the wake of Macondo incident, BOEM established guidelines for calculation of worst case discharge (WCD) to improve the wellbore safety (Bowman, 2012; Moyer et al., 2012). As per BOEM, the worst case discharge is described as “the daily rate of an uncontrolled flow from all producing reservoirs into the open wellbore.” WCD includes all hydrocarbon-bearing zones in each open-hole section as it is planned to be drilled. The uncontrolled flow is considered as unobstructed casing and liner, and no drill pipe in the hole. WCD rates for deep-water wells are calculated based on the uncontrolled flow at the sea floor with a hydrostatic water head or atmospheric pressure at sea level with well work on an existing platform. In past few years, many developments have been made to estimate the flow conditions and calculate operational

parameters in general for such unforeseen events. However, these calculations are based on existing flow models which were not developed for WCD calculations in extreme conditions.

Although the WCD has a limited chance of occurrence, it can be experienced while drilling. In case of insufficient drilling margin, over pressurized formations penetrated during well construction, leads to an influx of formation fluid in the annulus at small scale, and ultimately can lead to uncontrolled fluid flow and WCD. Over-pressurized formations are usually naturally occurring or created due to water or gas injections in nearby wells. The WCD rate significantly varies among wells based on reservoir inflow and wellbore outflow parameters and can be implemented in risk assessment process. Containment of such scenario is actually dependent on the accurate prediction of WCD rate, and consequently can be handled by proper designing and holistic monitoring of the operation. As the core of such scenario is WCD rate predictions, the critical step is to identify the building blocks. WCD estimation is dependent on several parameters accounting for reservoir inflow and wellbore outflow. Reservoir characteristics (such as permeability, porosity, pressure, and temperature) in inflow model and wellbore parameters (such as depth, flow pattern, phase velocity, geometry) in outflow model play a crucial role. The permeability and porosity of a formation mainly impact the fluid movement in the formation which governs the rate of influx from the formation. The bottom-hole pressure and temperature set a differential condition and provides impetus to the fluid, to flow from bottom to the surface of the wellbore. Increase in temperature results in the thermal expansion of wellbore fluids in sealed annuli and can exacerbate the flow issues (Oudemans and Kerem, 2006). Well depth directly influences the pressure gradient inside the annulus and consequently affect the discharge rate. Other factors including the multiphase flow characteristics such as phase velocity, flow patterns, and geometry also influence WCD.

Multiphase flow is a common occurrence in oil and gas operations. This fluid dynamics problem leads to the question of understanding the mechanisms behind the multiphase flow system. The efforts to understand and characterize the intricacies of flow started with the development of empirical correlations and with time-shifted towards numerical modeling and simulation approach. The empirical correlations are based on the statistical interpretation of the lab results. The numerical approach is based on the understanding of the mechanism and developing mathematical representations of the process using governing equations with the imposed boundary conditions.

The fundamental postulate of every approach is the based on flow patterns or flow configurations. Then, it becomes essential to answer that which model most closely replicate the in-situ phenomenon. On this front, several confusions and disagreements are existing. Different models have been developed to improve the understanding of two-phase flows; however, every model has limitations. As a result, the models cannot describe the full complexity of the flow occurring in real life. There is also disagreement sometimes between experimentalist and theoreticians: the experimentalists argue that empirical models provide reasonable prediction than the theoretical models. The theoreticians dispute that theoretical models provide better prediction than the

empirical models for a wide range of field conditions, which cannot be replicated by a laboratory experiment. The theoretical models are based on the physics of the flow. However, their development involves some assumptions and simplifications. Hence, it is highly desirable to look into the details of the problem and find common ground between these two approaches.

Besides in-situ conditions, the time dependence of the flow also influences the WCD rate. A steady-state condition refers to the case in which flow characteristics are not changing with time and do not include the real-time input. On the other hand, a transient condition means the flow characteristics varying with time. In harsh well control scenarios, the transient approach is more realistic which can effectively mimic the in-situ dynamic pressure and temperature, and allows to define the control sequence for the occurrence within the operational limitations. The discharge rate is affected by the characteristics of reservoir such as pressure, temperature, its drive mechanisms, completion type, wellbore geometry, and production history (Replogle, 2009).

There are several models used in the industry to estimate the WCD rate (Beggs and Brill, 1973; Duns and Ros, 1963; Hasan and Kabir, 2007). The primary models to evaluate the well inflow characteristics are based on the nodal analysis which incorporates the factors mentioned earlier. However, the main limitation of this model is its steady-state assumption. The details of the nodal analysis are described in Section 3.2. Other models including empirical, analytical, mechanistic, and numerical are used in wellbore outflow as a complementary to inflow model for WCD rate predictions. The detailed descriptions of these models are provided in modeling section. Apart from the theoretical work, experimental investigations are also necessary to validate and verify the model. Hence, a dedicated section for past experimental studies is included in Section 4.

Though the advancement in multiphase flow modeling, the estimation of WCD rate in the past was mostly limited to evaluations based on generic models and simple experimental data that do represent the severe conditions as specified by regulatory bodies in post Macondo era. One of the main WCD conditions, which is not investigated is high Mach number multiphase flow. Mach number, a dimensionless quantity, is defined as the ratio of flow velocity to the speed of the sound at the in situ condition. The speed having Mach number 1, represents the speed of sound. The existing WCD models are two-phase flow models, developed for low Mach number ( $Ma$ ) flows (i.e.,  $Ma < 0.1$ ). In order to meet the requirements of the regulatory bodies and current field conditions, these models need to be tested and improved for high Mach number flow and other existing limitations. The detailed description of these intricacies is presented in Section 5.

### 3. Mathematical Modeling of WCD

#### 3.1. Multiphase Flow

Multiphase flow is a common physical phenomenon encountered during fluid flow. There are several examples of multiphase flow systems such as chemical reactors, power plants, heat exchangers, biological systems, nuclear reactors, and transport systems, apart from the petroleum industry. The underlying flow phenomenon exhibits different characteristics in each system. Hence, various correlations and models are developed for the analysis of the particular system due to lack of the generalization. Apparently, because of the lack of generalization, the dynamics of multiphase flow has evolved slowly over time. The design of engineering system is also limited to available experimental data and fitting conceptual mathematical models depicting the accuracy of physical processes. To understand and replicate the real-time scenarios, various characteristics and physics of multiphase flow are required.

For single-phase flow, the continuum concept is used and the governing laws of physics are applied. To obtain the solution, the governing equations are combined with other models such as the thermodynamic equilibrium equations, constitute equations and heat transfer models. The continuum concept is difficult to apply for multiphase flow. The complexity of multiphase flow originates from the existence of multiple interfaces and non-homogeneous material discontinuities (Ishii and Hibiki, 2010).

As the petroleum industry deals with the flow of hydrocarbons on a regular basis, the study of multiphase flow is imminent. One of the critical elements of the petroleum industry is the wellbore construction. The wellbore construction requires drilling. During this process, two-phase flow of hydrocarbon (gas or liquid) and drilling fluid may exist in the wellbore. The phase composition changes due to change in the in-situ wellbore temperature and pressure with depth and time. The origins of this change are variations in density and miscibility. To characterize these variations and associated phenomenon, the term flow pattern is introduced. Flow pattern helps in distinguishing the consistent change based on the relative magnitude of forces involved. Several other terms such as liquid holdup, superficial gas velocity, slip velocity, and superficial liquid velocity are introduced to assist the understanding of the flow patterns and multiphase flow hydraulics. Before going into more details, it is essential to have a knowledge of these terminologies in context of multiphase flow in the wellbore.

The liquid holdup is the in-situ volumetric fraction of the liquid phase in the wellbore. The void fraction, which is the gas holdup, is also used in two-phase flow analysis. It represents the volume fraction occupied by the gas at the in-situ condition. Due to the difference in viscosity and density, the two phases travel at different velocities and the flow is considered to be slip flow. The no-slip liquid holdup is defined as a liquid holdup that would exist if the liquid and gas phases travel at the same speed at the in situ condition. Another common term is the superficial velocity, which is an average velocity of each phase calculated based on flow rate and the total

cross-sectional area of the flow. The mixture velocity is the main velocity of the two phases together. The in-situ speed is the actual velocity of a given phase when it flows with other phases simultaneously. Properties of the mixture are calculated for no-slip and slip cases. Mixture density and viscosity are determined by applying the weighted averaging technique.

Different flow patterns develop due to variation in the distribution of the phases in the flow. The flow pattern is generally affected by gas and liquid rates, wellbore geometry, and thermodynamic properties of the phases. In addition, flow pattern varies with wellbore pressure and temperature. Flow patterns in multiphase flow can be classified from different perspectives. One approach is based on the existence of interfaces and discontinuities at the interfaces. According to this concept, it can be classified as a gas-solid mixture, gas-liquid mixture, liquid-liquid mixture, and immiscible liquid mixture (Pai, 2013). Another approach is based on continuity of medium and can be categorized as continuous and discontinuous flows. In continuous flow, there is no interruption between the phases and both phase travels simultaneously. Discontinuous-flow is based on consideration of both phases as a discrete entity.

In this study, the scope of work is limited to the flow of gas and liquid in the vertical pipe and annulus. Hewitt and Hall-Taylor (1970) classified the gas-liquid flow pattern of vertical upward flow based on the geometry of the interfaces. Hence, the flow pattern is described as bubbly flow, slug flow, churn flow, and annular flow. Similar flow patterns are also observed and reported in many other studies (Mcquillan and Whalley, 1985; Rozenblit et al., 2006; Taitel et al., 1980; Weisman et al., 1979). **Figure 3.1** shows most commonly used flow pattern classifications in vertical pipes.

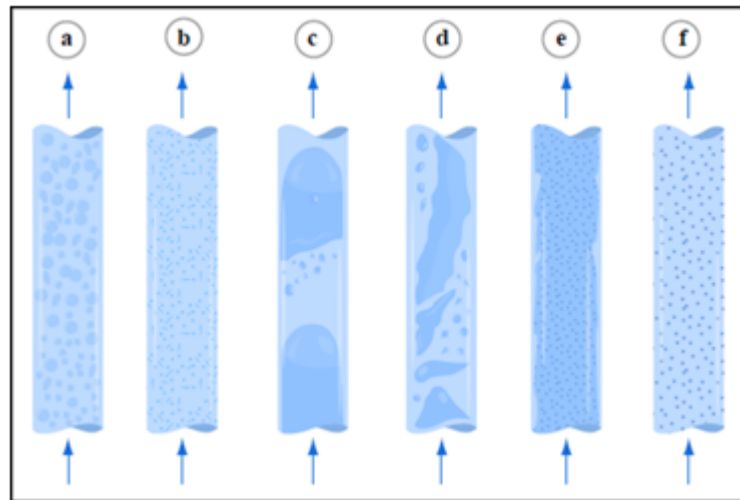


**Figure 3.1 Typical flow pattern of in vertical pipeline: a) bubbly flow, b) dispersed bubbly, c) plug/slug flow, d) churn flow, e) annular flow, and f) mist flow (After Image by MIT-OCW)**

Bubbly flows exist in vertical pipes at low gas flow rates. With increasing the gas flow rate, the bubbles coalesce and form larger bubbles. With further increase in gas flow rates, the coalesced

bubbles grow and occupy the full pipe cross-section. The large bubbles (Taylor bubbles) split the liquid phase and form gas and liquid slugs. The liquid slugs regularly have small entrained-gas bubbles. A thin liquid film surrounds the gas slugs. This type of flow pattern is categorized as slug flow. Increasing gas flow rate further increases the shear stress between the Taylor bubble and the liquid film. The stress increase eventually ruptures the liquid film resulting in churning motion, which is often categorized the churn flow pattern. At the extremely high gas rate, the gas phase flows as a plug occupying the central part of the pipe and the pattern is recognized as annular flow. Depending on the flow condition, limited amount of liquid droplets can be entrained in the gas while the remaining part of the liquid flows as a film. In the vertical wellbore, different flow-patterns are expected to develop at various depths. For instance, near the bottom of the hole, a single-phase fluid is expected. As the fluid moves upward, the in-situ pressure gradually decreases causing the dissolved gas to liberate and form the bubbly flow pattern. As pressure decreases further, more gas may come out of the solution and slug type flow-pattern develops.

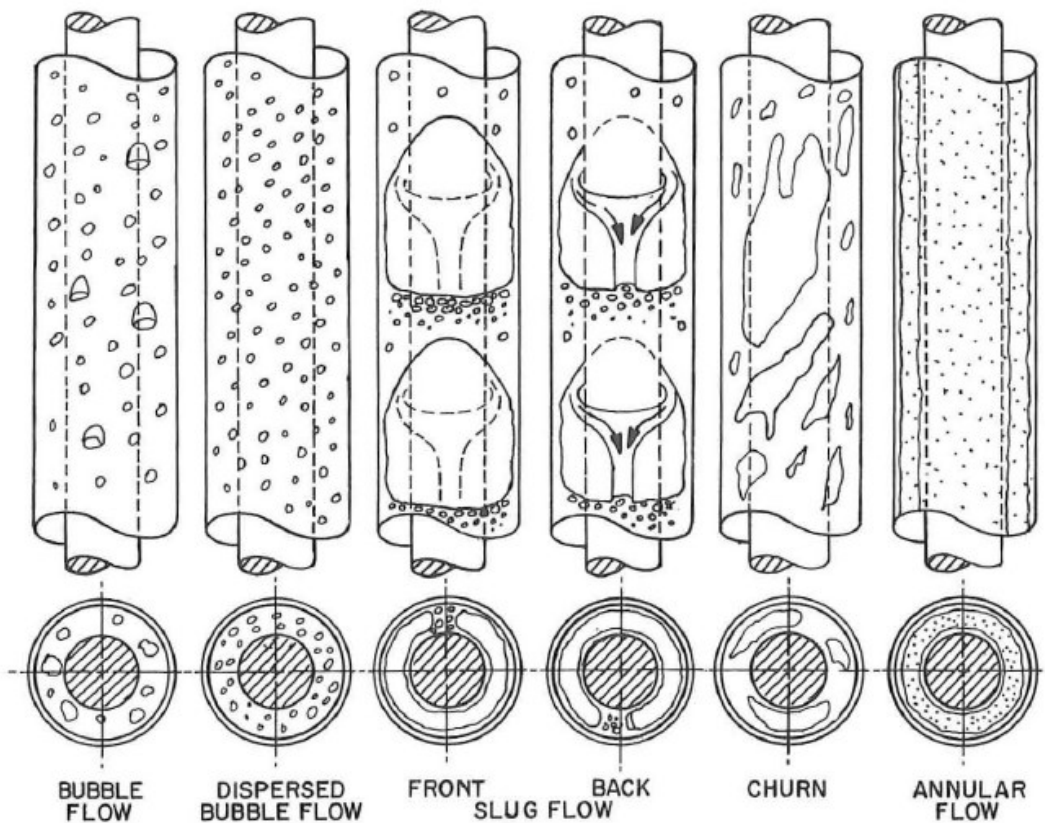


Figure 3.2 Flow Patterns in Annular Geometry (Caetano et al., 1992a)

Overall, the flow pattern maps in the annulus and pipe are resemble. Caetano et al. (1992a) collected experimental data to establish flow pattern map for a vertical annulus and revealed that

the flow pattern map is similar to a pipe; however, some differences exist (**Figure 3.2**). The flow patterns observed in annuli were mainly: bubbly, dispersed bubbly, slug, churn, and annular. In the bubbly flow, the gas phase is uniformly dispersed in the liquid phase as discrete bubbles. The bubbles have mainly two shapes: spherical and cap-type bubbles. The upward movement of spherical bubbles is random, while the cap-type bubbles move at a faster speed in a straight line. The dispersed bubble flow contains only small spherical discrete bubbles, moving upward in a straight path. The mixture velocity is same as the liquid velocity with no slippage between the phases. Slug flow comprised of moving large bubbles, accompanied with liquid slugs at the tail. The large bubbles are termed as Taylor bubbles similar to the pipe flow. Liquid phase moves backward in the form of films, which creates a high turbulence behind the Taylor bubble. Churn flow is more chaotic and independent of geometry in comparison to the slug flow. With high gas concentration, the Taylor bubbles are destroyed and liquid falls backward. In the annular flow, continuous gas phase flow constitutes the core of the annulus. Liquid films form at the casing and tubing walls and move upward. Some liquid droplets are entrained in the gas core. The casing wall film is thicker than the tubing wall film. Overall, the Taylor bubbles in annular geometry are asymmetric, and liquid phase moves backward through a flow channel. The flow pattern is a function of tubing to casing diameter ratio (Caetano et al., 1992a).

It is essential to understand the features of various two-phase flow patterns. Flow pattern maps are developed as a means of characterizing two-phase flows. They can be used to predict transitional boundaries between two or more distinct flow patterns and other relevant flow parameters needed to perform the hydraulic analysis. The maps have consistent principles for the flow patterns, a broad database, and a semi-theoretical basis for determining flow pattern boundaries. Flow pattern maps are drawn in a two-dimensional graph, to split the map into regions of different flow patterns. Simple flow pattern maps employ identical coordinates for all flow patterns and transitions, while complex flow-pattern maps utilize different coordinates for flow transitions (Awad, 2010). Variety of flow pattern maps for vertical upward flow can be found in the literature. These are produced based on different coordinate systems such as modified superficial velocities (Hewitt and Roberts, 1969; Hewitt and Hall-Taylor, 1970), dimensionless parameters (Dun and Ros, 1963), and superficial velocities (Ansari et al., 1994). The coordinate parameters are based on flow conditions, gas-liquid physical properties, pipe material and diameter, and superficial velocities. A typical flow-pattern map for vertical pipes, which is based on the superficial velocity of liquid and gas, is presented in **Figure 3.3** (Griffith, 1984).

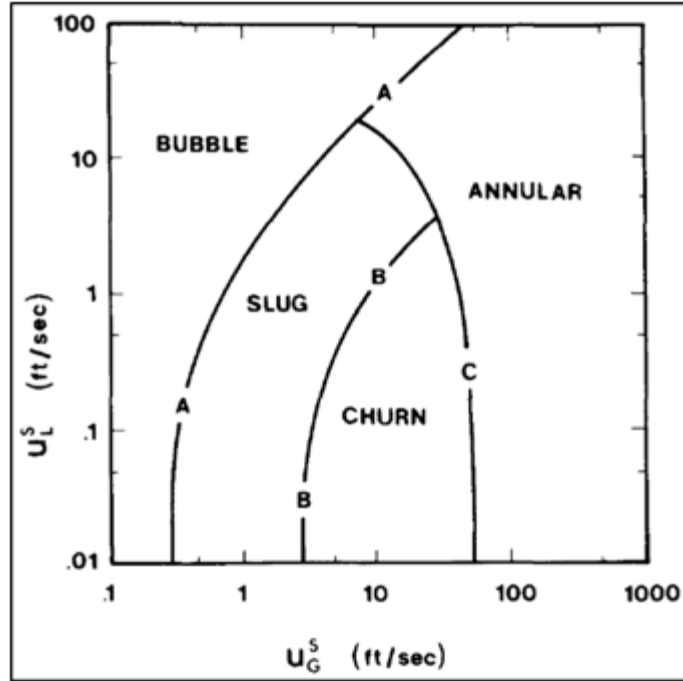


Figure 3.3 Flow pattern map for air and water in vertical up flow (Griffith, 1984)

Figure 3.4 shows different flow patterns existing in a pipe, based on dimensionless gas velocity number (RN) and liquid velocity number (N), which can be computed using Equations 3.1 and 3.2. Waltrich et al. (2015) conducted an experimental analysis and established the existence of annular flow in case of high superficial gas velocity where the ratio of gas and liquid velocity is greater than 100. The experimental data was put on the flow pattern map developed by Duns and Ros (1963).

$$RN = V_{sg} \sqrt[4]{\frac{\rho_l}{g\sigma}} \quad (3.1)$$

$$N = V_{sl} \sqrt[4]{\frac{\rho_l}{g\sigma}} \quad (3.2)$$

where,  $V_{sg}$  denotes the superficial gas velocity,  $V_{sl}$  denotes the superficial liquid velocity,  $\sigma$  represents the surface tension,  $\rho_l$  represents the liquid density, and  $g$  acceleration due to gravity. Black solid lines in the figure represent flow regime based on Dun and Ros (1963) model. The dashed line indicates the transition model based on Waltrich et al. (2015) study. Green, red and blue shaded regions are bubbly, churn, and annular flow regime, respectively.

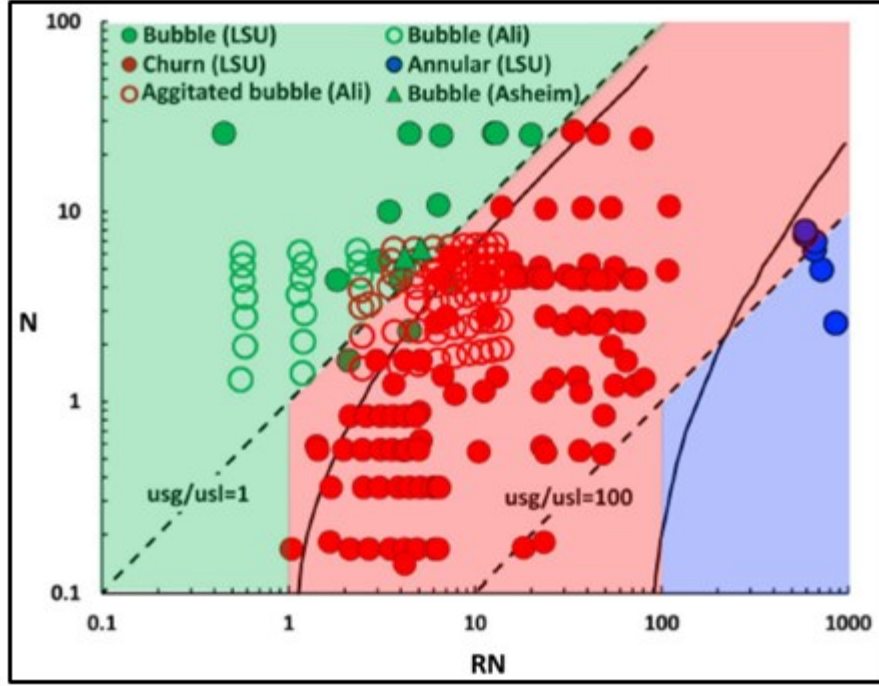


Figure 3.4 Experimental flow regime map (After Waltrich et al., 2015)

Even though flow patterns in the annulus and pipe are similar, there are some differences. Caetano et al. (1992a) proposed different flow pattern maps for air-water and air-kerosene flow through a concentric annulus (Figures 3.5 and 3.6). Air-kerosene mixture had lower flow transition superficial gas velocities, which is attributed to the change in the fluid properties. Hence, the impact of fluid properties on transition from one flow pattern to another is important. To characterize these transitions, models have been proposed based on the flow characteristics. Mathematically, the bubble flow regime occurs in case of high Taylor velocity in comparison with discrete bubble velocity as described in Equation 3.3.

$$0.345\sqrt{gD_{EP}} \geq 1.53 \left[ \frac{(\rho_l - \rho_g)g\sigma}{\rho_l^2} \right]^{0.25} \quad (3.3)$$

where  $D_{EP}$  represents equi-periphery diameter (sum of tubing and casing diameter),  $g$  is acceleration due to gravity,  $\rho_l$  is liquid density,  $\rho_g$  is the gas density,  $\sigma$  is surface tension of the liquid in the presence of air. The bubble to slug transition is dictated by agglomeration mechanism at low superficial velocity. During the test, the gas void fraction was 0.20. The in-situ liquid and gas superficial velocities are related by Equation 3.4 (Caetano et al., 1992a).

$$V_{sg} = \frac{V_{sl}}{4} + 0.306 \left[ \frac{(\rho_l - \rho_g)g\sigma}{\rho_l^2} \right]^{0.25} \quad (3.4)$$

where  $V_{sg}$  represents superficial gas velocity,  $V_{sl}$  represents superficial liquid velocity,  $g$  is acceleration due to gravity,  $\rho_l$  is liquid density,  $\rho_g$  is the gas density,  $\sigma$  is surface tension of the liquid in the presence of air.

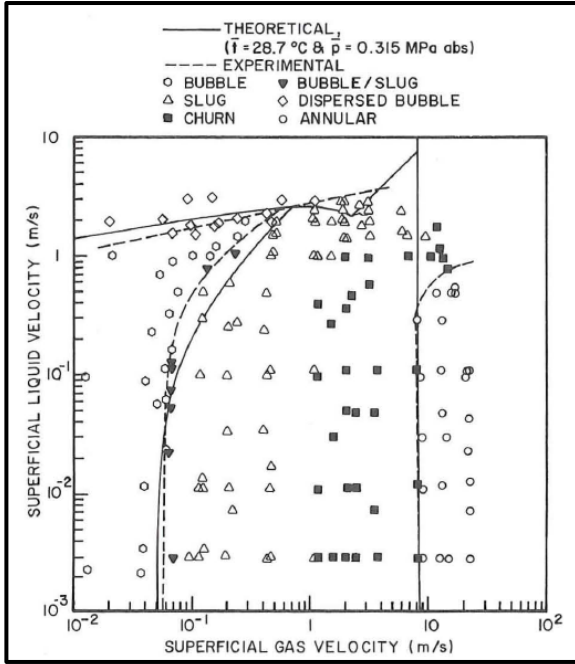


**Figure 3.5 Flow pattern map for air-water mixture in concentric annulus (Caetano et al., 1992a)**

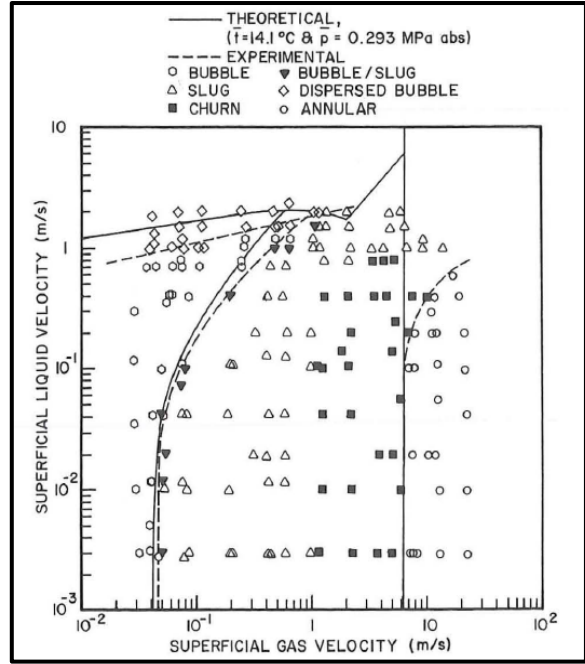


**Figure 3.6 Flow pattern map for air-kerosene in concentric annulus (Caetano et al., 1992a)**

The transition from bubble to slug is also modeled using the concept of hydraulic diameter in which high turbulent forces break the gas phase into the dispersed bubbles. The transition is defined by the following relation:

$$2 \left[ \frac{0.4\sigma}{(\rho_l - \rho_g)g} \right]^{0.5} \left( \frac{\rho_l}{\sigma} \right)^{0.6} \left( \frac{2}{D_H} \right)^{0.4} (f)^{0.4} (V_m)^{1.2} = 0.725 + 4.15 \left( \frac{V_{sg}}{V_m} \right)^{0.5} \quad (3.5)$$

where  $V_{sg}$  represents superficial gas velocity,  $V_m$  represents mixture superficial velocity,  $g$  is acceleration due to gravity,  $\rho_l$  is liquid density,  $\rho_g$  is the gas density,  $\sigma$  is surface tension of the liquid in the presence of air,  $D_H$  is a hydraulic diameter, and  $f$  is fanning friction factor.

The establishment of annular flow is dependent on the minimum gas velocity to move the largest liquid droplet entrained in the gas core and can be determined by comparing the gravity and drag forces. Equation 3.6 gives the transition condition after neglecting the effect of film thickness at the wall.

$$V_{sg} \geq 3.1 \left[ \frac{(\rho_l - \rho_g)g\sigma}{\rho_l^2} \right]^{0.25} \quad (3.6)$$

where  $V_{sg}$  represents superficial gas velocity,  $g$  is acceleration due to gravity,  $\rho_l$  is liquid density,  $\rho_g$  is the gas density,  $\sigma$  is surface tension of the liquid in the presence of air.

Besides the regular flow, the critical flow conditions might present in worst case discharge. The critical flow of a single phase gas occurs, when the Mach number is equal to 1 at the smallest cross-section or chokes (Wallis, 1980). For a single-phase flow, the sonic velocity can be determined based on the isentropic and equilibrium assumptions (Hsu, 1972). A number of studies were conducted on supersonic two-phase flows. For two-phase flow, due to the existence of interfacial transports of mass, heat, and momentum, the isentropic and equilibrium assumptions will be no longer valid, and the dominant flow pattern plays a crucial role in flow characterization (Brown et al., 1960; Baxendell and Thomas, 1961). In these critical flow conditions, the subsonic and supersonic flow conditions occur. These conditions are represented by different Mach numbers. The subsonic condition refers to the Mach number 0.3 to 1. The supersonic condition is represented by Mach number above 1. The supersonic phenomenon is accompanied by shock generation in the system.

The supersonic shock phenomena in the two-phase tunnel were investigated by Eddington (1970). It was observed that the propagation velocity of a shock wave in a two-phase continuum corresponds to the velocity obtained by considering the two-phase medium as an isothermal continuum for the propagation of pressure waves. These waves exhibit finite structure, which depends on volume ratio, phase distribution, and wave strength of both phases. Later, Hsu (1972) extensively investigated the critical flow rate and sonic velocity in two-phase flow. The study investigated the flow pattern and slip ratio. A semi-empirical model was developed and validated using experimental measurements. Then, a theoretical model (Wallis, 1980) has been developed applying two-phase flow theories and conservation equations. Due to simplifying assumptions, theoretical models also require calibration to fit the experimental data. Furthermore, accurate critical flow models need to account for non-equilibrium (transient flow) phenomena. A model to predict sonic velocity in one-dimensional stratified, slug, and homogeneous two-phase flow in a vertical pipe was presented by Nguyen et al. (1981). This model is based on the theory of pressure propagation without phase transformation. According to the modern, the interface of one phase acts as an elastic wall of the other phase. The critical limitation of this model was neglecting frictional forces and surface tensions.

The treatment of multiphase flow at lower velocity is explained in detail in this section, but the dynamics of flow in critical conditions (subsonic and supersonic) are different. A brief outline of supersonic/subsonic flow is provided in this section. However, Section 5 is fully dedicated to subsonic/supersonic multiphase flow.

### **3.2. Nodal Analysis**

As mentioned in Section 2.2, the WCD estimation is based on two models, namely inflow and outflow model. The inflow model deals with the fluid influx into the well from the reservoir. These models are mainly based on the nodal analysis. This study is not mainly focused on inflow

models, hence, before going into detail about outflow models, which describes the flow characteristics in the wellbore, the nodal analysis is briefly presented in this section.

Nodal analysis is based on the construction of inflow performance relationship (IPR), which is developed using the flowing bottom-hole pressure (BHP) and liquid production rate. The inception of nodal analysis came with work done by Gilbert (1954) when two-phase flow and well capabilities were analyzed by matching the inflow performance and outflow performance. This approach was named nodal analysis by Brown and Lea (1985). Afterwards, this technique has evolved over time to monitor the optimum production from oil and gas wells. Every component in the production systems, static reservoir pressure including inflow performance, as well as flow across the completion packer, up the tubing string, across the surface choke, through horizontal flow lines, and into the separation facilities and many others, can be determined to have an economical production. The well components of this system have a broader impact on the nodal analysis.

A typical oil and gas production system consists of flow through a porous medium, wellbore, choke, and surface pipelines. **Figure 3.7** shows a schematic of a simple production system with nodal analysis architecture. Each system component affects production rate and pressure loss in different ways. The existing pressure gradient between reservoir and surface facility is the main driving force for fluid flow in oil and gas well. In the nodal analysis, the system is divided into several nodes comprising of surface line, choke, wellhead, tubing, bottom hole, and reservoir. There are two methodologies involved in the analysis of this system. First, the bottom hole pressure (BHP) is calculated using inflow performance relationship (IPR) and outflow performance relationship (generally known as tubing performance relationship, TPR) at the given production rate. Inflow performance relationship is estimated using different correlations such as Vogel and Fetkovich (Guo et al., 2007).

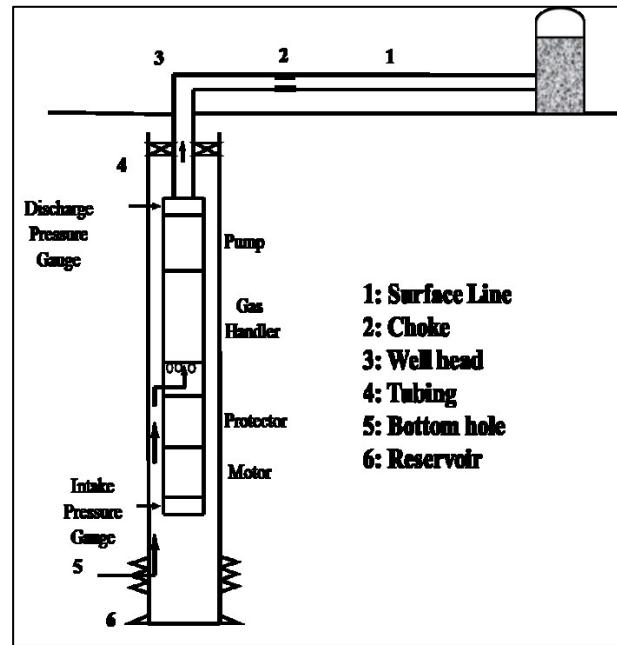


Figure 3.7 Flow across the Operation system

Vogel (1968) came up with the equation to calculate BHP and flow rate for pressure below bubble point. Bubble point refers to a pressure below which the free gas starts leaving the liquid phase from the crude oil. Vogel equation is represented by:

$$q = q_{\max} \left[ 1 - 0.2 \left( \frac{p_{wf}}{\bar{p}} \right) - 0.8 \left( \frac{p_{wf}}{\bar{p}} \right)^2 \right] \quad (3.7)$$

where,  $q_{\max}$  is absolute open flow (theoretically estimated based on reservoir pressure and productivity index above bubble point pressure),  $p_{wf}$  is the bottom hole pressure, and  $\bar{p}$  is the average pressure. However, for the pseudo-steady state (transient conditions), the absolute open flow is given by:

$$q_{\max} = \frac{J^* \bar{p}}{1.8} \quad (3.8)$$

Another known equation for IPR is given by Fetkovich (1973) and considered more accurate. This method was tested for reservoirs having permeability ranging from 6 to 1000 mD. It is given by:

$$q = q_{\max} \left[ 1 - \left( \frac{p_{wf}}{\bar{p}} \right)^2 \right]^n \quad (3.9)$$

After simplifying, Equation 3.9 can be expressed as:

$$q = C(\bar{p}^2 - p_{wf}^2)^n \quad (3.10)$$

where

$$C = \frac{q_{\max}}{\bar{p}^{2n}} \quad (3.11)$$

Brown and Lea (1985) considered the non-Darcy flow and turbulence, which gives pressure difference between reservoir and BHP as a function of a second order polynomial in flow rate. Standing incorporated depletion effect in Vogel's equation by defining the concept of zero drawdown, which depicts the productivity index, when BHP tends to reservoir pressure. This equation uses average pressure,  $\bar{p}$  which is dependent on relative permeability of oil, viscosity of oil, and formation volume factor. The equation represents the single-phase flow. Hence, it can be valid for flow at the bottom of the well. However, other part of the wellbore can be under multiphase flow conditions. Some free gas is produced along with the liquid and it complicates the pressure loss calculation. As the pressure changes, the phase change takes place, and consequently there is change in density, velocity, volume of each phase, and fluid property. Besides this, the pressure change is also accompanied with the change in temperature, which also affects the fluid flow. The primary equations characterizing the fluid flow is based on the general energy equation. The differential form of the energy equation is given below:

$$dU + d\left(\frac{P}{\rho}\right) + \frac{v dv}{g_c} + \frac{g}{g_c} dZ + dq + dW = 0 \quad (3.12)$$

Applying the first law of thermodynamics, Equation 3.12 becomes:

$$\frac{dP}{dL} = \frac{\rho v dv}{g_c dL} + \frac{\rho g}{g_c} + \left(\frac{dP}{dL}\right)_f \quad (3.13)$$

Equation 3.13 is applicable for vertical pipes and annuli. The first term from the right side represents the acceleration term, which is dependent on the kinetic energy of the system. The last term,  $\left(\frac{dP}{dL}\right)_f$  represents the pressure loss due to friction, which can be calculated using existing correlations. In order to determine the two-phase friction factor accurately, the effects of liquid holdup, density, velocity, viscosity, and surface tension need to be investigated. The two-phase friction factor is more complicated due to the presence of different flow patterns. The two-phase flow pattern is dependent on the superficial gas and liquid velocity. The methods of multiphase flow modeling are described in details in Section 3.3.

### 3.3. Multiphase Flow Modeling

There are different types of modeling approach (empirical, analytical, mechanistic, and numerical) existed in the industry in order to predict pressure drop, volumetric liquid holdup, and flow pattern of two-phase flow in pipes and annuli. The review of these models is presented in the sub-sections below.

#### 3.3.1. Empirical Models

The most simplistic approach for two-phase flow characterization is based on experimental data. Often empirical models can be formulated by establishing the mathematical correlations based on statistical evaluation of experimental results. Although, this technique yields reasonably accurate prediction, its application is limited to the range of data that is used to create the model. In addition, the accuracy of empirical correlations is strongly affected by the flow pattern (Dukler et al., 1964).

The pressure drop in multiphase flow in comparison to single-phase flow is different in several aspects. One of them is slippage arising between the phases. The slippage is the consequence of two phases with different velocities, which in turn, depend on the fluid properties. Based on this characteristic, empirical correlations can be divided into three categories, i) no-slip no-flow pattern (Poettman and Carpenter, 1952); ii) slip no-flow pattern (Eaton et al., 1967, Hagedorn and Brown, 1965; Zuber and Findlay, 1965); and iii) slip and flow pattern (Beggs and Brill, 1973; Hasan and Kabir, 1992; Mukherjee and Brill, 1985; Shi et al., 2005). Based on the geometry of the flow, different correlations (Beggs and Brill, 1973; Hagedorn and Brown, 1965; Dun and Ros, 1963; Hagedorn and Brown, 1965) and models (Orkizewski, 1967) have been developed.

Hagedorn and Brown (1965) developed a flow-pattern independent correlation using measurements from a 1500-ft long vertical wellbores with tubing diameters ranging from 1-2 in.

Five test fluids (water and four types of oil with viscosities ranging from 10 to 110 cp at 80°F) were considered during the experimental investigation. A similar correlation (Duns and Ros, 1963) was developed for vertical flow of gas and liquid mixtures. Although it was developed for dry oil-gas mixtures, it can be utilized to analyze flow of wet mixtures with some corrections. Later, Orkizewski (1967) formulated a two-phase flow model for vertical wellbores, which is valid for different flow regimes such as bubbly, slug, transition, and annular mist flows. Beggs and Brill (1973) presented most widely used correlation, which is developed from experimental measurements obtained from a small-scale test facility. Most of these studies (Duns and Ros, 1963; Orkizewski, 1967; Beggs and Brill, 1973) investigated flow regimes in vertical pipes including bubbly flow, slug flow, transition flow, and mist flow.

In bubbly flow, the pipe is full of liquid and free gas presents as small bubbles. The bubbles move faster than the liquid. The pipe is largely in contact with the liquid phase. In slug flow, the gas phase is more distinct. The liquid phase remains as continuous; however, the gas bubbles establish plugs or slugs across the pipe section. Gas velocity is more than liquid and liquid film around bubble moves downward with relatively low velocity. Both phases have a noticeable effect on pressure gradient.

In transitional flow, gas bubbles become more significant, and liquid entrains between the gas bubbles. Gas phase has a more dominant effect than liquid phase in this case. Mist flow has a continuous gas phase, and liquid droplets are formed in the gas. Most of the correlations presented by Duns and Ros (1963) are applicable in mist region. The summary of some of the correlations developed over time is presented in **Table 3.1**.

**Table 3.1 Summary of empirical correlations**

Authors	Flow Patterns addressed	Validation	Remark
Poettmann and Carpenter (1952)	No flow patterns considered	Flow rate > 420 STB/day; GLR < 1500 scf/STB; 2-3 in. pipe; Oil, water and air	Used solubility concepts
Duns and Ros (1963)	Bubble, slug, transition, annular-mist	3.5 in tubing; Oil and gas	3-10% deviation from the measure data
Hagedorn and Brown (1965)	No flow patterns considered	1500 ft experimental well data; 1, 1.25, 1.5 in tubing; Oil (10-110 cp) and gas	Correlation for friction factors and liquid holdup developed based on Reynolds number
Orkiszewski (1966)	Bubble, slug, transition, annular mist	1-3 in pipe size; Oil, water, and air	Griffith Wallis work extended to high-velocity, Annular-mist flow pattern not evaluated, Flow in casing annulus not evaluated
Bregg and Brills (1973)	Mist, bubble, slug, plug, annular, wavy, stratified	90 ft long pipe Gas flow rate (0-300 Mscf/D) Liquid flow rate (0-30 gal/min) System pressure (35-95 psia) Liquid holdup (0-0.87) Pressure gradient (0-0.8 psi/ft)	Correlation for inclination angle correction, Froude number, liquid content, and no slip holdup Correlation for predicting two-phase friction factor normalized with no slip friction factor from Moody diagram

\*GLR: Gas Liquid ratio

### 3.3.2. Analytical Models

As we know, the multiphase flow can be characterized using the conservation laws. The analytical equations are derived using these conservation principles with certain assumptions and simplifications. These models quite successfully handle wide ranges of flow parameters with certain limitation in their accuracy due to modeling constraints and simplifications considered. Different analytical modeling approaches (Homogenous Model, Separated Flow Model, Interfacial Pressure Gradient (IPG) Model, Two-Fluid Model and Drift-Flux Model) have been developed and used for designing and optimization purposes in the petroleum industry. In this section, a review of different analytical models is presented.

One of the simplistic analytical models is the homogeneous model, also known as a no-slip model (Darcy, 1857), which considers a multiphase flow as a single-phase flow with average fluid properties that depend on phase composition. The main constraint of this model is the consideration of no-slip condition and neglect of flow pattern effect. This model is often not applied in practice, except with single-phase simulators to obtain an estimate of two-phase flow

effect. In addition, the model utilized to assess the performance of advance multiphase models that consider slip effects.

Another analytical model is separated flow model, which was introduced by Lockhart and Martinelli (1949) and later improved by Martinelli and Nelson (1948). In this model, liquid and gas phases are considered individually. The models accounts for slippage between phases. It is one of the simplest methods for determining two-phase flow pressure drop and liquid holdup (Awad, 2012). The Lockhart-Martinelli technique is applied for all flow patterns. It uses only one parameter to differentiate between two phases.

In advanced separated models, equations of continuity, momentum, energy, and rate equations are considered for each phase. Different formulations of separated flow models (Muzychka and Awad, 2010; Turner, 1966) are presented in the literature. In continuation of the Lockhart-Martinelli scheme, the interfacial pressure gradient is also used to characterize gas-liquid flows. The interfacial pressure gradient approach/model considers small and large Lockhart-Martinelli parameters ( $X_m$  and  $Y_m$ ), which represent gas and liquid phases, respectively. The two-phase frictional pressure gradient is determined from three pressure gradients (single-phase liquid, single-phase gas, and interfacial pressure gradients). It can be formulated as one, two, or multiple-parameter model depending on the flow pattern.

The drift-flux model has been extensively applied in bubbly and plug flow analysis with acceptable accuracy. The merit of the model is that it simplifies the calculation procedure by reducing number equations. The model uses four basic equations: the mass, momentum and energy balance equations of the mixture, and the gas phase mass balance. Rouhani and Axelsson (1970) validated the drift-flux model using wide range of experimental data and they reported negligible error. A similar study was performed to analyze flow in vertical wells. The drift-flux model was used for predicting the void fraction in tubing for bubbly flow. The model was validated based on the different source of experimental data, and the acceptable match was reported. Moreover, to improve the accuracy of the drift-flux model, studies were conducted to develop correlations for predicting model parameters for vertical and inclined pipe flows. The accuracy of the drift-flux model highly depends on the flow pattern (slug and churn flow) of gas-oil flow in vertical and inclined wells (Hasan and Kabir 1992, Kabir and Hasan 1990).

The most advanced model in the area of analytical modeling is the two-fluid model, which is used as a predictive tool for two-phase flow characterization in engineering applications. The real benefit of this model is that it accounts for the dynamic and non-equilibrium interactions existing between the phases. The model considers each phase as a distinct fluid and applies the governing equations. As a result, each phase has its own pressure, temperature, and velocity profiles. In this manner, the differences between two phases can be accurately pinpointed. Also, this model has been well applied for analyzing two-phase flow in shell-sides of large heat exchangers with different gas and liquid velocity directions such as steam generators and kettle reboilers. However, the model is computationally very expensive in comparison to other

analytical models (Schlegel et al., 2010). In addition, the use of two momentum equations presents considerable complications in modeling interfacial interaction between the two phases (Hibiki and Ishii (2003)). **Table 3.2** presents the summary of different well know analytical models developed for two-phase flow.

**Table 3.2 Summary of analytical models**

Authors	Model type	Validation	Remark
Kawanishi et al. (1990)	Drift Flux model	Steam-water/Air-water ID: 0.6-61 cm	Relative error was 0.168 Annular condition not studied in detail
Shi et al. (2003)	Steady-state Drift-Flux model	Oil, water, and Nitrogen gas 15.2 cm diameter and 10.9 m long test section	Optimized drift flux parameters to study large diameter, vertical and inclined pipes
Hibiki and Ishii (2003)	Steady-state Drift Flux model	Air-water adiabatic flow 2 in pipe diameter	Constitutive equation developed for bubble, slug, churn, and annular flow Model showed 70% deviation for velocity at 10 m/s
Schegel et al. (2010)	Drift Flux model	Test sections under 0.15 and 0.20 m Liquid velocity up to 1 m/s Void fractions up to 0.85	Review of drift-flux models for different diameter No effect on drift flux parameter for non-dimensional diameter above 30
Bhagwat et al. (2014)	Drift-Flux model	Range of Parameters: Diameter: 0.5-305 mm Liquid Viscosity: 0.0001-0.6 Pa-s System pressure: 0.1-18.1 MPa	Correlation development: Distribution parameter and drift velocity as function of pipe diameter, pipe orientation, phase flow rate, fluid properties, and void fraction Void fraction independent of flow patterns

\*ID: Inner diameter

Due to reasonable efficiency and accuracy, the drift-flux model is frequently used in Petroleum industry. The same model can be used for the WCD study, considering the steady-state formulation. Drift-flux model (DFM) has been consistently used and improved in the Petroleum industry since its inception due to its simplicity, and continuous and differentiable behavior (Zuber and Findlay, 1965; Hasan and Kabir, 1988; Ansari et al., 1994). DFM relies on slip property between gas and liquid, which is determined by two factors namely, gas concentration and the tendency of the gas to move upward due to buoyancy. The effect is generally modeled in terms of velocity and can be described as:

$$V_g = C_0 V_m + V_{slip} \quad (3.14)$$

where  $V_g$  is the average gas phase flow velocity across the cross-section,  $C_0$  is distribution coefficient,  $V_m$  is the average velocity of the mixture, and  $V_{slip}$  is the drift velocity of the gas. The variation of  $C_0$  is essential due to its dependence on flow regimes. Several researchers have reported different values over time.

A mathematical model for two-phase flow can be formulated using the drift flux model. The model includes solving the conservation of continuity and momentum using the closure equations and boundary conditions. The basic equations are:

Conservation of Mass (Liquid Component):

$$\frac{\partial}{\partial t}(\alpha_l \rho_l) + \frac{\partial}{\partial x}(\alpha_l \rho_l v_l) = \Gamma \quad (3.15)$$

where  $\alpha_l$  is the liquid fraction,  $\rho_l$  is the density of the liquid,  $v_l$  is the velocity of the liquid phase, and  $\Gamma$  represents the gas dissolution rate from the gaseous phase to liquid phase and is often considered to be 0.

Conservation of Mass (Gas Component):

$$\frac{\partial}{\partial t}(\alpha_g \rho_g) + \frac{\partial}{\partial x}(\alpha_g \rho_g v_g) = -\Gamma \quad (3.16)$$

where  $\alpha_g$  is the gas fraction,  $\rho_g$  is the density of the gas,  $v_g$  is the velocity of the gas phase, and  $\Gamma$  represents the gas dissolution rate from the gaseous phase to liquid phase and is frequently considered to be 0.

Conservation of Momentum (Liquid Component):

$$\frac{\partial(\alpha_l \rho_l v_l + \alpha_g \rho_g v_g)}{\partial t} + \frac{\partial(\alpha_l \rho_l v_l^2 + \alpha_g \rho_g v_g^2)}{\partial x} + P = -F + G \quad (3.17)$$

where  $P$  is the pressure at the calculation point,  $F$  is the force due to frictional pressure loss,  $G$  is the gravity force. The boundary conditions and closure relations are given by Equations 3.18 to 3.24.

Boundary conditions and closure equations:

$$\alpha_l + \alpha_g = 1 \quad (3.18)$$

Density variation:

$$\rho_l = \rho_{l,0} + \frac{P - P_0}{\alpha_l^2} \quad (3.19)$$

where  $\rho_l$  is the density of the liquid phase,  $\rho_{l,0}$  is the density of the liquid at reference pressure ( $P_0$ ), and  $\alpha_l$  is the liquid fraction.

$$\rho_g = \frac{P}{\alpha_g^2} \quad (3.20)$$

where  $\rho_g$  is the density of the gas phase,  $P$  is the pressure, and  $\alpha_g$  is the gas fraction.

Velocity Variation:

$$v_g = \frac{C_0 \alpha_l v_l + v_{slip}}{1 - C_0 \alpha_g} \quad (3.21)$$

where  $V_g$  is the superficial gas velocity,  $V_l$  is the superficial liquid velocity,  $C_0$  is the distribution coefficient,  $V_{slip}$  is the slip velocity,  $\alpha_l$  is the liquid fraction, and  $\alpha_g$  is the gas fraction.

Mixture Density:

$$\rho_{mix} = \alpha_l \rho_l + \alpha_g \rho_g \quad (3.22)$$

where  $\rho_{mix}$  is the density of the mixture,  $\rho_l$  is the density of the liquid phase,  $\rho_g$  is the density of the gas phase,  $\alpha_l$  is the liquid fraction, and  $\alpha_g$  is the gas fraction.

Mixture Viscosity:

$$\mu_{mix} = \alpha_l \mu_l + \alpha_g \mu_g \quad (3.23)$$

where  $\mu_{mix}$  is the viscosity of the mixture,  $\rho_l$  is the density of the liquid phase,  $\rho_g$  is the density of the gas phase,  $\mu_l$  is the viscosity of the liquid, and  $\mu_g$  is the viscosity of the gas.

Slip Velocity:

$$v_{slip} = 0.35 \sqrt{\frac{gD(\rho_l - \rho_g)}{\rho_l}} \quad (3.24)$$

where  $V_{slip}$  is the slip velocity,  $g$  is acceleration due to gravity,  $D$  is the diameter of the pipe,  $V_{slip}$  is the slip velocity,  $\rho_l$  is the density of the liquid phase, and  $\rho_g$  is the density of the gas phase.

### 3.3.3. Mechanistic Model

The complex physical phenomena of multiphase flow cannot be simply addressed by the generalized empirical correlations and simplified analytical models. Mechanistic models have been introduced to predict flow behavior more accurately under different flow conditions. These classes of models are based on a phenomenological approach that takes into account the governing laws. Continuity is preserved by applying simultaneous mass balances of the phases. The early mechanistic models (Orkiszewski 1967, Caetano et al., 1992a; 1992b) were developed to predict flow pattern transition and pressure drop during steady gas-liquid flows in vertical tubes. The models incorporate the effect of fluid properties and flow geometry. The models do

not have severe limitations as the empirical models. Later, improved and more advanced mechanistic models (Ansari et al. 1994; Hasan and Kabir, 1988; Gomez et al. 2000) for two-phase gas-liquid flow were developed considering different flow patterns and geometries. To simulate real flow in oil and gas wells, the models are coupled with PVT models. Other applications of mechanistic models in analyzing two-phase flows have been widely reported in the literature (Gomez et al., 2000; Liu et al., 2005). The most relevant characteristic of mechanistic models is their ability to predict the flow regime.

A number of mechanistic models have been reviewed to examine the assumptions under which they were established and their limitations. Bijleveld et al., (1988) developed the first steady state mechanistic model that predicts bottom-hole pressure and two-phase flow parameters. The model uses an iterative procedure. First, it assumes a stratified flow condition and then checked for its validity. In case of non-existence of stratified flow, another flow pattern is assumed. The procedure is repeated until a good agreement between assumption and prediction is established. An average error of 10%, which is less than that of Beggs and Brill correlation (12% average error), was reported. Furthermore, several mechanistic models have been developed to characterize different flow parameters such as flow pattern, film thickness, bubble rise velocity in liquid columns, and liquid holdup. Gomez et al. (2000) used a unified mechanistic model to predict the two-phase flow parameters.

Caetano et al. (1992b) presented a model for upward vertical flow in the annulus. The model predicts the bubble to slug transition at void fraction of 0.2; however, other studies (Hasan and Kabir, 1988; Kelessidis and Dukler, 1989; Lage and Time, 2000) proposed slightly different transition point (void fraction of 0.25). Hasan and Kabir (1988) developed a model to predict two-phase upward flow in annuli. The model predicts the gas void fraction using the drift-flux approach considering liquid slugs and Taylor bubbles. Other similar model (Ansari et al. 1994) predicts the flow variables and flow pattern (bubble flow, slug flow, churn flow and annular flow) shown in **Figure 3.1**. The study conducted by Ansari et al. (1994) suggests the significant improvement in annular flow model which is presented in **Table 3.3**. After determining the flow pattern, the flow variables are determined. The model was validated using a wide range of experimental data and field measurements. Recently, an improved mechanistic model was developed (Lage and Time, 2000) to analyze two-phase upward flow in concentric annulus.

**Table 3.3 Statistical result of comparative study of models for annular flow (After Ansari et al. 1994)**

<b>Model</b>	<b>Relative Performance Factor</b>
<b>Aziz et al. (1972)</b>	5.9
<b>Hagedorn and Brown</b>	8.6
<b>Duns and Ros</b>	11.3
<b>Mukherjee and Brill</b>	17.4
<b>Beggs and Brill</b>	20.5
<b>Orkiszewski</b>	45.8
<b>Ansari et al. (1994)</b>	5

More recently, a comprehensive mechanistic model (Perez-Tellez et al. 2003) was formulated for a steady-state two-phase flow in wellbores. The predictions of the model demonstrated reasonable agreement (average error of less than 5%) with field and full-scale flow loop measurements. **Table 3.4** summarizes the mechanistic models developed by different studies over time. Two of the most popular models for two-phase flow in pipe and annulus are presented next.

**Table 3.4 Summary of mechanistic models**

Authors	Flow Patterns addressed	Validation	Remark
Aziz et al. (1972)	Bubbly, slug, and froth	Field data: ID: 1.992-2.436 in Oil rate: 44-1850 bbl/d GOR: 143-9975 Scf/bbl API: 18.7-47.3	Model for flow in Pipe Error similar to Orkiszewski but superior to Hagedorn and Brown and Duns and Ros
Hasan and Kabir (1988)	Bubble, slug, and annular	Beggs and Brill data and Lau's data	Model for flow in pipe and annulus New correlation for flow parameters for bubbly flow Maximum error of 4.6%
Hasan and Kabir (1992)	Bubbly, slug, churn, and annular	Test data Maximum OD: 127 mm Maximum ID: 87 mm Maximum V <sub>sg</sub> : 15.24 m/s	Model for flow in annulus Drift flux approach adapted to model slip
Caetano (1992 a and b)	Bubble, dispersed bubble, slug, and annular	Experimental data Air-water and Air-Kerosene 3 X 1.66 in test section	Model for flow in annulus Strong dependence on liquid entrainment Film thickness ratio dependent on adopted droplet deposition mechanism
Ansari et al. (1994)	Bubble, slug, and annular	Field data from different sources	Model for flow in pipe Used the concept of Caetano (1992 a and b) model for slug flow Better performance than other empirical correlations and Aziz et al. (1972) and Hasan and Kabir (1988) model
Gomez et al. (2000)	Stratified, slug, bubble, annular, and dispersed bubble	Lab data: Maximum ID: 3 in	Unified model for flow in Pipe Absolute average Error for databank: 12.6%
Lage and Time (2000)	Bubble, dispersed bubble, slug, and annular	Used Caetano (1985) data and another full-scale Experiment setup with 6.276 X 2.764 in test section	Model for flow in annulus Same film thickness to tubing and Casing wall Less than 10% absolute errors

**Pipe Flow Model (Based on Ansari et al., 1994)**

Ansari et al. (1994) developed a comprehensive mechanistic model for pipe flow considering different flow regimes. The bubbly flow regime characteristics are established based on observations of Caetano et al. (1992a; 1992b). The liquid holdup is predicted by solving the following implicit equation:

$$1.53 \left[ \frac{g\sigma(\rho_l - \rho_g)}{\rho_l^2} \right]^{0.25} H_L^{0.5} = \frac{V_{sg}}{1 - H_L} - 1.2V_M \quad (3.25)$$

where  $V_{sg}$  represents superficial gas velocity,  $V_m$  represents mixture velocity,  $\rho_l$  is liquid density,  $\rho_g$  is the gas density,  $\sigma$  is surface tension of the liquid in the presence of gas, and  $H_L$  is the liquid holdup. The pressure gradient is given by the following equation:

$$\left(\frac{dp}{dz}\right)_T = \rho g + \frac{f\rho V^2}{2d} \quad (3.26)$$

where  $(dp/dz)_T$  represents the total pressure gradient,  $V$  represents the mixture velocity,  $d$  is the pipe diameter of the casing, and  $f$  is fanning friction factor.

The slug flow model is developed based on modeling formulations of Caetano et al. (1992a; 1992b). Accordingly, the holdup is calculated by solving the following implicit equation.

$$\begin{aligned} & \left(9.916\sqrt{gd}\right)\left(1-\sqrt{1-H_{LTB}}\right)^{0.5} H_{LTB} - V_{TB}(1-H_{LTB}) + H_{gLS}V_{TB} + (1-H_{gLS}) \\ & \times \left[ V_M - H_{gLS} \left\{ 1.53 \left[ \frac{\sigma g(\rho_l - \rho_g)}{\rho_l^2} \right]^{0.25} (1-H_{gLS})^{0.5} \right\} \right] \end{aligned} \quad (3.27)$$

where  $H_{gLS}$  is liquid slug void fraction,  $H_{LTB}$  liquid Taylor bubble holdup,  $V_{TB}$  is the velocity of the Taylor bubble.

Following a similar modeling procedure, the annular flow model is formulated considering the conservation of mass and momentum. The momentum is conserved for the liquid film. The gas core is assumed a homogenous mixture of gas and entrained liquid droplets moving at the same speed. The final equations comprise of the pressure gradient that can be solved implicitly with the initial guess of dimensionless film thickness.

$$\frac{Z}{4\bar{\delta}(1-\bar{\delta})(1-2\bar{\delta})^5} \left(\frac{dp}{dz}\right)_{SC} - (\rho_L - \rho_C)g - \frac{(1-Fe)^2}{64\bar{\delta}^3(1-\bar{\delta})^3} \frac{f_f}{f_{SL}} \left(\frac{dp}{dz}\right)_{SL} = 0 \quad (3.28)$$

where  $Z$  is the correction factor for interfacial friction. The film thickness is obtained using equations given by Wallis (1969).  $\bar{\delta}$  is dimensionless film thickness,  $(dp/dz)_{SC}$  is the superficial friction pressure gradient in the core,  $(dp/dz)_{SL}$  is the superficial liquid friction pressure gradient,  $Fe$  is the entrained liquid fraction in the gas core and calculated using the Wallis equation,  $f_f$  is the fanning friction factor in the film, and  $f_{SL}$  is the fanning friction factor for the superficial liquid velocity. The non-dimensional form of Lockhart Martinelli parameter can be applied to determine the total pressure gradient using the following equation:

$$\left(\frac{dp}{dz}\right)_T = \phi_c^2 \left(\frac{dp}{dz}\right)_{SC} + \rho_c g = \phi_F^2 \left(\frac{dp}{dz}\right)_{SL} + \rho_L g \quad (3.29)$$

where the non-dimensional parameter can be calculated using Equations 3.30 and 3.31.

$$\phi_c^2 = \frac{\left(\frac{dp}{dz}\right)_c - g\rho_c}{\left(\frac{dp}{dz}\right)_{SC}} \quad (3.30)$$

$$\phi_F^2 = \frac{\left(\frac{dp}{dz}\right)_F - g\rho_L}{\left(\frac{dp}{dz}\right)_{SL}} \quad (3.31)$$

where  $(dp/dz)_T$  is the total pressure gradient,  $(dp/dz)_C$  is the pressure gradient in the core,  $(dp/dz)_F$  is the pressure gradient in the film.

#### Annular Geometry Model (Based on Caetano et al., 1992b)

Caetano et al. (1992b) developed a mechanistic model for flow in concentric annulus considering different flow regimes.

**Bubbly Flow:** In the bubbly flow, the slippage between the gas and liquid is a primary concept for modeling. The liquid holdup in the bubble phase is given by the implicit equation as depicted below.

$$H_L^{n+2} - H_L^{n+1} + \frac{(V_{sl} + V_{sg})H_L}{1.53 \left[ \frac{(\rho_l - \rho_g)g\sigma}{\rho_l^2} \right]^{0.25}} - \frac{(V_{sl})}{1.53 \left[ \frac{(\rho_l - \rho_g)g\sigma}{\rho_l^2} \right]^{0.25}} = 0 \quad (3.32)$$

where n is index number which is considered to be 0.5 (Fernandes et al., 1983). The total pressure gradient is defined as the sum of pressure gradients due to gravity, friction loss, and kinetic energy or convective acceleration change. Generally, the change in acceleration is negligible and total pressure gradient is given by Equation 3.33.

$$\left(\frac{dp}{dz}\right)_T = \rho_s g + \frac{4f}{D_c - D_T} \rho_s \frac{(V_{sl} + V_{sg})^2}{2} \quad (3.33)$$

where  $D_c$  is the inner diameter of the casing,  $D_T$  is the outer diameter of the tubing,  $\rho_s$  is the slip density, and f is fanning friction factor.

The concept of dispersed bubble phase is originated due to its nature of homogenous flow without slippage, and consequently, the in-situ velocities of both phases are considered the same. The liquid holdup is given by the following the equation:

$$\lambda_L = \frac{V_{sl}}{V_{sl} + V_{sg}} \quad (3.34)$$

where  $\lambda_L$  represents the no-slip liquid holdup. The total pressure gradient is using Equation 3.33; however the slip density should be replaced with mixture density which is obtained using the no-slip liquid holdup.

**Slug Flow:** Slug flow model is the most challenging flow regime to model considering the intermittent nature of the flow and complicated phase distribution. Caetano et al. (1992a) developed the model for slug flow considering the two possible configurations: fully developed Taylor bubble and developing Taylor bubble. The liquid holdup and total pressure gradient are given by Equations 3.35 and 3.36.

$$H_{SU} = \left( \frac{L_{LS}}{L_{SU}} \right) H_{LS} + \left( 1 - \frac{L_{LS}}{L_{SU}} \right) H_{LF} \quad (3.35)$$

where  $H_{SU}$  is the unit average liquid holdup,  $L_{LS}$  is liquid slug length,  $L_{SU}$  is unit slug length,  $H_{SL}$  is liquid holdup in liquid slug zone and considered to be 0.8,  $H_{LF}$  is the liquid holdup in the liquid film.

$$\left( \frac{dp}{dz} \right)_T = \left[ \rho_s g L_{LS} + \rho_L H_{LF} (V_{LLF} + V_T) (V_{LLF} + V_{LLS}) + \frac{2f}{D_H} \rho_s (V_{sg} + V_{sl})^2 L_{LS} \right] \frac{1}{L_{SU}} \quad (3.36)$$

where  $L_{LS}$  is liquid slug length,  $L_{SU}$  is unit slug length, and  $H_{LF}$  is the liquid holdup in the liquid film.

**Annular Flow:** The annular flow occurs at high superficial gas velocities where the continuous gas phase is moving as a core. The mathematical model is based on the equilibrium of fully developed flow. The phases are considered to be incompressible, and film with on both walls of uniform thickness. The flow equations are derived using the conservation of linear momentum and continuity accompanied by the equilibrium equations for the stability of gas and liquid interfaces. The conservation of linear momentum at casing wall liquid film is derived based on the pressure gradient, shear stresses at the walls and liquid film-gas core interface. The conservation of linear momentums at the walls can be given by Equations 3.37 and 3.38.

$$\left( \frac{dp}{dz} \right)_{CL} + \tau_{CW} \frac{S_{CW}}{A_{CL}} - \tau_{CI} \frac{S_{CI}}{A_{CL}} + \rho_l g = 0 \quad (3.37)$$

where  $(dp/dz)_{CL}$  represents the total pressure gradient for casing wall film,  $\Gamma_{CW}$  represents the shear stresses at casing wall,  $\Gamma_{CI}$  represents the shear stresses at casing film-gas core interface,  $S_{CW}$  is the wetted liquid perimeter on casing wall,  $S_{CI}$  is the wetted liquid perimeters on casing film-gas core interface, and  $A_{CL}$  is the area of the casing film.

$$\left( \frac{dp}{dz} \right)_{TL} + \tau_{TW} \frac{S_{TW}}{A_{TL}} - \tau_{TI} \frac{S_{TI}}{A_{TL}} + \rho_l g = 0 \quad (3.38)$$

where  $(dp/dz)_{TL}$  represents the total pressure gradient for tubing wall film,  $\Gamma_{TW}$  represents the shear stresses at tubing wall,  $\Gamma_{TI}$  represents the shear stresses at tubing film-gas core interface,  $S_{TW}$  is the wetted liquid perimeter on tubing wall,  $S_{TI}$  is the wetted liquid perimeters on tubing film-gas core interface, and  $A_{TL}$  is the area of the tubing film.

The conservation of linear momentums for the gas cores is expressed as:

$$\left(\frac{dp}{dz}\right)_{core} + \tau_{CI} \frac{S_{CI}}{A_{core}} + \tau_{TI} \frac{S_{TI}}{A_{core}} + \rho_{core} g = 0 \quad (3.39)$$

where  $(dp/dz)_{core}$  represents the total pressure gradient for gas core,  $\Gamma_{CI}$  represents the shear stresses at casing film-gas core interface,  $\Gamma_{TI}$  represents the shear stresses at tubing film-gas core interface,  $S_{CI}$  is the wetted liquid perimeters on casing film-gas core interface,  $S_{TI}$  is the wetted liquid perimeters on tubing film-gas core interface, and  $A_{core}$  is the area of the mixture core. Since the equilibrium exists at the liquid film and gas core interface, the pressure gradients will be equal. Thus:

$$\left(\frac{dp}{dz}\right)_{CL} = \left(\frac{dp}{dz}\right)_{TL} = \left(\frac{dp}{dz}\right)_{core} \quad (3.40)$$

Another conservation equation is based on the continuity of gas and liquid phase. The liquid phase continuity can be defined by Equation 3.41.

$$V_{SL} = V_{TL}H_{TL} + V_{CL}H_{CL} + Fe \quad (3.41)$$

where  $V_{SL}$  is the liquid superficial velocity,  $V_{TL}$  is tubing wall liquid film velocity,  $V_{CL}$  is casing wall liquid film velocity,  $H_{TL}$  is the in-situ liquid holdup in the tubing wall film,  $H_{CL}$  is the in-situ liquid holdup in the casing wall film, and  $Fe$  is the liquid entrainment fraction in the gas core of the annuli. The continuity for gas phase is given by:

$$V_{SG} = V_{core}(1 - H_{L\_total}) \quad (3.42)$$

where  $V_{SG}$  is the superficial gas velocity,  $V_{core}$  is in-situ gas core velocity, and  $H_{L\_total}$  is the liquid holdup in the annulus. The wall shear stresses are calculated using the Blasius expression:

$$\tau_w = f_w \rho \frac{V^2}{2} \quad (3.43)$$

where  $\tau_w$  represents the shear stresses at the wall,  $f_w$  is the fanning friction factor,  $V$  is the in-situ average phase velocity,  $\rho$  is the phase density at the wall. The shear stress at the interface is expressed similarly, except the velocity is replaced with in-situ velocity in the core, phase density is replaced with the density of the core, and fanning friction factor is determined according to the friction at the interface. In addition, the entrained liquid fraction in the gas core is given by (Wallis 1969):

$$Fe = 1 - \exp(-0.125(\phi - 1.5)) \quad (3.44)$$

where the dimensionless number  $\Phi$  is represented by the following equation.

$$\phi = 10^4 V_{SG} \frac{\mu_g}{\sigma} \left( \frac{\rho_g}{\rho_l} \right)^{0.5} \quad (3.45)$$

where  $\mu_g$  is the viscosity of the gas, Another closure parameter is the tubing and casing wall film thickness ratio, which is defined as:

$$T = \frac{\delta_T}{\delta_C} = \frac{\langle W_T' \rangle}{(2\pi - \langle W_T' \rangle)K} \quad (3.46)$$

where T is thickness ratio between casing and tubing liquid film, K is the casing-tubing diameter ratio,  $\langle WT' \rangle$  is the angle associated with the tubing wall and averaged over the whole annular cross-sectional area. Mathematically, it is expressed as:

$$\langle W_T' \rangle = \frac{1}{(1-K^2)} \left[ 2\text{Sin}^{-1}(K) + 2K\sqrt{1-K^2} - K^2\pi \right] \quad (3.47)$$

Combining the above equations, the following dimensionless relationships can be developed:

$$\tilde{V}_{CL}^{2-m} = \frac{\tilde{\delta}_c \left[ 1 - \tilde{\delta}_c(1-K) \right]}{X_M^2 \tilde{D}_{CL}^{-m}} \left\{ \begin{array}{l} \tilde{V}_{core}^2 \left[ 1 + 300 \tilde{\delta}_c(1-K) \right] \left[ 1 + 2 \tilde{\delta}_c(1-K) \right] \left( \frac{1}{G_1} + \frac{1}{G_2} \right) \\ \tilde{V}_{core}^2 \left[ 1 + 300 \tilde{\delta}_c T \left( \frac{1-K}{K} \right) \right] \left[ 1 + 2 \tilde{\delta}_c T \left( \frac{1-K}{K} \right) \right] \left( \frac{1}{G_3} \right) - 4Y_M \end{array} \right\} \quad (3.48)$$

$$\tilde{V}_{TL}^{2-m} = \frac{T \tilde{\delta}_c \left[ 1 + \tilde{\delta}_c \left( \frac{1-K}{K} \right) \right]}{X_M^2 \tilde{D}_{TL}^{-m}} \left\{ \begin{array}{l} \tilde{V}_{core}^2 \left[ 1 + 300 \tilde{\delta}_c T \left( \frac{1-K}{K} \right) \right] \left[ 1 + 2 \tilde{\delta}_c T \left( \frac{1-K}{K} \right) \right] \left( \frac{1}{G_3} + \frac{1}{G_4} \right) \\ + \tilde{V}_{core}^2 \left[ 1 + 300 \tilde{\delta}_c(1-K) \right] \left[ 1 + 2 \tilde{\delta}_c(1-K) \right] \left( \frac{1}{G_2} \right) - 4Y_M \end{array} \right\} \quad (3.49)$$

where  $X_M$  is the modified Martinelli parameter,  $Y_M$  is the dimensionless group parameter. The dimensionless groups are given as follows:

$$G_1 = \tilde{\delta}_c \left[ 1 - \tilde{\delta}_c(1-K) \right] \quad (3.50)$$

$$G_2 = \frac{1+K}{4} - \tilde{\delta}_c \left[ 1 - \tilde{\delta}_c(1-K) \right] - \tilde{\delta}_c TK \left[ 1 + \tilde{\delta}_c T \left( \frac{1-K}{K} \right) \right] \quad (3.51)$$

$$G_3 = \frac{1+K}{4K} - \frac{\tilde{\delta}_c}{K} \left[ 1 - \tilde{\delta}_c(1-K) \right] - \tilde{\delta}_c T \left[ 1 + \tilde{\delta}_c T \left( \frac{1-K}{K} \right) \right] \quad (3.52)$$

$$G_4 = \tilde{\delta}_c T \left[ 1 + \tilde{\delta}_c T \left( \frac{1-K}{K} \right) \right] \quad (3.53)$$

Model evaluation (Caetano et al. 1992b) for all flow patterns except the annular flow demonstrated discrepancy of less than 5 percent between predictions and measurements. The annular flow model performance was strongly dependent on the liquid entrained fraction. In addition, the liquid film thickness ratio is dependent on the scattering isotropy and independent of liquid droplet size. However, previous studies state that the rate of deposition is highly dependent on the liquid droplet size.

A study conducted by Aggour et al. (1996) on the field data concluded that the Beggs and Brill correlation has an overall minimum relative error for tubing size as well total liquid rate in the pipe flow. However, at the higher flow rate more than 20,000 B/D, Hasan and Kabir's model exhibits better accuracy. The findings are presented in **Figures 3.8** and **3.9**.

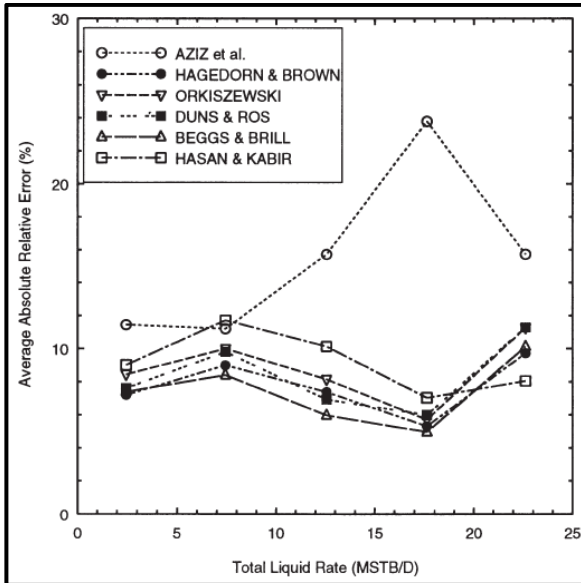


**Figure 3.8** Effect of rate of liquid on the accuracy of different flow correlations (Aggour et al., 1996)

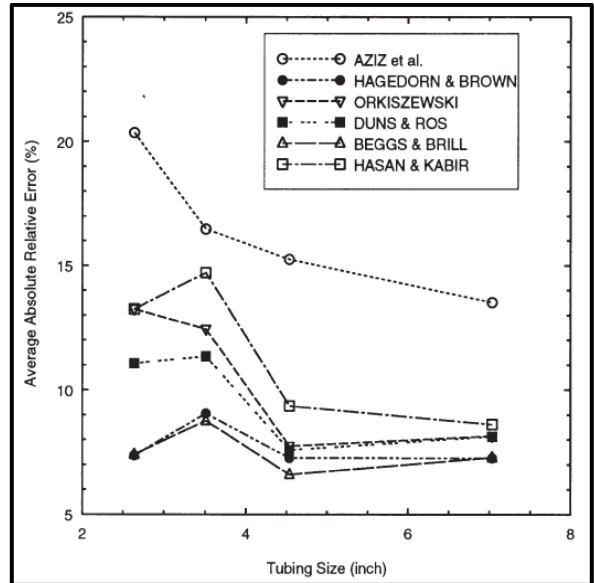


**Figure 3.9** Effect of tubing size on the accuracy of different flow correlations (Aggour et al., 1996)

Another model is developed by Lage and Time (2000) which is based on the assumption of the same thickness of the liquid film at casing and tubing wall. The model was evaluated and compared with measurements of Caetano et al. (1992a and b). The comparative study showed better performance as compared to other models.

### 3.3.4. Numerical Models

With the advancement of computational power, complex flow problems are nowadays tackled by the numerical approach. Two-phase flow, which is encountered in a wide range of industrial applications and natural situations can be analyzed using numerical models. For many years, because of their complexity, two-phase flows were predominantly investigated experimentally.

Although lots of facts were revealed through experimental investigation, its application is very limited due to the inherent constraints of experimental approaches such as equipment size, high pressure, high temperature and high flow rates. The main issue is upscaling of small-scale experimental results to real field case. New computational prowesses provide the flexibility to construct complicated models which can be easily adapted to different physical conditions without the actual construction of a large-scale prototype or expensive test rigs. A number of numerical techniques are presented in the literature including differential analysis, integral analysis, artificial neural network (Osman and Aggour, 2002; Selli and Selegim, 2007), and Computational Fluid Dynamics (CFD).

The CFD approach has become a more cost-effective tool for characterizing multiphase flows. CFD is a fluid mechanics approach developed for modeling fluid-flow problems involving complex flows in terms of flow geometry and/or fluid type. It is based on obtaining numerical solutions to the equations of motion, utilizing other required closure models. The Continuity equation under dynamic condition is expressed as:

$$\frac{\partial \rho}{\partial t} + \frac{\partial}{\partial x_i} (\rho u_i) = 0 \quad (3.54)$$

where  $\rho$  is density,  $u_i$  is the velocity in individual direction,  $x_i$  is the corresponding position vector, and  $t$  is the time. Another conservation principle used is the momentum balance, which is expressed in a generalized form as:

$$\frac{\partial}{\partial t} (\rho u_i) + \frac{\partial}{\partial x_j} (\rho u_i u_j) = -\frac{\partial P}{\partial x_i} + \frac{\partial}{\partial x_j} \left( \mu \frac{\partial u_i}{\partial x_j} - \overline{\rho u_i' u_j'} \right) + S_i \quad (3.55)$$

where  $\rho$  is density,  $u_i$  and  $u_j$  are the velocities in individual direction,  $x_i$  and  $x_j$  are the corresponding position vector,  $t$  is the time,  $P$  is the pressure,  $\mu$  is the viscosity, and  $S$  is the body force. The Conservation of energy for a flowing fluid is mathematically described in following form:

$$\frac{\partial (\rho T)}{\partial t} + \frac{\partial}{\partial x_i} (\rho u_i T) = \frac{\partial}{\partial x_i} \left( \frac{\lambda}{C_a} \text{grad} T \right) + S_T \quad (3.56)$$

where  $\rho$  is the density,  $u_i$  is the velocity vector,  $x_i$  is the corresponding position vector,  $t$  is the time,  $T$  is the temperature,  $\lambda$  is the viscosity, and  $S$  is the body force.

There are mainly two approaches in CFD simulation, Eulerian-Lagrangian, and Eulerian-Eulerian. In Eulerian-Lagrangian approach, discrete phase modeling is considered. The continuous phase is treated as a continuum, and the analysis is performed by tracking the dispersed phase such as particles, bubbles, or droplets. The dispersed phase exchanges momentum, mass, and energy with the continuous fluid phase. The main limitation of this

method is that it is unsuitable for modeling when the volume fraction of the dispersed phase is considerable.

In Eulerian-Eulerian method, the two phases are considered as interpenetrating continua. The method uses the concept of phase volume fraction and conservation principles are applied to each phase individually. The model is closed by empirical correlations or by applying the kinetic theory. The most suitable model for WCD modeling is Eulerian-Eulerian approach that has three types of models, Volume of fluid (VOF), mixture, and Eulerian models. In VOF model, two or more phases can be handled. Then, the equations of motion are solved applying the boundary conditions and the volume fraction of each of phase is tracked. It can be applied in the steady or transient tracking of any liquid-gas interface, the motion of large bubbles in the liquid. In mixture model, multiphase flow is considered as different phases moving with distinct velocities, but local equilibrium over short spatial length scales are assumed. Subsequently, the governing equations (conservation of mass, momentum, and energy) are applied for the mixture. In addition, volume fraction equations for the secondary phase, and algebraic closure expressions for the relative velocities are incorporated to obtain the solution.

In petroleum field, CFD has been used in limited multiphase flow cases. In other engineering disciplines however, the application of CFD in two-phase flow is well established over the past 20 years. Many experimental and analytical studies were performed to validate CFD simulations (Taha and Cui, 2006). A number of studies demonstrate the reliability of CFD modeling of gas-liquid flow. CFD modeling provided an accurate prediction of wellbore flow parameters in complex wells (Yuan and Bello 2014). The three-phase flow (oil/water/gas) characterization depends on several factors such as well geometry, fluid properties, flow patterns, pressure, and temperature. The CFD simulation results showed reasonable agreement with measured field data and predictions of the finite difference-based mechanistic model.

### **3.4. Current WCD Modeling**

The NTL No. 2015-N01 indicates that the WCD scenario should consider all hydrocarbon-bearing zones in each open-hole section as it is planned to be drilled. Accounting for changes in rock and fluid properties, multiphase flow pattern, saturation, operating pressure and temperature, and relative permeability with respect to a position over time is essential for accurate estimation of WCD (Hopper, 2015). Comprehensive modeling of such a dynamic and complex scenario cannot be decoded with conventional analytical models. With the advent of modern technology, the blowout tends to decrease. Nevertheless, unfortunate combinations of equipment failure and geological uncertainty, still regularly give rise to incidents that may lead to loss of wells, equipment, and even human life. To keep these risks to a minimum, a priori estimation of WCD through holistic modeling is necessary.

There are several models which have evolved over time to predict the discharge rate in case of blow-out or explosion. One of the earlier work was carried out by Das et al. (1993). The model incorporated fluid dynamics, heat transfer, and pollutant dispersion effect. It has the capability

to predict the quantity of spill, velocity, and the temperature at the outgoing jet, radiation intensity profile, and pollutant dispersion around the well. However, the effect of formation damage, sand migration, collapse, and coning are not included in the model. Similarly, a blowout simulator was developed by Oudeman et al. (1993) to conduct sensitivity analysis of input parameters such as reservoir properties and consequently define the suitable relief well design or well killing sequence. It includes the inflow and outflow performances calculations to determine the existence of multiphase sonic flow condition across the choke geometries in a blowout well. The earlier presumption regarding the blow-out rate calculation at the point of intersection of inflow performance curve with well intake pressure curve for ambient pressure was studied. It was concluded that the above presumption was true only for low to medium blow-out rate and in case of extreme blow-out rate, the outflow rate at sonic conditions across choke is more realistic. Pressure and temperature profiles are calculated simultaneously, using a modified form of Gray's correlations for wet gas and high GLR (Gas/liquid ratio) wells and, Dun and Ros correlation for low GLR wells. In addition to that, Joule-Thompson effect was considered to simulate the fluid properties. They observed that when the actual flow velocity approaches the sonic velocity, the total pressure drop tends to increase sharply resulting in an equilibrium flow rate (maximum flow rate).

Oudeman (2010) presented a validation for blowout rate simulator for subsea wells encompassing a comparison of calculated rate and estimates based on observable phenomena such as flame length and heat release rate. The nodal analysis method was applied for matching the inflow performance of the well to the vertical lift performance of the wellbore to estimate the blowout rate. It was observed that for onshore wells, the blowout rate is often controlled by the sonic outflow conditions because the pressure in the well exceeds atmospheric pressure by a factor of two or more. Another earlier study showed that the connection between high noise level around the well and erosion of wellhead components to the establishment of supersonic conditions at the surface (Oudeman et al., 1993). On the other hand, in offshore wells, there is hydrostatic pressure of water column at the mudline, which can be used for determining the flowing wellhead pressure of the blowing well. Hence, in offshore wells, the sonic condition is not likely to develop at the wellhead, and the total system performance is the critical factor.

Hasan et al. (1998) developed a combine wellbore-reservoir simulator to investigate the pressure-transient behavior of two-phase flow in deviated and vertical wellbores. The model analyzes wellbore flow numerically, and reservoir flows analytically. The convective and conductive heat transport mechanisms are considered in the formulation of the model. A transient model was used to simulate the flow conditions at the onset of the maximum discharge. The model uses a numerical method to solve the mass, momentum, and energy balance equations for the wellbore fluid and analytical models for fluid flow in the reservoir. Fluid properties are estimated using black-oil model and a mechanistic model (Hasan and Kabir 1992) was used to characterize the liquid holdup based on flow patterns. Another important consideration in this model was the tracking of gas bubble migration throughout the wellbore. Isentropic expansion was assumed to

compute the theoretical sonic velocity. According to the model, the flow rate increases with increasing well productivity, tube diameter, pressure in the reservoir, and the gas-oil ratio (GOR).

Blowout rate simulators have been useful tools to forecast and manage a blowout. In 1990, dynamic flow simulator OLGA (a Schlumberger proprietary software) was used in a blowout well control in the North Sea by Rygg and Gilhuus. The dynamic blowout rate, wellbore flowing temperature and dynamic wellbore pressure profiles were considered in their analysis. Liu et al. (2014) developed a simulator using wellbore flow and heat transfer model. The model formulation combines flow in the reservoir, wellbore, and their interaction. The model treats a blowout as a type of drawdown changing over time. Therefore, flow equations applied for drawdown test analysis are used by neglecting the superposition in time for blowout calculation. It was reported that the existence of sonic velocity rarely occurs for single-phase oil well blowout because of high hydrostatic pressure gradient, which does not allow such high velocity in the wellbore. Recently, the more advanced version of OLGA, a dynamic kill simulator was used to analyze worst-case blowout scenarios and evaluate the impacts of different operational parameters during the killing process (Yuan et al., 2015). Among several other available multiphase flow models implemented in simulators, the OLGA steady-state model (OLGAS, 2016), the LedaFlow Point model (Ledaflow, 2016), and the TUFFP Unified model are capable of analyzing two-phase gas-liquid flows for all inclination angles, pipe diameters, and fluid properties (Shippen and Bailey, 2012). OLGAS has the capability to analyze 300-1320 psia operating pressure, superficial gas velocity up to 43 ft/s, and liquid superficial velocity up to 13 ft/s. This simulator was validated using TILDA databased. LEDA-PM was also confirmed using additional experimental data to TILDA database. TUFF unified model is based on the rule of 10. According to the rule of the tomb, this simulator can be used in deviation angles in the range of +/- 10°, liquid holdup more than 10%, internal pipe diameter less than 10 in., and oil viscosities less than 10 cP. The comparison of the software is presented in **Table 3.5**. The Gemini simulator developed by Gemini Solutions predicts the WCD rate of oil and gas well blowouts. However, the basis of worst case discharge calculation in this software is based on nodal analysis and uses empirical correlations for the estimation of pressure drop in the system (Worst Case Discharge, 2016). The limitation of the empirical correlations is well known and discussed in details in Section 3.3.1.

**Table 3.5 Comparison of Industry software**

Features	TUFF	Leda-PM	OLGAS
Continuity	Three mass Equation	Nine Mass Equations	Five Mass Equations
Momentum	Three Equations: Gas pocket in slug Oil and water in film zone Oil and water in slug body	Three Equations: Gas bulk + liquid Droplets Oil bulk + gas bubble and water droplet Water bulk + gas bubble and water droplet	Three Equations: Gas-liquid Droplets Hydrocarbon Film Water Film
Viscosity Model	Brinkman	Continuous Phase	Pal and Rhodes
Flow Regimes	Stratified Intermittent Annular Bubbly Dispersed Bubble	Stratified smooth Stratified wavy Slug Annular Bubbly	Stratified smooth Stratified wavy Slug Annular Bubbly
Model type	Unified mechanistic	Transient mechanistic	Steady-state Mechanistic

## 4. Experimental Study

Experimental investigations are essential aspects of multiphase flow, which can provide insight into the flow characteristics. Besides this, experimental measurements can be used for model calibration and validation purposes. The problems with gas-liquid flows at high velocities and large pipe diameters have not been explored yet. Several experimental studies have been conducted in the past. However, the studies were limited to low velocity and small diameter pipes. Some of the experimental data and field measurements are presented in this section.

### 4.1 Field Case Study

Asheim (1986) formulated a new model (MONA) based on phase slippage to predict the two-phase flow characteristics. The developed model included the parametric description of holdup and well friction. The flow characteristic parameters were obtained by nonlinear minimization program for optimal data matching. The study used three field (forties, Ekofisk, and Prudhoe Bay field) data to evaluate the accuracy of the model. The well data is presented in **Table 4.1**. Out of 116 data points presented, only 4 datasets were vertical flow data (**Table 4.2**).

**Table 4.1 Well data used for modern validation (Asheim, 1986)**

Parameters	Data range
Inner diameter	2.764-15.312 in
Oil flow rate	720 - 143087 STB/D
Gas flow rate	738 - 110015 MMscf/D
Inlet pressure	586 - 6891 psig
Outlet pressure	136 - 4417 psig
Average temperature	119.5-260 °F
Oil specific gravity	0.647-0.884
Gas specific gravity	0.667-1.122
Flow length	6899-14762 ft
Average inclination	0° - 90.221°

**Table 4.2 Field data for multiphase flow (After Asheim, 1986)**

Field	ID (in.)	Q <sub>o</sub> (STB/D)	Q <sub>g</sub> (MMscf/D)	P <sub>i</sub> (psig)	P <sub>o</sub> (psig)	T <sub>avg</sub> (°F)	S <sub>o</sub>	S <sub>g</sub>	L <sub>f</sub> (ft)
Forties	6.184	12,300	4143	2,477	388	188.5	0.842	1.122	7,133
Ekofisk	3.958	16,080	20,690	4,267	1,275	238.5	0.772	0.700	10,049
Ekofisk	2.764	10,872	12,140	6,695	1,620	227	0.778	0.700	10,039
Ekofisk	3.826	15,696	23,130	6,502	3,300	215	0.773	0.700	9,746

where ID is the inner diameter (in.),  $Q_0$  is the oil flow rate (STB/D),  $Q_g$  is gas flow rate (MMscf/D),  $P_i$  is inlet pressure (psig),  $P_o$  is the outlet pressure (psig),  $T_{avg}$  is the average temperature ( $^{\circ}$ F),  $S_o$  is the oil specific gravity,  $S_g$  is the gas specific gravity, and  $L_f$  is the flow length (ft).

#### 4.2 Two-phase flow in large pipe diameter (ID > 6 in)

Shen et al. (2010) conducted an experimental study on two-phase flow in vertical large diameter pipe. The study aimed to investigate distribution parameter and drift velocity for two-phase flow. The experimental flow loop has a test section with a dimension of 199.89 mm (7.87 in) ID and 24.99 m (82 ft) length (**Figure 4.1**). The superficial velocities of gas and liquid phase were varied in the range of 0.0016 - 0.093 m/s and 0.0501 - 0.311 m/s, respectively, which is considered very low velocity. The measured test parameters include void fraction, gas and liquid velocity, and pressure drop. New localized measurement methods such as hot-film probe and optical multi-sensor techniques were applied to measure two-phase flow characteristics. The experimental results are compared to various existing correlations. Under the test conditions, three dominant flow patterns were observed including bubbly flow, churn flow and slug flow (**Figure 4.2**). The flow patterns were dependent on the gas and liquid superficial velocities and they developed at various locations of the test section. For instance, the bubbly flow was observed at a low superficial gas velocity or high superficial liquid velocity, and mostly established in the main flow direction.

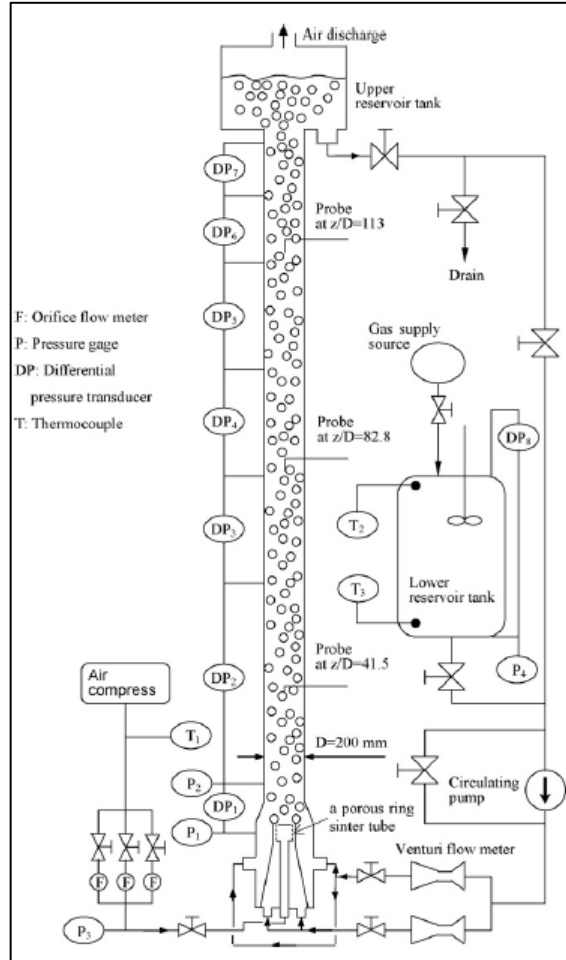


**Figure 4.1 Schematic of the experimental flow loop (Shen et al. 2010)**

The churn flow pattern established at low liquid and high gas superficial velocities. At the entrance of the test section, the flow was developing. The churn flow was distinguished by the existence of large deformed bubbles disturbing the flow and producing strong localized turbulence and secondary flows. For slug flow developed at the end of the test section and characterized by the occurrence of large coalescent cap bubbles. Relatively high superficial gas velocity is required to develop slug pattern in two-phase vertical pipe flow.

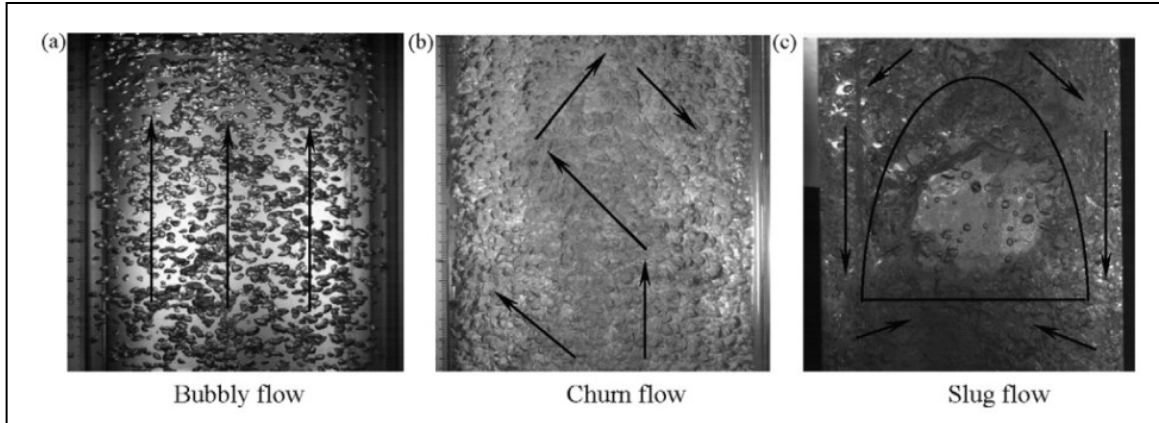


**Figure 4.2 Dominant flow regimes: (a) bubbly flow, (b) churn flow, and (c) slug flow (Shen et al. 2010)**

In the earlier study of Shen et al. (2005), the characteristics and phase distribution patterns of two-phase flow in a vertical large pipe were investigated using the same test setup. The air-water flow tests were carried out varying gas and liquid superficial velocities. The test measurements were void fraction and pressure drop. Based on their experimental observations, phase distribution patterns are classified into two categories: wall peak and core peak. In addition, pressure drop considerably decreased with the superficial gas velocity due to reduction in the void fraction and increased with superficial liquid velocity.

Another large-scale two-phase flow experiment was performed by Schoppa et al. (2013). The experimental setup (**Figure 4.3**) consisted of vertical pipe having a length of 12.19 m (40 ft) and the inner diameter of 279.4 mm (11 in). Structural supports were provided for both the flow line and riser. The wall thickness was chosen as to provide maximum operating pressure of 40 psig. Water was pumped into flow line from large storage tank using a centrifugal pump and metered with turbine flow meter. Air was used as the gas phase and supplied through compressed air flow system and measured using four different sized orifice plates. Both air and water entered through a pipe tee. Water flow rate was limited to 200 gpm and air flow to 1200 scf/min at 100 psi. The exit of the vertical pipe was connected to a gas-liquid separator, which had a large volume and exposed to atmospheric conditions. Various differential pressure transducers and thermocouples were installed at different locations to track the pressure and temperature. The test was comprised of two operational phases. In the first operational phase, when the gas entered at different flow rates, different flow characteristics were observed. **Figures 4.4, 4.5, and 4.6** show the flow data generated in the experiment.

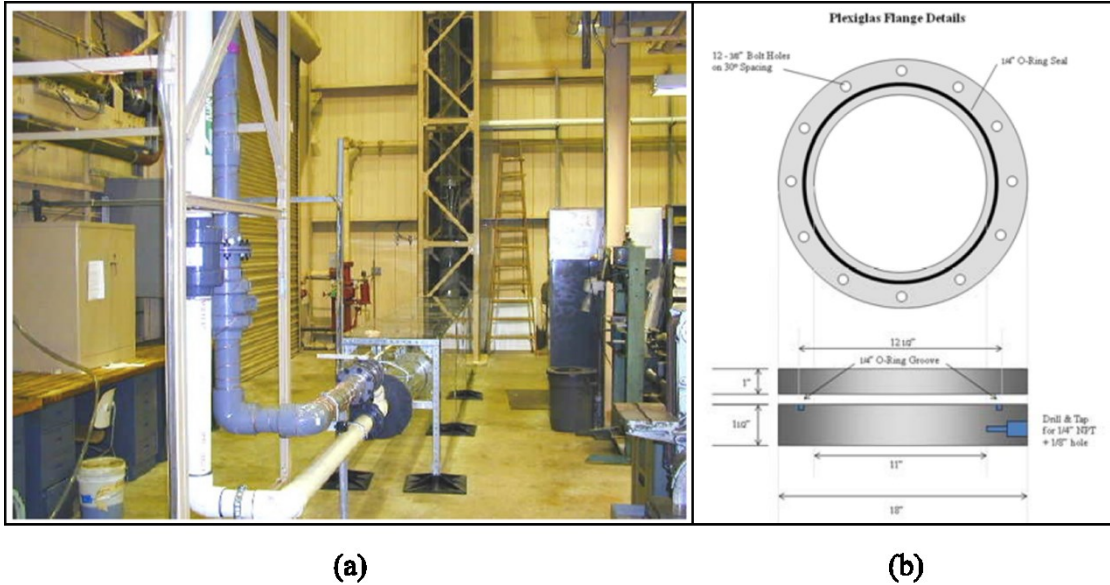


Figure 4.3 Test setup: (a) gas-liquid flow loop; and (b) plexiglas pipe configuration (Schoppa et al., 2013)

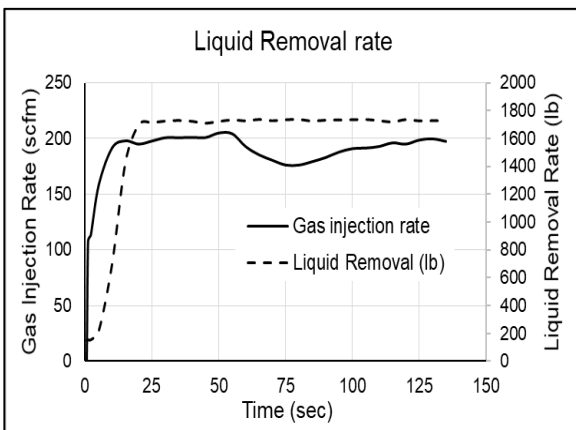


Figure 4.4 Liquid removal rate with rate of gas injection (After Schoppa et al., 2013)

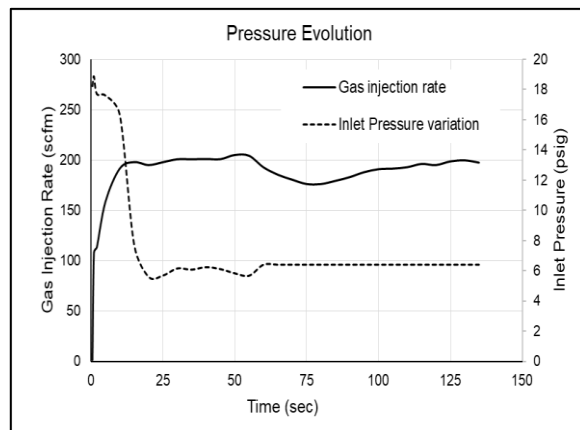


Figure 4.5 Pressure variation and gas injection rate with time (After Schoppa et al., 2013)

More recently, Louisiana State University (LSU) research group (Waltrich et al. 2015) conducted an extensive experimental study to investigate two-phase flow behavior in large pipes. A large-scale experimental setup (**Figure 4.7**) consisted of: i) vertical-clear PVC pipe segments of four different diameters (2, 4, 8 and 12 in), ii) water injection system; iii) air supply system; and iv) gas and liquid phase flowmeters were used. Experimental measurements were obtained over a wide range of water flow rates (6.26 to 795 gpm), and air flow rates (4.17 to 1666 scf/min). To carry out the experiments, three centrifugal pumps with different flow capacities (60, 300 and 600 gpm) were used. To attain desired air flow rate, two air compressors were employed. Test measurements were flow pattern, liquid holdup, and pressure gradient.

After analyzing test measurement, the experimental data obtained from the 2 in test section was found inconsistent with previous measurements under similar test conditions. Therefore, the data were eliminated and replaced by another data reported by Waltrich et al. (2013). Visual observations and high-speed camera images revealed different flow patterns including bubbly, slug, churn, and annular flows during the experiment. Based on the criteria for each flow regime, combined with two-phase flow data reported in previous studies (Ohnuki and Akimoto 1996, Ohnuki and Akimoto 2000, Ali 2009), a new flow regime/pattern map (Figure 4.8) for large-diameter pipes (4 – 12 in) has been developed. This flow pattern map defines two major transition zones: bubbly to non-bubbly transition zone (gray-shaded) and churn to annular transition zone (orange-shaded).

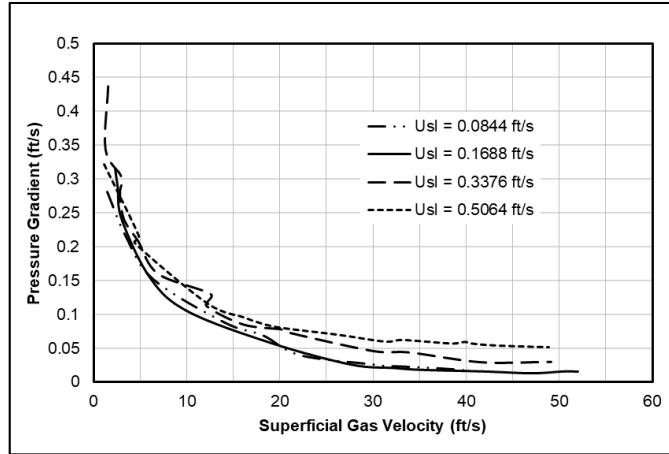


Figure 4.6 Variation of pressure gradient with superficial gas velocity (After Schoppa et al., 2013)

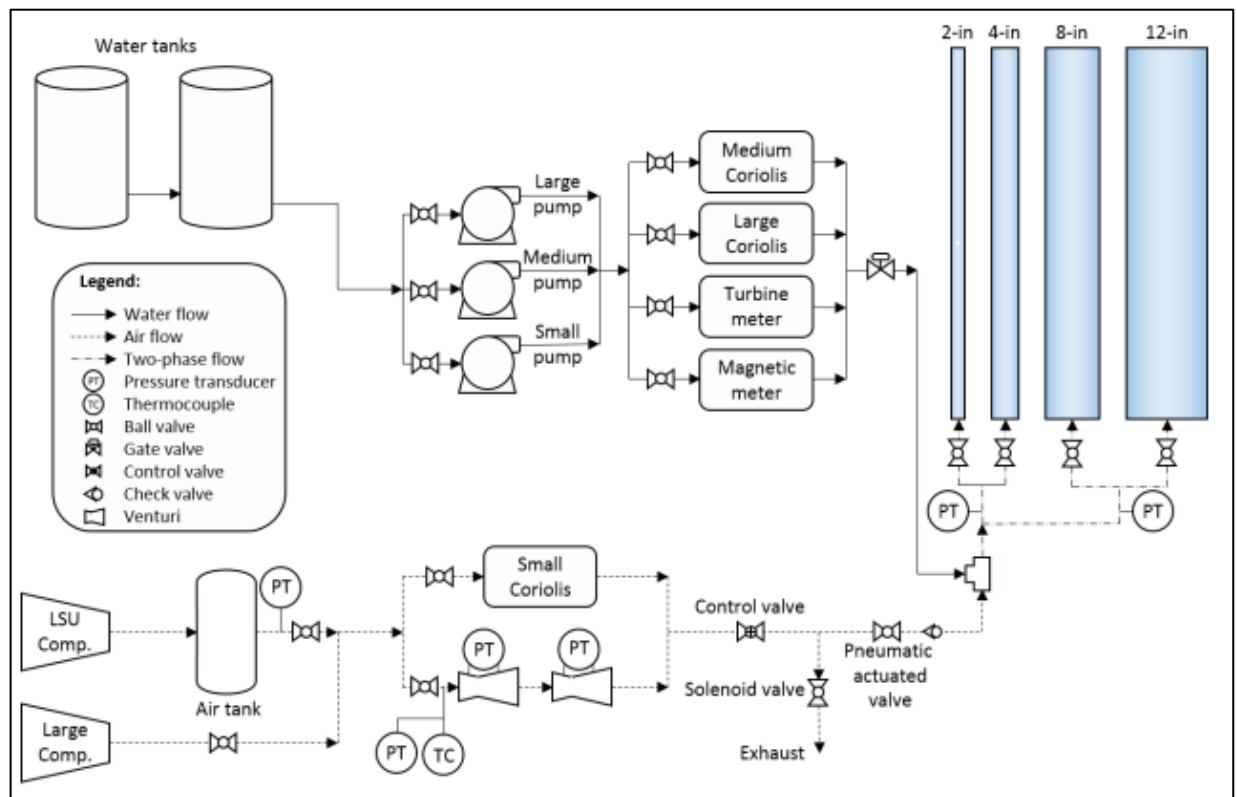


Figure 4.7 Schematic diagram of test setup ((Waltrich et al. 2015, LSU report)

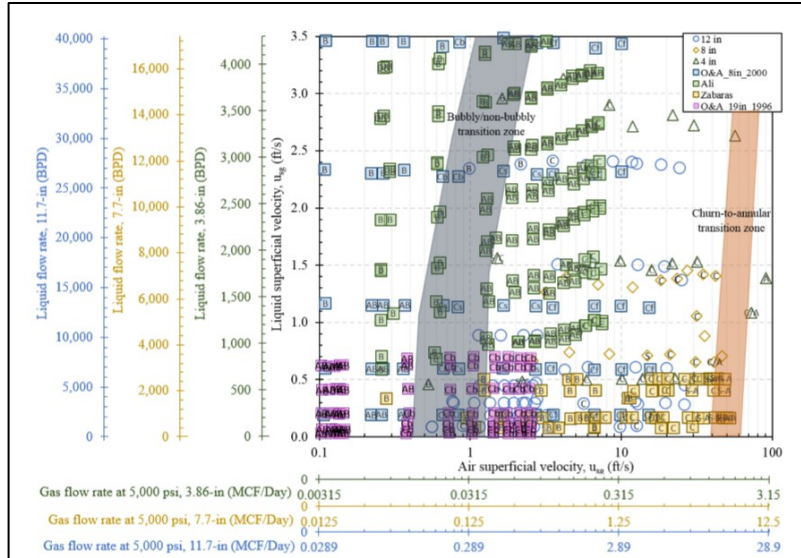
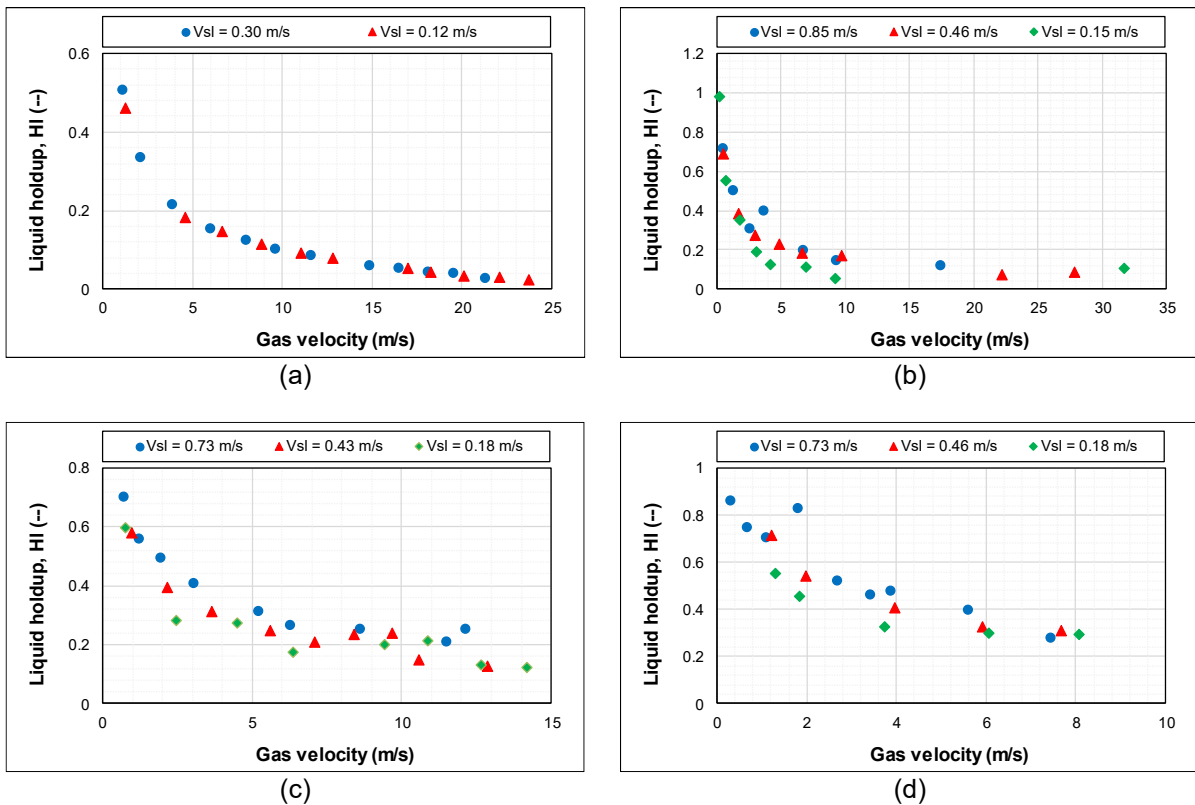


Figure 4.8 Flow regime map for large ID pipes (Waltrich et al. 2015, LSU report)

The volume of water accumulated in the test section (liquid holdup) was calculated from the pressure measurement at the bottom of the test section. In another word, the liquid holdup is defined by the ratio between volume collected water in test section after stopping the flow of gas and water and the total volume of the test section. The liquid holdup measurements for different pipe diameters and superficial liquid velocities are presented in **Figure 4.9**. As expected, the liquid hold up decreased dramatically with gas velocity, regardless of pipe diameter. It can also be inferred that the accumulated amount of water in the test section increased with the diameter. At low pipe diameters (below 4 in), results revealed that liquid holdup was insensitive to the change in liquid velocity, particularly data obtained from the 2 in pipe (**Figure 4.9a**). However, in the large pipe diameter (above 4 in), noticeable increase in the liquid holdup measurement was observed with significant variation in liquid velocity (**Figures 4.9b** and **4.9c**). It is worthy to note that liquid holdup trend for 4 in pipe was different from that of large diameter pipes (8 and 12 in) due to the occurrence of slug flow in 4 in pipe.



**Figure 4.9 Measured liquid holdup versus gas velocity at various liquid velocities and pipe sizes: a) 2 in; b) 4 in; c) 8 in; and d) 12 in (Waltrich et al. 2015, LSU report; Waltrich et al. 2013)**

In the LSU study, pressure gradient measurements for different pipe diameters were also reported (**Figure 4.10**). The measurements demonstrated a trend similar to that of the liquid holdup in which the pressure gradient significantly declined with the gas velocity. This trend indicates that the total pressure gradient was more dominated by the gravitational gradient rather than frictional gradient (Shoham, 2005). For 4-in pipe, the total pressure gradient versus gas velocity curve shows trend reversal at relatively high gas and liquid velocities (Figure 4.10b). The trend reversal implies that the frictional pressure gradient becomes a significant element of the total pressure gradient. In addition, these measurements suggest that the flow pattern was most likely annular. For small pipe diameter (2 in), pressure gradient slightly increased with liquid velocity (Figure 4.10a). For large diameter pipes (larger than 4 in), the pressure gradient was not significantly affected by the change in pipe diameter for all levels of superficial liquid velocity tested, especially for 8 and 12 in pipes. One possible explanation could be pressure gradient is more sensitive to superficial gas velocity. For large-diameter pipes, it is expected that the friction against the pipe wall is negligible compared to the interfacial friction.

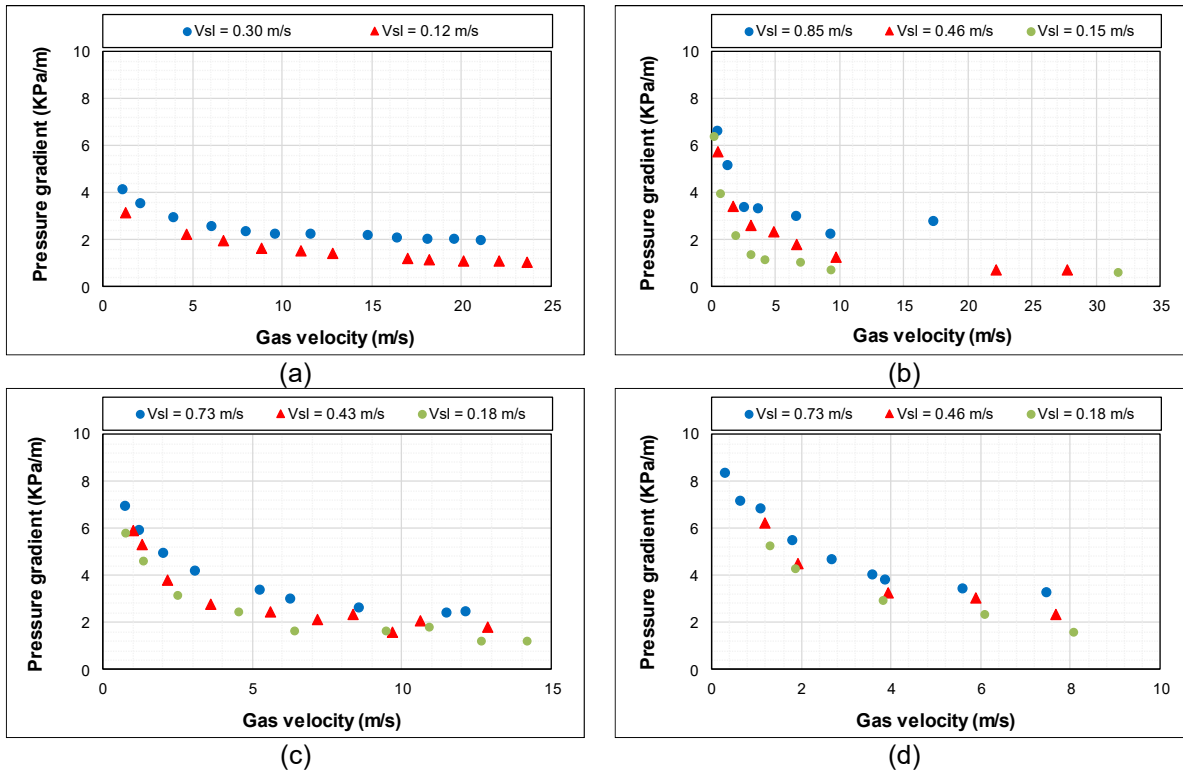


**Figure 4.10 Measured pressure gradient vs. gas velocity at various liquid velocities and pipe sizes: a) 2 in; b) 4 in; c) 8 in; and d) 12 in (Waltrich et al. 2015, LSU report; Waltrich et al. 2013)**

To assess the LSU data, the measurements reported are compared with the data available in the literature (not reported in the LSU study) under similar test conditions. The measured pressure gradient data is compared with test results reported by Biria (2013) and Perez (2008). Biria (2013) also obtained data using a 50 mm (2 in) pipe test section and varying superficial liquid velocity (0.12 – 0.72 m/s) and superficial gas velocity (0.33 – 13.25 m/s). In Perez (2008) study, the two-phase flow experiments were conducted using 38 and 67 mm pipes. The gas and liquid velocities were in the range of 0.15 – 8.9 m/s and 0.04 – 0.7 m/s, respectively. Detailed reviews of these studies are provided in Section 4.3. To compare the results, the data from these studies and LSU report are digitized and re-plotted together (**Figure 4.11**). Generally, the LSU measurements showed similar pressure gradient trend with respect to gas and liquid velocities when compared with the data from these studies (Biria 2013; Perez 2008). The findings of LSU report showed a considerable decline in pressure gradient with superficial gas velocity and slight increase with superficial liquid velocity. Under similar test conditions (ID = 50.8 mm,  $V_{sg} = 0.33 - 13.25$  m/s, and  $V_{sl} = 0.12 - 0.30$  m/s), the comparison shows good agreement between LSU data and measurement reported by Biria (2013). Furthermore, LSU pressure gradient measurements agree with the results reported by Perez (2008) for different pipe diameters. The change in pipe diameter has a negligible impact on pressure gradient, particularly at low liquid velocities. Similarly, the liquid holdup data is compared (**Figure 4.12**) with measurements reported by Perez (2008). Overall, LSU data showed the expected liquid holdup trend with respect to superficial gas velocity. This finding suggests that the LSU data is consistent with the existing data at relatively low superficial gas velocities. Additionally, in small diameter pipe (less than 50.8 mm

or 2 in), there is a consensus that increasing superficial liquid velocity has a minor impact on the liquid holdup. This comparison ensures the accuracy and reliability of the LSU data. The LSU data is combined with other data (**Figure 5.7**) to assess two-phase flow characteristics at high superficial gas velocities.

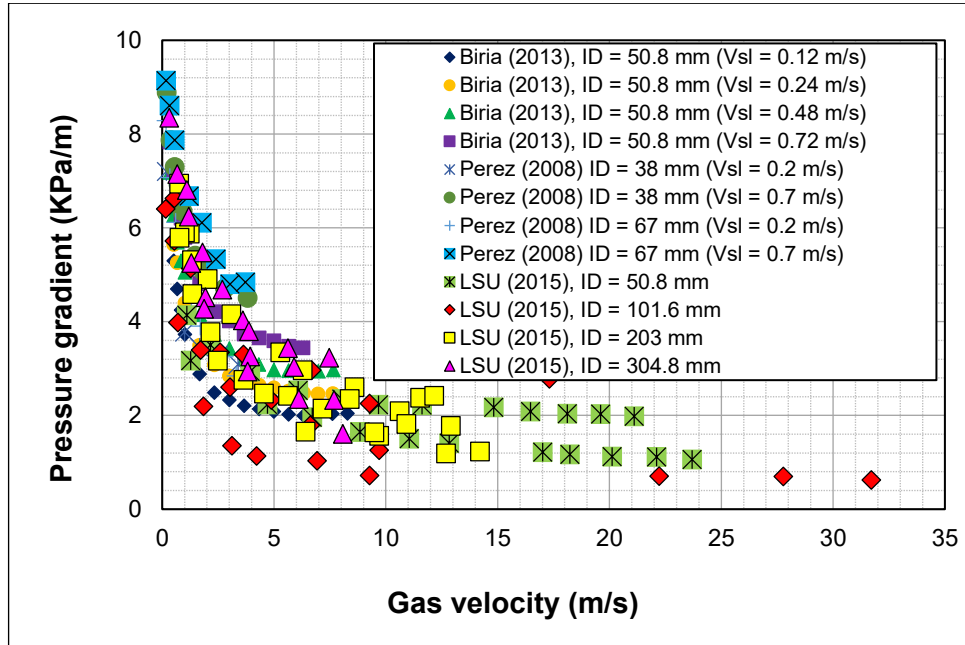


Figure 4.11 Comparison of pressure gradient data from previous studies and LSU report (Waltrich et al. 2015)

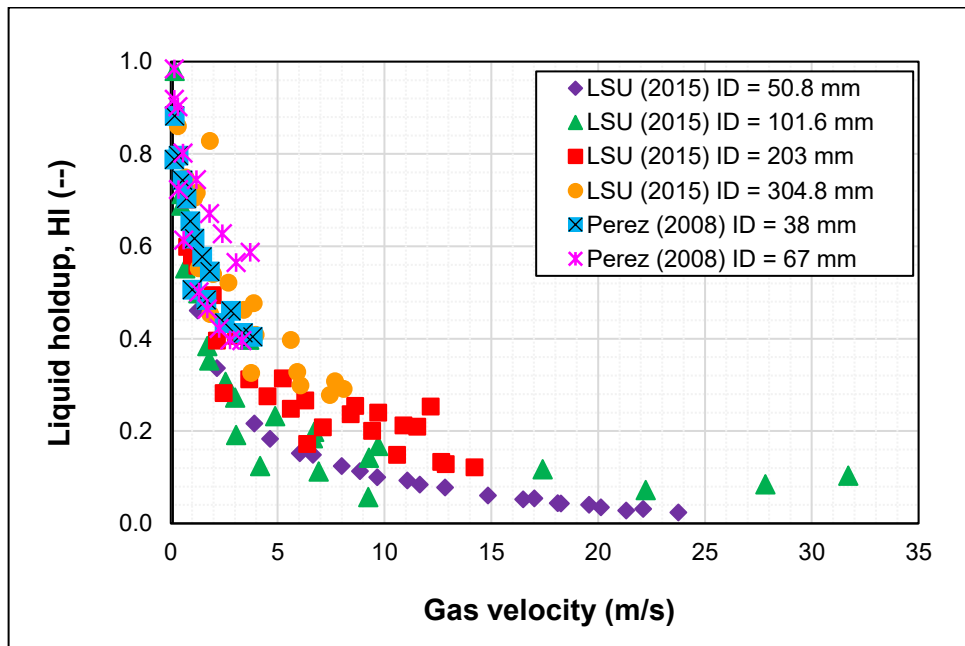


Figure 4.12 Comparison of liquid holdup data from previous studies and LSU report (Waltrich et al. 2015)

### 4.3 Two-phase flow in small pipe diameter (ID < 6 in)

An experimental investigation (Zangana et al. 2010) was conducted using large diameter vertical pipes to study the impact of gas and liquid velocities on frictional pressure loss. A large-scale flow loop with a test section of 127 mm diameter and 10.97 m long was used. A schematic of the loop is presented in **Figure 4.13**. Six hundred set of experiments were carried while measuring the total pressure drop and liquid holdup for wide range of superficial liquid (0.01 to 0.7 m/s) and gas (3 to 16.25 m/s) velocities. By applying steady momentum equation for vertical upward annulus and accounting for the liquid holdup (Sawai et al. 2004), the frictional pressure drop is calculated from total pressure drop as:

$$-\left(\frac{dp}{dx}\right)_t = F_{wl} + [(1-\beta^*)\rho_g + \beta^*\rho_l] \cdot g \quad (4.1)$$

where  $\left(\frac{dp}{dx}\right)_t$  is total pressure drop,  $F_{wl}$  is the frictional pressure drop,  $\beta^*$  is the liquid holdup,  $g$  is gravitational acceleration,  $\rho_g$  and  $\rho_l$  are density of gas and liquid, respectively.

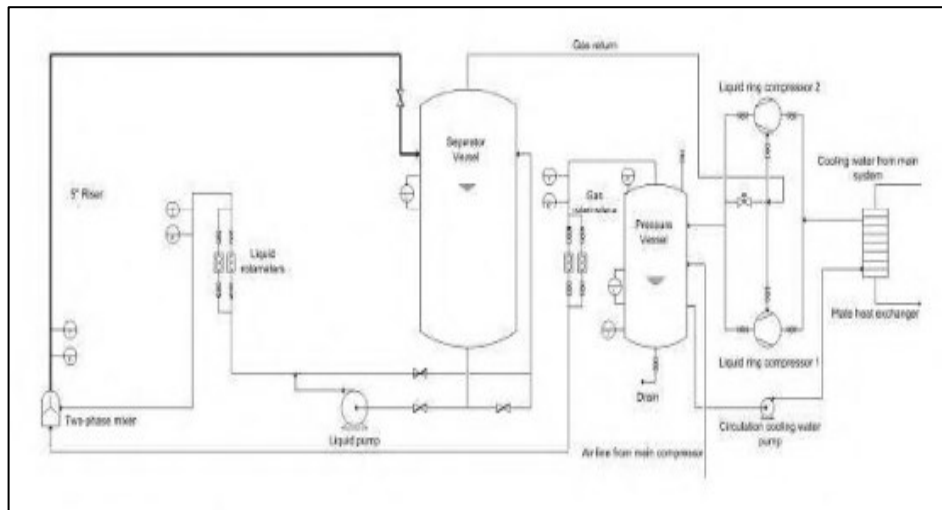


**Figure 4.13 Large-scale closed flow loop (Zangana et al. 2010)**

The measured and calculated total frictional pressure drops are presented in **Figure 4.14** as a function of superficial gas velocity for various superficial liquid velocities. Three main flow regimes are identified considering superficial gas and liquid velocity changes. The first regime which occurs at low superficial liquid velocity range (0.014 – 0.04 m/s), the total pressure declined significantly with the superficial gas velocity. Afterward, a gradual decline in pressure drop was observed with further increase in superficial gas velocity. In the second regime, the frictional pressure drop and total pressure drop exhibited similar behavior at different superficial gas velocity. Smooth trends of frictional and total pressure drops were observed when the superficial liquid velocity was in the range of 0.05 – 0.06 m/s. In the third regime, with increasing superficial liquid velocity (from 0.07 to 0.7 m/s), both frictional and total pressure increased. In

general, the study concluded that the frictional pressure drop is significantly affected by superficial liquid velocity. Recently, the same test setup was used by Damir (2012) to investigate two-phase flow characteristic in large diameter pipes. A total of 81 experiments were carried out measuring void fraction, pressure drop, and flow rates. During the experiments, superficial gas and liquid velocities were ranging from 3 – 16 m/s and 0.0165 – 0.51 m/s, respectively. Experiments were performed at different pressures 0.1 and 2 bar (0, 14.5, and 29 psi). Predominantly, annular and churn flow pattern were observed during the test. The void fraction increased with superficial gas velocity and decreased with superficial liquid velocity. In addition, results showed a continual reduction in liquid film thickness with superficial gas velocity.

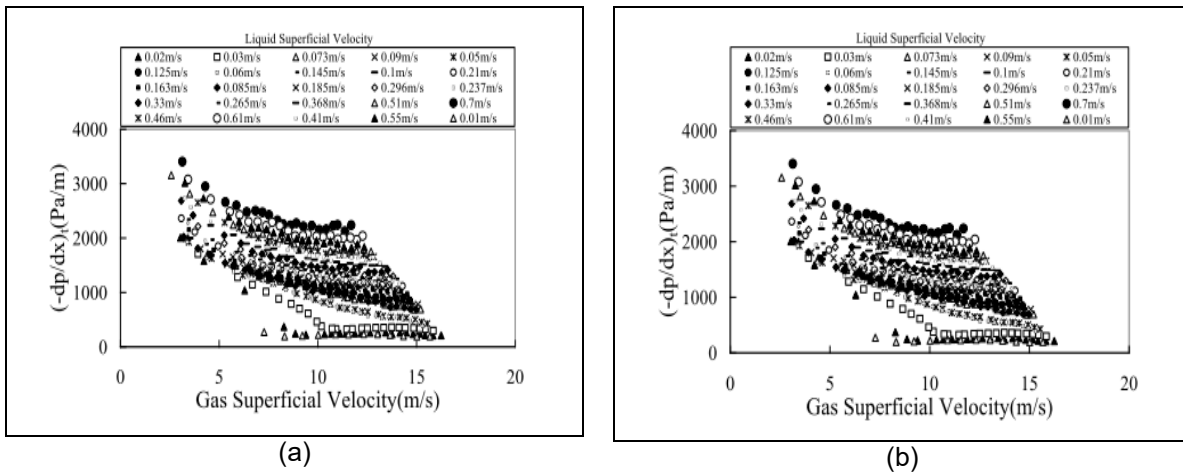


**Figure 4.14 Pressure drop versus gas superficial velocity: a) total pressure drop, and b) frictional pressure drop (Zangana et al., 2010)**

Tang et al. (2013) carried out an extensive experimental study to investigate the effect of void fraction and superficial gas velocity on pressure drop in upward vertical pipe flow. The experimental setup consisted of a test section that has 157.4 cm long flow visualization part and 220.1 cm long void fraction measurement section. The test section (**Figure 4.15**) has 1.27 cm inner diameter (0.5 in). **Figure 4.16** shows the schematic of the experimental setup, which was equipped with facilities for measuring void fraction, pressure drop and flow visualization to identify flow patterns.

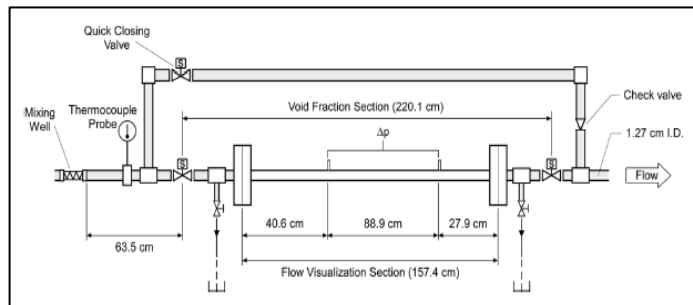


**Figure 4.15 Schematic of test section (Tang et al. 2013)**

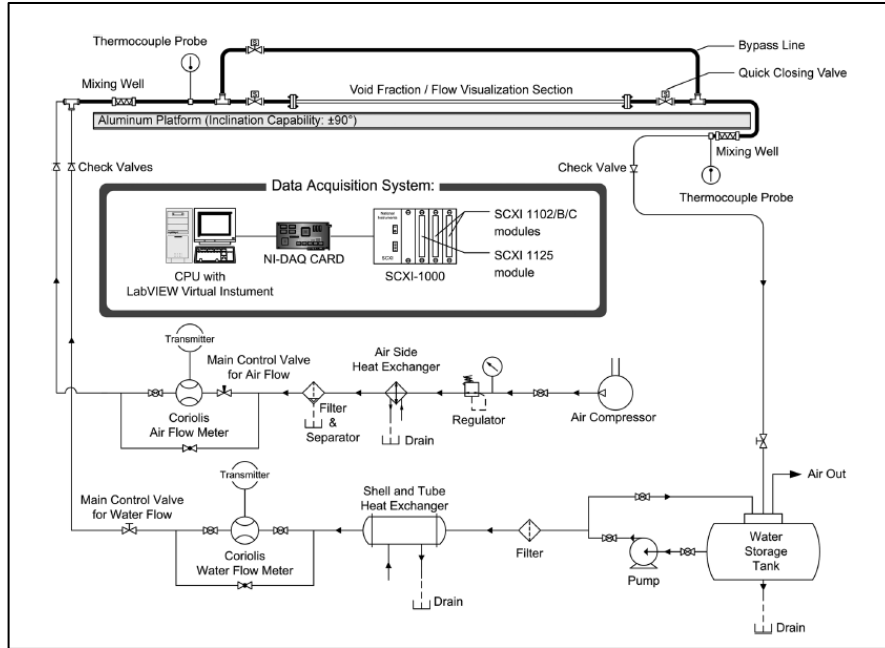


Figure 4.16 Schematic of experimental setup (Tang et al. 2013)

As presented in Figure 4.17, bubbly and slug flow patterns were established at low superficial gas velocities. The bubbly and slug flow patterns were observed with void fraction range of  $0.05 < \alpha < 0.5$  and  $0.2 < \alpha < 0.7$ , respectively. In the mid-range of the superficial gas velocities and void fraction range of  $0.3 < \alpha < 0.8$ , churn and froth flow patterns were established. Churn flow has a higher void fraction than froth flow at a specific superficial gas velocity. In high superficial gas velocity region and void fraction range of  $0.7 < \alpha < 0.9$ , experimental results showed annular flow pattern.

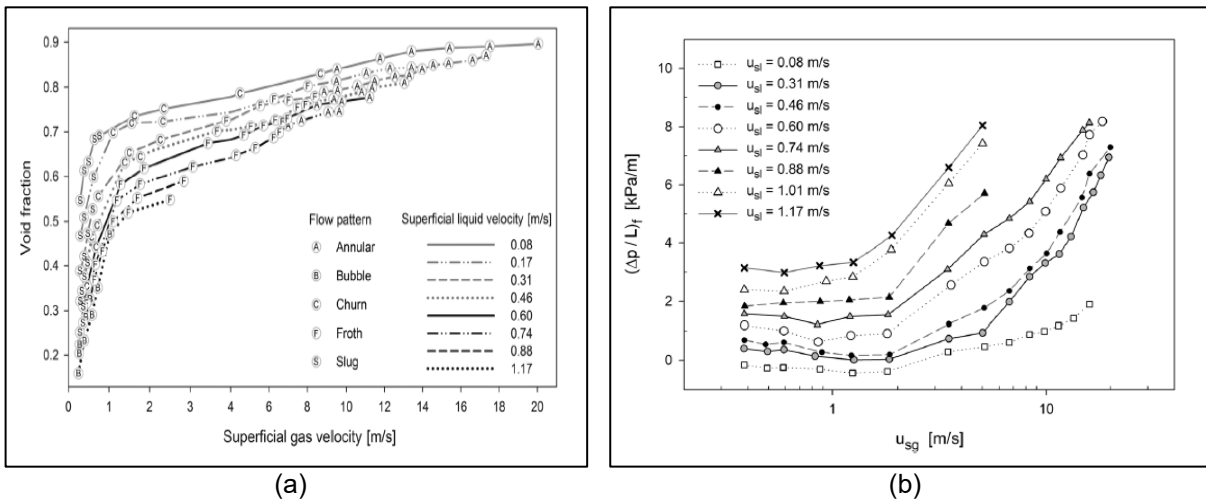
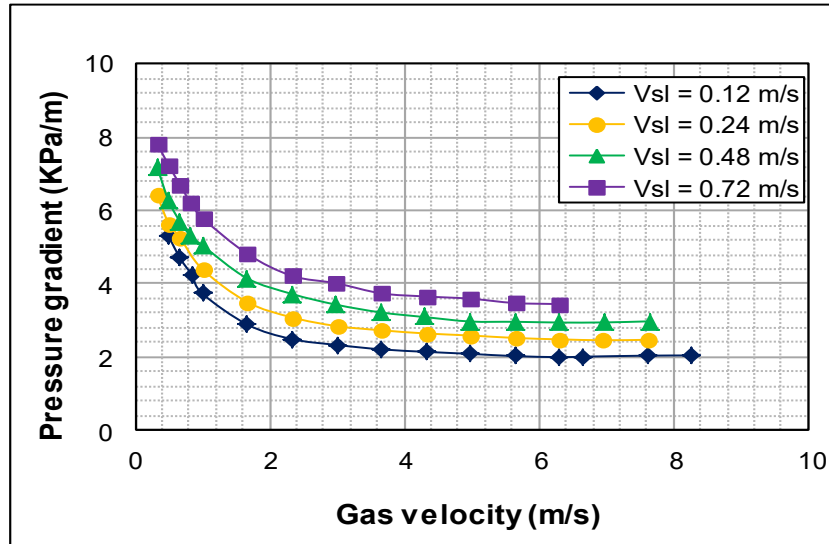


Figure 4.17 Variation of the test parameter measurements with superficial gas velocity for upward vertical two-phase flow: a) void fraction and b) friction pressure gradient (Tang et al. 2013)

According to the test results (Figure 4.17b), the frictional pressure loss is highly dependent on liquid and gas velocities. In general, the pressure loss increased with the superficial liquid velocity. At low superficial gas velocities (0.35 – 1.3 m/s), the results exhibited a flat linear relationship between the frictional pressure drop and superficial gas velocity. A significant change in the pressure loss was observed at high superficial gas velocities (above 1.3 m/s) in which the pressure drop rapidly increased with gas velocity. It was indicated that at a high gas mass fraction, the two-phase frictional pressure loss is highly sensitive to void fraction.

The measurements are also compared with other reported data (Biria 2013) obtained with relatively larger pipe diameter test sections. Biria (2013) used a flow loop consisted of a 10 m (32.8 ft) test section with 50.8 mm (2.0 in) inner diameter. Test flow rates were in the range of 0.12 - 0.72 m/s for the superficial liquid velocity and 0.33 - 13.25 m/s for the superficial gas velocity. **Figure 4.18** presents the measured total pressure gradient drop versus superficial gas velocity at various superficial liquid velocities.



**Figure 4.18** Total pressure drop vs. gas superficial velocity at various  $V_{SL}$  (Biria, 2013)

Results (Figure 4.18) are consistent with the previous findings (Tang et al. 2013; Zangana et al. 2010; Shen et al. 2005). The total pressure drop increased with superficial liquid velocity regardless of the superficial gas velocity. Total pressure gradient behavior of air-water vertical pipe flow can be classified into two flow regimes depending on superficial gas velocity. At relatively low superficial gas velocity (less than 4 m/s), a sharp decline in pressure gradient was observed with superficial gas velocity. This reduction is attributed to the decline in the hydrostatic head which is the most dominant part of the total pressure drop. Afterward, total pressure gradient remains steady with further increase in superficial gas velocity. Similar total pressure gradient versus superficial gas velocity curves were generated for various liquid superficial velocities. Measured pressure drop was compared with predictions of six different models (Hagedorn and Brown 1965, Duns and Ros 1963, Orkiszewski 1967, Aziz et al. 1972,

Mukherjee and Brill 1985, and Hasan and Kabir 1990). A reasonable agreement between model predictions and experimental data was observed. Mostly the Hasan and Kabir (1990) model exhibited the best predictions. A detail of the model comparison is provided in the original document (Biria, 2013).

The two-phase vertical flow was experimentally investigated by Zubir and Zainon (2011) using three different pipe sizes. Test measurements included void fraction using Constant Electric Current method (CECM) and flow pattern recognition using a high-speed video camera. **Figure 4.19** shows schematic of the flow test setup. Three 9.84-ft long pipe sections with different inner diameters (0.83, 1.85 and 3.74 in) were used. The test sections were divided into four equal segments of length 2.46 ft.

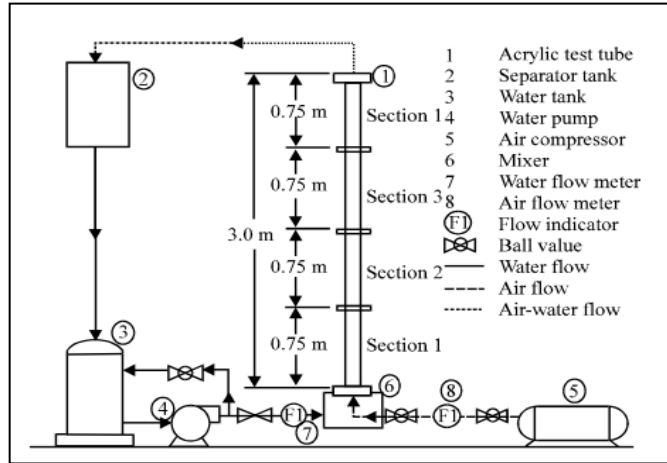


**Figure 4.19 Schematic of two-phase flow setup (Zubir and Zainon 2011)**

During the test, superficial gas velocity was ranging from 0.1 to 2 m/s. Various flow patterns including bubbly-slug, slug, and churn flow were observed in different pipes (**Figure 4.20**). At a fixed liquid superficial velocity, the flow pattern changed with superficial gas velocity. The bubbly-slug flow pattern appeared in short range of the test section at low gas superficial velocities. As gas velocity increased, slug flow formed due to the coalescing of the bubbles. The slug length was influenced by the pipe diameter. For instance, the maximum length of slug formed in the 1.85 in pipe was much shorter than the one formed in the 0.83 in pipe. Due to the easy breakdown of the liquid film, it was challenging to develop slug flow pattern inside 3.74 in pipe, which eventually resulted in the formation of churn flow. The slug flow occurred commonly in the third and the fourth sections after the coalescing of the bubbles in the first and the second sections.

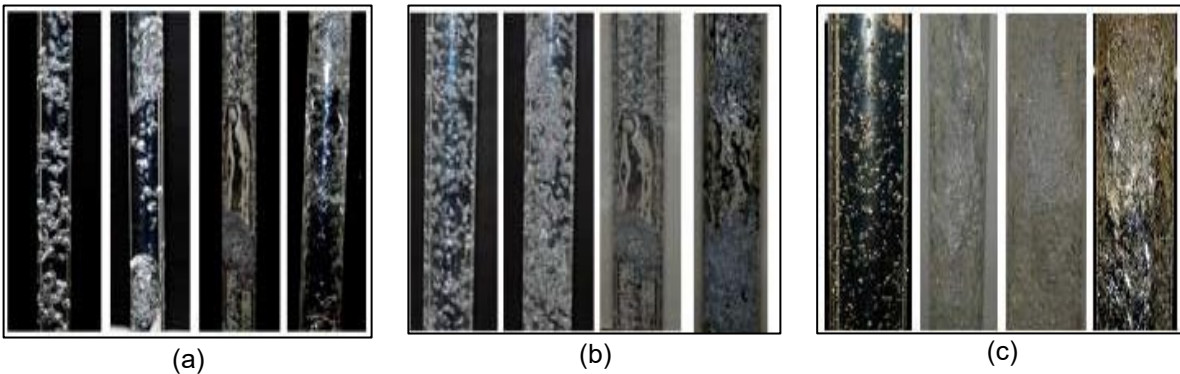


**Figure 4.20 Flow pattern inside a) 0.83 in; b) 1.85 in; and c) 3.74 in pipe (Zubir and Zainon 2011)**

Based on the experimental observations, a flow map was developed for each pipe size. Each flow map displays the transition of flow pattern including bubbly, bubbly-slug, and slug-churn. In addition, the effect of gas and liquid superficial velocities on the void fraction was investigated. The void fraction consistently increased with superficial gas velocity and decreased with superficial liquid velocity. The measurement of void fraction using CECM was compared with results from the Bestion drift- flux model. A fair agreement between model predictions and measurement was observed (**Figure 4.21**).

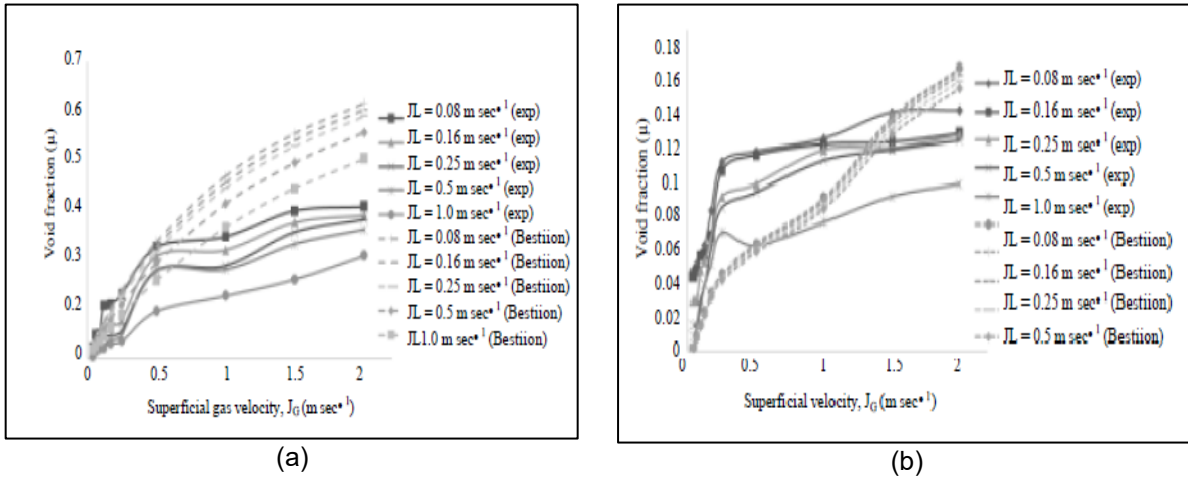


**Figure 4.21** Comparison measured void fraction and prediction by Bestion correlation at various gas and liquid superficial velocities for different pipes: a) 0.83 in and b) 3.74 in (Zubir and Zainon 2011)

An extensive experimental work (Perez 2008) was undertaken to have a better understanding of two-phase flow behavior in inclined pipes. Two different pipe diameters (38 and 67 mm) were used in the study. The total length of the test section was 6.50 m. The test fluids were air and water. Experiments were carried out by varying superficial gas and liquid velocities in the range of 0.15 - 8.9 m/s and 0.04 - 0.7 m/s, respectively. During the experiment, two-phase flow characteristics including flow patterns, liquid holdup, and pressure gradient were measured. In addition, a high-speed camera was used to record the flow pattern under different test conditions. Various types of flow patterns were observed including bubbly, churn, slug and highly aerated slugs or waves (**Figure 4.22**). The test results is summarized in **Table 4.3**.

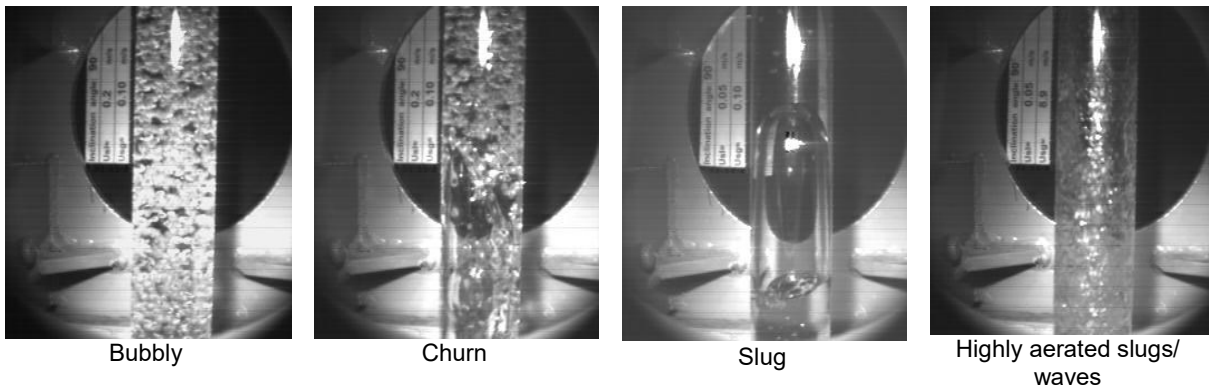


**Figure 4.22** Observed flow pattern at various gas and liquid superficial velocities (Perez, 2008)

**Table 4.3 Summary of flow pattern observations and test conditions**

Test No #	Gas superficial velocity (m/s)	Liquid superficial velocity (m/s)	Flow pattern
1	0.15	0.2	Bubbly
2	0.45	0.2	Churn
3	0.1	0.05	Slug
4	8.9	0.2	Highly aerated slugs or waves

**Figure 4.23** compares liquid holdup measurement data obtained during the experiment at different pipe diameters (38 and 67 mm) and superficial liquid velocities (0.2 and 0.7 m/s). In general, liquid holdup decreased significantly with superficial gas velocity, regardless of pipe diameter and liquid velocity. This result is consistent with previous findings. Interestingly, at low superficial liquid velocity (0.2 m/s), varying pipe diameter had a negligible effect on the liquid holdup and measurements from two different pipe diameters exactly coincide with each other (Figure 4.23a). When the superficial liquid velocity was increased to 0.7 m/s, different liquid holdup measurements were obtained from the pipes (Figure 4.23b). The increase in the liquid holdup with pipe diameter can be attributed to the difference in interfacial shear stress. In the small diameter pipe, the interfacial shear stress is higher than the one in the large pipe. Due to high interfacial stress, more water is removed from the test section causing reduction liquid holdup.

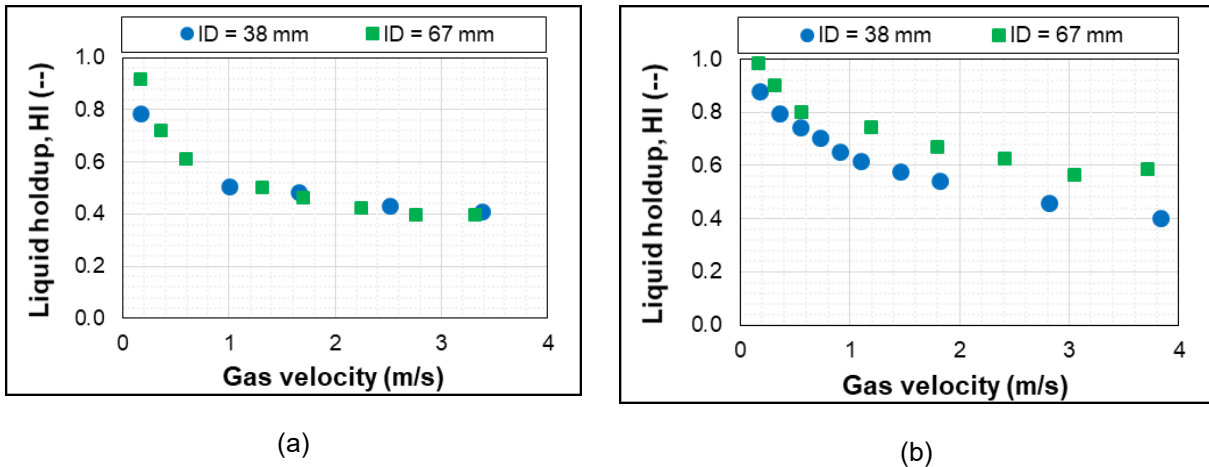


**Figure 4.23 Effect of pipe diameter on liquid holdup at different  $V_{SL}$ : a) 0.2 m/s; and b) 0.7 m/s (Perez, 2008)**

**Figure 4.24** presents pressure gradients obtained from two pipe diameter sections. The pressure gradient and liquid holdup exhibited similar trends which decrease with increase in superficial gas velocity. This behavior is expected, since the contribution of hydrostatic pressure drop to total pressure gradient dominates that of frictional pressure loss, particularly in large diameter pipes. At the same superficial gas and liquid velocities, the change in pressure gradient with pipe diameter was insignificant (Figure 4.24a). However, slight difference in pressure gradient measurements due to pipe diameters was observed at approximately 1.5 m/s superficial gas

velocity and 0.7 m/s liquid velocity (Figure 4.24b). Interestingly, under the same conditions, the effect of pipe diameter on the liquid holdup was significant (Figure 4.23b). This observation indicated that the influence of the frictional component on the total pressure gradient is relatively important.

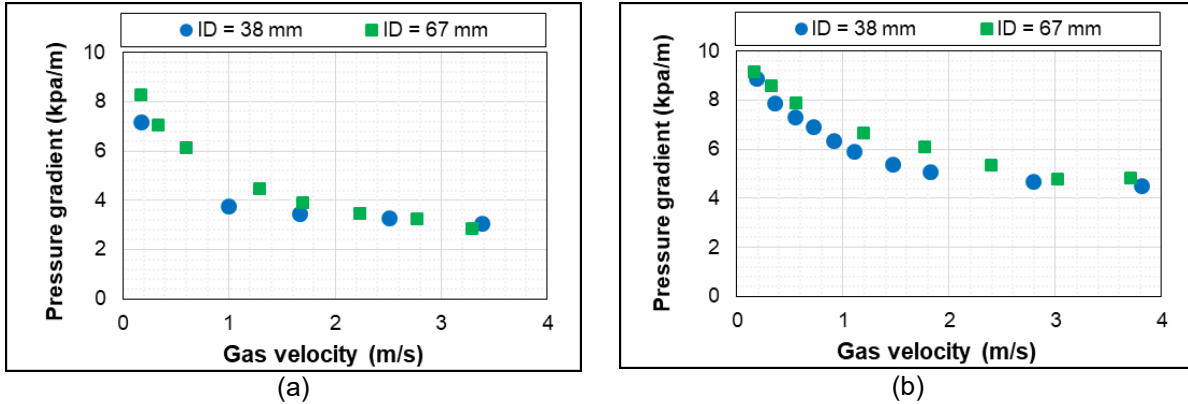


Figure 4.24 Effect of pipe size on pressure gradient at different  $V_{SL}$ : a) 0.2 m/s; and b) 0.7 m/s (Perez 2008)

Waltrich et al. (2013) performed a multiphase flow study in a long vertical tube. The experimental setup consists of: series of 0.048 m (1.89 in) transparent PVC pipes with a total tube length of 42 m (137 ft); a centrifugal pump with a variable speed driver to circulate water; Coriolis and vortex flow meters; and a screw compressor to provide the compressed air. Actuated valves were installed to control the pressure and gas flow rate. A mixing tee with perforated nipple is used to mix air and water. Also, the setup has one high-speed camera and three CCD cameras to observe the flow pattern and conductivity probes for liquid holdup measurement. In addition,

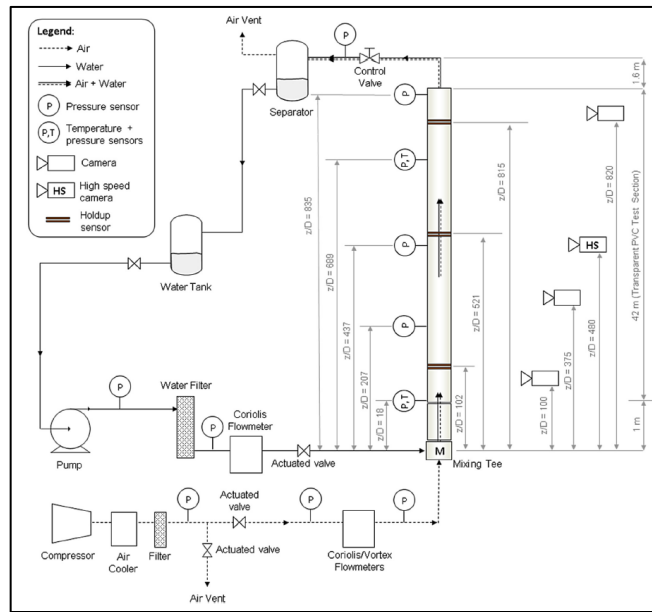


Figure 4.25 Schematic diagram of the two-phase flow loop (Waltrich et al. 2013)

pressure and strain-gauge transducers, and T-type thermocouple probes are installed to measure test parameters. The study was mainly focused on capturing the flow development in vertical pipes. In addition to visual flow pattern observation, the test equipment allowed measurement of pressure gradient, liquid holdup and slug/wave frequency over a wide range of pressures, and gas and liquid flow rates. The schematic of the test setup is shown in Figure 4.25.

The measured pressure gradient is shown in Figures 4.26 and 4.27. The measurements exhibit an inflection point where the flow transition occurred from churn to annular. For churn to annular

flow regime transition, the results suggest that the criterion developed by Turner et al. (1969) exhibits good agreement with experimental data for high superficial gas velocity while another approach (Wallis 1969) provides useful predictions at low superficial gas velocities. The flow pattern transition was found insensitive to the liquid superficial velocity. The criterion developed by Turner et al. (1969) accounts for surface tension, even though it ignores the effect of tube diameter.

$$U_{gs} \geq 3.08 \times \left( \frac{g\sigma(\rho_L - \rho_g)}{\rho_g^2} \right)^{0.25} \quad (4.1)$$

In addition, the experimental result shows good agreement with Hagedorn and Brown correlation at various flow conditions.

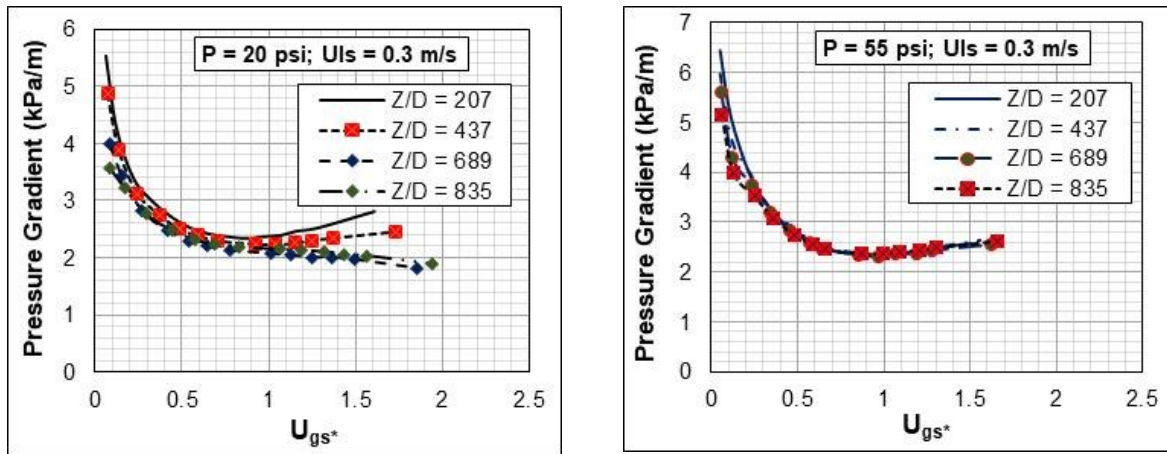
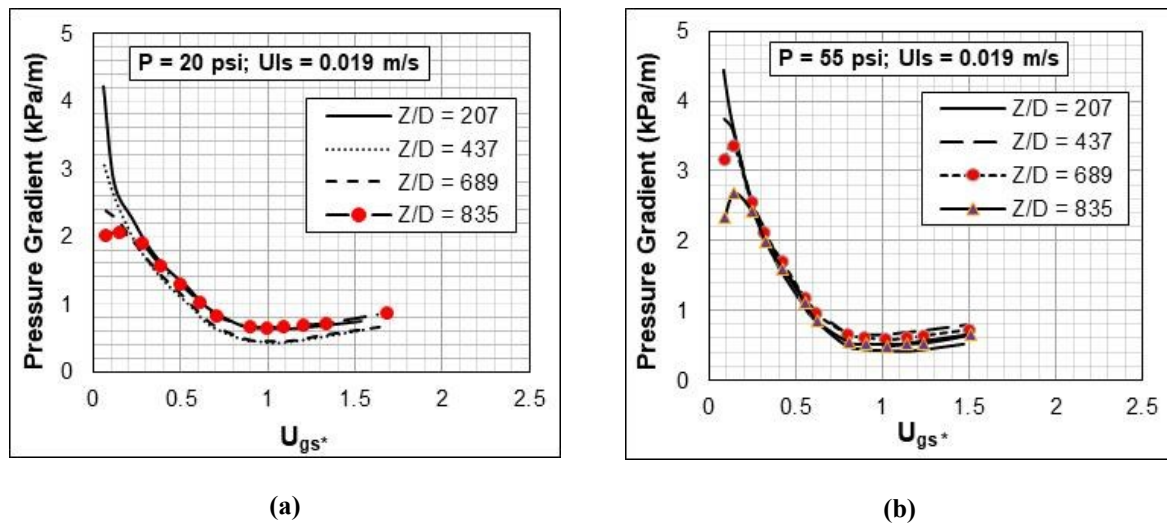
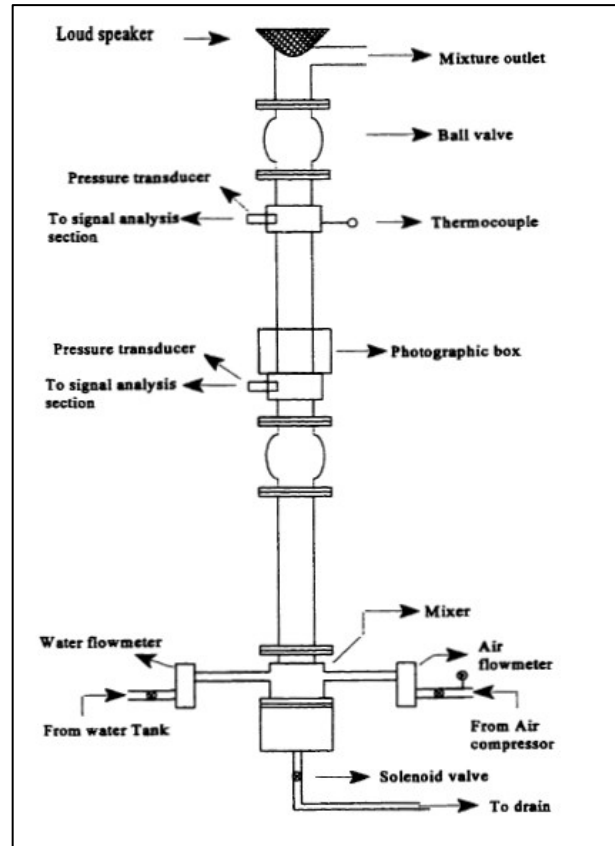


Figure 4.26 Pressure Gradient versus dimensionless superficial gas velocity at  $V_{sl} = 0.3$  m/s for different pressure drops: a) 20 psi, and b) 55 psi (Waltrich et al., 2013)



**Figure 4.27 Pressure gradient versus dimensionless superficial gas velocity at  $V_{sl} = 0.019$  m/s for different pressure drops a) 20 psi, and b) 55 psi (Waltrich et al., 2013)**

Pressure wave propagation is a natural phenomenon occurring in various industrial operations. Sultan (1999) performed an experimental study to investigate the propagation of pressure pulses in two-phase mixture flowing in a vertical pipe under steady flow condition. Additionally, the two-phase flow parameters such as flow pattern, void fraction, and pressure drop were measured during the experiment. The flow patterns were determined through visual observation and images analysis. Two quick-closing pneumatically actuated ball valves were used to determine the relative amount of liquid and gas trapped in the test section. The void fraction was obtained using liquid holdup and total pressure measurement, assuming that gravitational force is dominant in the total pressure drop. Two pressure transducers were used to measure the total pressure drop across test section and also to indicate the time for propagation wave to travel between the pressure transducers. To carry out the experiments, a test setup was developed. The setup (Figure 4.28) consisted of test section, submersible pump, compressor, gas and liquid flow meters, mixer, and two ball valves.



**Figure 4.28 Schematic of two-phase flow test setup (Sultan 1999)**

The setup (Figure 4.28) consisted of test section, submersible pump, compressor, gas and liquid flow meters, mixer, and two ball valves.

An air inducer, which has one axial inlet and four side inlets (Figure 4.29) was used to mix the two phases and attain desired flow pattern. For bubble, slug, and forth flow; the side inlets were used to inject air and water (Figure 4.29a). On the other hand, for high void fraction regime (i.e. annular or mist flow pattern), the gas phase (air) was injected from the main axial inlet while the liquid phase (water) was injected from the upper and lower side entrance, as shown in Figure 4.29b. The test section had 28.6 mm (1.13 in) inner diameter and 2.7 m (8.86 ft) length. The test measurements were obtained by varying superficial gas and liquid velocities in the range of 0.0027 – 7.79 m/s and 0.0027 – 0.29 m/s, respectively. Experimental results revealed a significant reduction in wave velocity as it propagates in a bubbly fluid. For instance, the wave velocity was reduced from 1480 m/s in pure water to 340 m/s in the pure air. It was further decreased to 30 m/s at a void fraction of 20%. During the experiment, various flow patterns were identified including bubbly, slug, forth, and annular flow. The detailed flow patterns description and test

conditions at which they were developed are summarized in **Table 4.4**. The mist flow pattern was not observed due to the limitation of the setup.

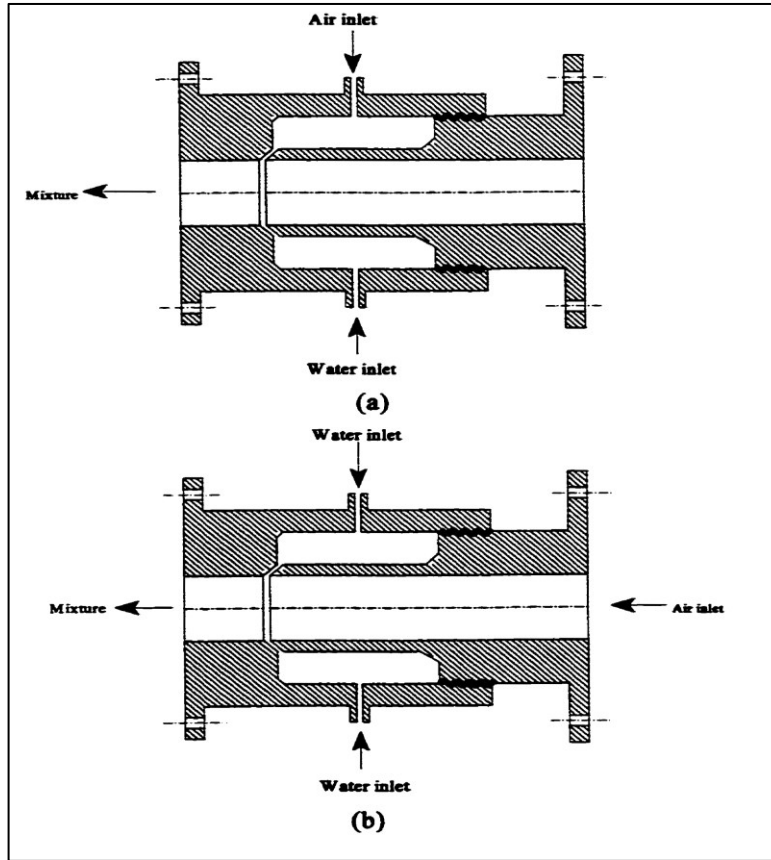


**Figure 4.29 Gas-Liquid mixer (a) bubbly/slug/froth flow (b) annular flow (Sultan 1999)**

**Table 4.4 Description of observed flow pattern**

Observed flow pattern	Void fraction	Water flow rate (cm <sup>3</sup> /s)	Flow Description
Bubbly	0.15, 0.16, and 0.23	63, 126, and 189	Number and size of the bubbles increases with the increment of gas flow rate Transition from bubbly to slug flow occurs due to small bubble collision which results in forming gas caps Distribution of the bubbles across the pipe diameter at various tested void fraction values was investigated.
Slug	0.15, 0.21, and 0.27	63, 126, and 189	Slugs formed due to the continues collision of small bubbles The diameter of slugs is roughly equal to pipe diameter while the length varies from 3 to 24 cm, depending on void fraction value.
Forth	0.63, 0.63 and 0.65	63, 126, and 189	Formed in the test section due to the breakdown of large gas slugs
Annular	0.86	63, 126, and 189	Described with high-speed gas flowing in the core of the pipe and carrying a thin film of liquid. The measured liquid film thickness is 4 mm

Void fraction is considered as one of the most essential parameters in determining two-phase flow characteristics. Sultan (1999) measured it at various gas and liquid flow rates. The void fraction is important because of its impact on the wave velocity. Besides this, it is necessary to calculate the components of the total pressure drop. **Figure 4.30** compares void fraction data obtained using two different techniques (quick-closing valves and pressure differential method) at liquid flow rate range of 1.75 – 63 cm<sup>3</sup>/s. As displayed in the figure, the void fraction measurement shows an expected trend. It increased with the air flow rate. In addition, a fairly reasonable agreement was found between the two methods, particularly at high air flow rate. At higher liquid flow rate range (7 – 189 cm<sup>3</sup>/s), a considerable discrepancy between the two methods was obviously observed throughout all the flow patterns (**Figure 4.31**). The discrepancy is attributed to the assumption that the gravitational pressure drop is the dominant component of the total pressure drop. This suggests that the contribution of friction drop becomes significant to the total pressure. The deviation of gravitational pressure drop measurement from the total pressure is shown in **Figure 4.32**.

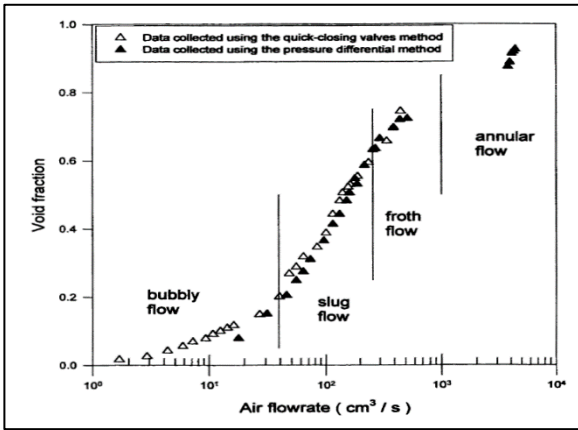


**Figure 4.30** Void fraction measurements versus air flow rate at water flow rate range of 1.75 - 63 cm<sup>3</sup>/s (Sultan 1999)

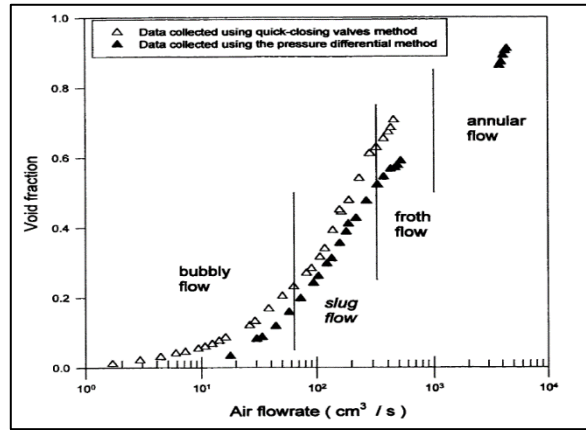


**Figure 4.31** Void fraction measurements versus air flow rate at water flow rate range of 7 - 189 cm<sup>3</sup>/s (Sultan 1999)

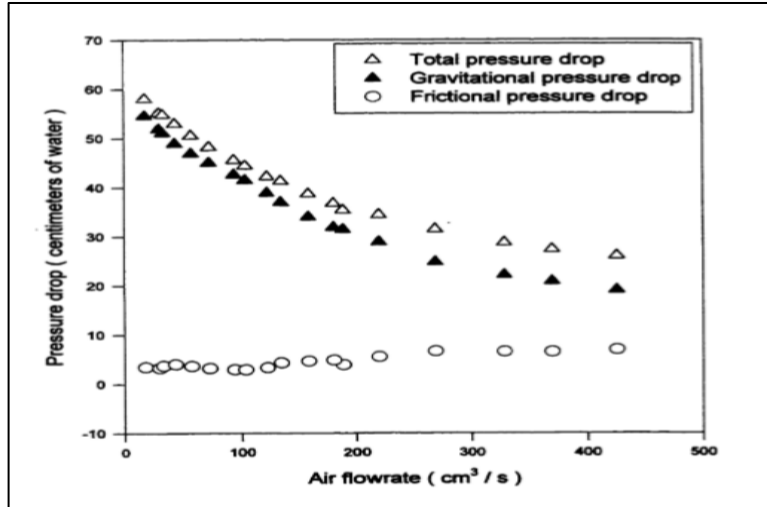


Figure 4.32 Pressure drop components for air-water mixture at water flow rate of 189 cm<sup>3</sup>/s (Sultan 1999)

Furthermore, the divergence of void fraction measurements is also attributed to the formation of nonhomogeneous flow exhibiting both the slug and forth regimes. The nonhomogeneous flow was developed due to the shortness of the test section. it is noteworthy that no liquid holdup (void fraction) was reported in the annular flow regime. Prior to pressure wave propagation test, the pressure drop across the test section was measured in the two-phase upward vertical flow. The measured pressure drop with respect to air flow rate at two different liquid flow rates (126 and 189 cm<sup>3</sup>/s) is presented in **Figure 4.33**. Consistent with previous findings, the pressure drop declined with air flow rate and increased with liquid flow rate. In addition, the results suggest that increasing liquid rate has a negligible impact on the pressure drop at low air flow rates (below 50 cm<sup>3</sup>/s). The results of past two-phase flow studies in vertical pipe are summarized in Table 4.5.

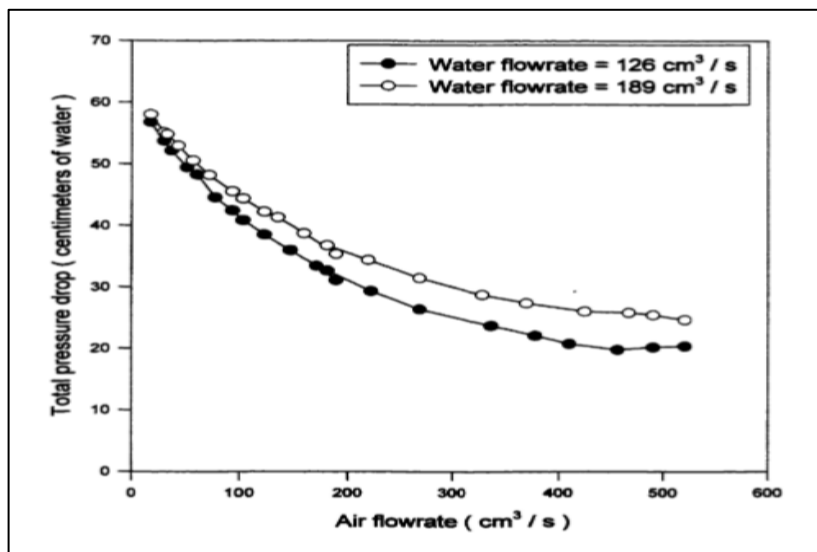


Figure 4.33 Measured total pressure drop versus air flow rate at various liquid flow rates (Sultan 1999)



**Table 4.5 Literature survey summary for two-phase flow in vertical pipe**

Reference	Test fluid	ID (in)	L/D	$U_{sg\ max}$ (m/s)	$U_{sl\ max}$ (m/s)	Pressure (Psi)	$\Delta P$ reported	Observed Flow pattern
Shiple (1984)	air-water	18	12.34	NA	NA	14.5	No	Bubbly
Ohnuki and Akimoto (1996)	air-water	18.9	4.2	0.06	0.02	14.5	Yes	Uniform bubbly, agitated bubbly, some cap bubbles and churn
Sultan (1999)	air-water	1.13	94	7.79	0.29	NA	Yes	Bubbly, slug, forth, and annular
Ohnuki and Akimoto (2000)	air-water	7.9	61.5	0.39	0.09	14.5	Yes	Undisturbed bubbly, agitated bubbly, churn bubbly, churn slug and churn forth
Prasser et al. (2002)	air-water	7.9	0.04	0.11	0.08	14.5	No	Uniform/ agitated bubbly and churn
Shen et al. (2005)	air-water	7.9	120	0.03	0.02	14.05	Yes	Bubbly
Shen et al. (2006)	air-water	7.9	60.5	0.02	0.09	14.5	Yes	Undisturbed bubbly, agitated bubbly, churn bubbly, churn slug and churn forth
Omebere et al. (2007)	nitrogen-naphtha	7.4	264.5	1.23 0.50	0.33 0.25	290 1305	Yes	Bubble, churn and annular
Perez (2008)	air-water	1.5& 2.64	97 & 171	8.90	0.70	NA	Yes	Bubbly, churn, slug and highly aerated slugs or waves
Ali (2009)	air-water	10	46	0.19	0.09	14.5	Yes	Dispersed bubbly flow, bubbly flow, agitated bubbly flow and churn/forth flow
Shen et al. (2010)	air-water	7.9	125	0.093	0.311	14.5	Yes	Bubbly, churn and slug
Zangana et al. (2010)	air-water	5	86.38	16.25	0.7	NA	Yes	-
Zubir and Zainon (2011)	air-water	0.83 -3.74	32 - 142	1.00	2.00	14.64	No	Bubbly-slug, slug, and churn flow
Schlegel et al (2012)	air-water	8	26	0.25	0.08	26.1	No	-
Damir (2012)	air-water	5	86.38	16	0.51	14.5& 29	No	Annular and churn flow some cap bubbles
Schoppa et al. (2013)	air-water	11	43.6	1.32	0.05	100	Yes	Bubbly, churn and annular
Tang et al. (2013)	air-water	0.5	173	20	1.17	NA	Yes	Bubbly, slug, churn, forth and annular
Waltrich et al. (2013)	air-water	1.89	870	1.95	0.30	20 & 55	Yes	Slug, churn and annular flow
Biria (2013)	air-water	2	197	13.25	0.72	NA	Yes	-
Waltrich et al. (2015)	air-water	2-12	20-216	31.6	0.85	14.5	Yes	Bubbly, slug, churn and annular flow
Luo et al. (2016)	air-water	2.5	126	196.50	1.97	145	Yes	Slug and annular flow

#### 4.4 Two-phase flow in annulus

Even though, most of two-phase flow investigations were conducted in horizontal and vertical pipes, limited studies had been carried out in the annuli. Available experimental data is only for low Mach number ( $Ma < 0.1$ ) flows. The first comprehensive study was performed by Caetano (1986) to investigate vertically upward gas-liquid flow in concentric and fully eccentric annuli. The modeling details of Caetano's work is presented in Section 3.3.3.2. The experimental setup used in the study consisted of transparent annular section. The outer pipe (casing) was made of cast acrylic with an inner diameter of 3 in while the inner pipe (tubing) is made of gray PVC with an outer diameter of 1.66 in. The total length of the test section was 16 m (52.5 ft). A schematic diagram of vertical annular flow test section is shown in **Figure 4.34**.

Air-water and air-kerosene were tested fluids used to simulate gas-liquid flow. A two-stage compressor with a maximum output capacity of 486 scf/min and 120 psig discharge pressure was employed to supply the gas phase. The liquid phase (water or kerosene) was injected into the test section using two separate single-stage centrifugal pumps. The maximum flow rate was 180 gpm at 125 psi. During the experiment, flow pattern was visually observed. Two pressure taps were used to measure pressure drop, and the quick-closing valve technique was utilized to measure liquid holdup. The flow velocities of the gas and liquid phases were ranging from 0.02 to 20 m/s and from 0.003 to 2 m/s, respectively. The experimental data revealed the occurrence of five flow patterns in the annulus including bubbly, dispersed bubbly, slug, churn and annular flow (**Figure 4.35**). Although similar flow patterns were generally exhibited in pipe and annular flows, their characteristics were markedly different. The detailed descriptions of two-phase flow patterns in the vertical annulus are provided in Caetano et al. (1992a).

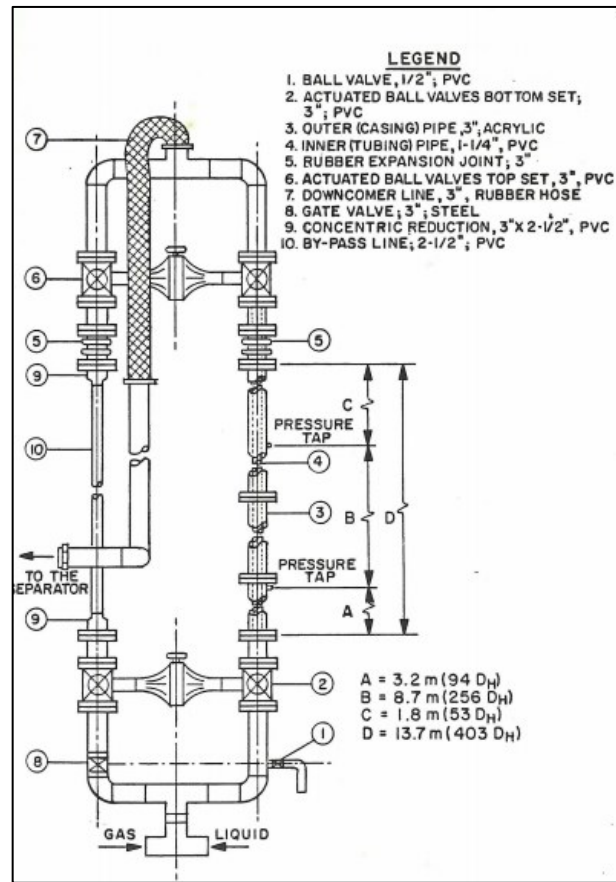


**Figure 4.34 Schematic diagram of two-phase annular flow test section (Caetano, 1985)**

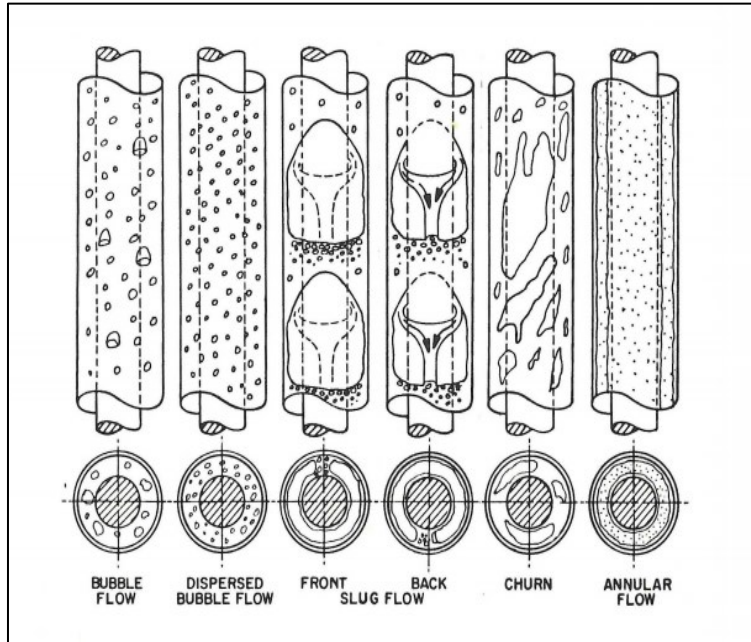


Figure 4.35 Flow patterns in upward vertical flow through a concentric annulus (Caetano, 1992a)

Furthermore, Caetano et al. (1992a) compared the flow patterns in pipe and annulus. The comparison revealed that the presence of an inner pipe in the annulus causes a change in flow pattern from slug to annular. Using flow pattern data obtained from their experiment, flow pattern maps (Figures 3.5 and 3.6) were developed for two test fluids (air-water and air-kerosene), based on the gas and liquid superficial velocities. The difference between the two maps is discussed in Section 3.1. The liquid holdup and pressure gradient measurements for various flow patterns were reported as a function of gas and liquid superficial velocities in the second part of the study (Caetano et al. 1992b).

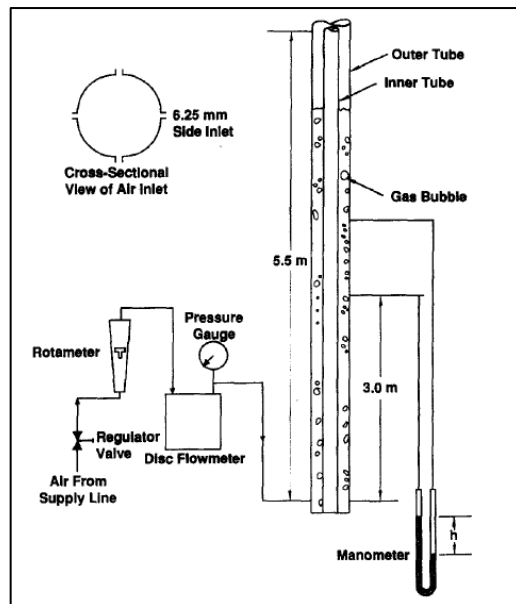


Figure 4.36 Schematic of experimental setup (Hasan and Kabir 1992)

Recently, a flow characteristic of two-phase flow (gas-liquid) in vertical annulus was experimentally investigated by Ozar et al. (2008). A 14.33-ft annular (0.75" × 1.5") test section was used. The superficial velocities were ranging from 0.05 to 3.89 m/s for the gas phase and from 0.26 to 3.31 m/s for the liquid phase. Three flow regimes including bubbly, cap-slug, and churn-turbulent were observed. Using their experimental data, a new correlation for predicting distribution parameter ( $C_0$ ) in the drift-flux model was developed.

Void fraction is an important flow parameters for calculating mixture density and pressure drop. Hasan and Kabir (1992) carried out an experimental study to estimate the void fraction in the upward co-current two-phase flow in the annulus and presented expressions for a void fraction in each regime. A flow loop consisted of Plexiglas tube with 127 mm inner diameter and 5.5 m length was utilized to carry out the tests (**Figure 4.36**). Three different inner pipe diameters (48, 57 and 87 mm) were used to simulate the annular geometry. During the test, the air was injected into stagnant water column through four 6.25 mm side inlets. The void fraction value was obtained using the pressure drop measurement ignoring the frictional pressure loss. The superficial air velocity was varied in the range of 0.0066 to 0.2 m/s. To avoid the entrance effect, the pressure drop measurement was obtained at 3 m away from the air inlets. Based on visual observation, four flow patterns including bubble, slug, churn and annular flow were identified. For various flow patterns (bubble, slug, and churn), the values of distribution parameters ( $C_0$  and  $C_1$ ) in the annulus were found consistent with those of a circular channel. The transition between bubbly and slug flow occurred at a void fraction of 0.25.

## 5. Subsonic and Supersonic Multiphase Flow

Supersonic and subsonic (Mach number greater than 0.3) multiphase flows generally occur in extreme circumstances. The flows are characterized by in-situ flow parameters such as a high-pressure drop and high superficial velocities. In this section, available high-speed (subsonic and supersonic) flow studies are presented. The experimental results indicate the roles of compressibility, phase transformation, vaporization of dissolved gas, which have a significant impact on the flow characteristics. It is crucial to establish a good understanding of the physical phenomena occurring during the critical flow condition. Apart from the laboratory conditions, critical flow situations are observed under specific field events such as discharge during volcanic eruptions and rupture of highly pressurized vessels, which exhibit similar characteristics of the worst-case discharge.

Mathematical models reveal that the dynamics of supersonic and subsonic two-phase flows is impacted by phase transformation and excessive gas expansion, which can lead to acceleration phenomenon that determines the flow characteristics. The primary challenge concerning mathematical modeling is lack of numerical stability and accuracy due to nonlinearity of the governing equations.

### 5.1 Subsonic/Supersonic Flow

Multiphase flows encountered in regular oil and gas operations have velocities of lower magnitude. However, very high velocities have also been reported at the time of catastrophic well control incidents. For instance, during the deepwater horizon blowout, it is believed that escaped gas resulted in cavitation, which led to supersonic conditions in the discharge line. In the light of such events, attention must be paid to the ground effect problems arising in the flow field beneath such high-velocity discharge. The existing frameworks only deal with low velocities, mapped to Mach number less than 0.3. Sophisticated testing methods are required for flow domains involving high Mach numbers ( $Ma > 0.3$ ), in which the flow characteristics are hugely implicated by phase transformation, gas expansion and turbulent mixing. The subsonic condition is described as flow with Mach number ranging from 0.3 to 1, while the supersonic condition is attributed to flows with Mach number greater than 1. The generated shock waves lead to change in velocity and density abruptly in the system and consequently induce a discontinuity in the flow system. Such phenomena were first theoretically established by Earnshaw (1851) while relating the thunder propagation with the supersonic velocity (Krehl, 2000). The shock wave propagation occurs in several engineering applications such as exploding coal dust in mines, accidental explosion in long pipes transmitting natural gas, exhaust pipes of reciprocating engines, volcanic eruptions, a rupture in nuclear vessels, and blast waves. The presence of shock waves in a flow presents challenging tasks to any theoretical algorithm.

Shock waves are often associated with the speed of sound. The speed of sound in two-phase fluid is different from that of single phase fluid. For instance, the sound speed is approximately 1440 m/s in water and 340 m/s in the air. However, introducing 1% air in water results in sound

speed of 100 m/s. Kieffer (1977) developed a model to predict the speed of sound in a two-component system. The model is applied in adiabatic or isothermal condition. The model is expressed as:

$$c = \eta \rho_{LA} \left( \frac{G_{air}}{P} \right)^{1/\gamma} + \exp\left(\frac{P_a - P}{K}\right) \left\{ [(1 + \eta) \rho_{LA}]^{1/2} \left[ \frac{\eta \rho_{LA} G_{air}^{1/\gamma}}{\gamma P^{(1+\gamma)/\gamma}} + \frac{1}{K} \exp\left(\frac{P_a - P}{K}\right) \right]^{1/2} \right\}^{-1} \quad (5.1)$$

where  $c$  is the speed of sound,  $\eta$  is the gas mass fraction,  $\rho_{LA}$  is the density of the liquid in the reference state (considered as 1 g/cm<sup>3</sup> at atmospheric condition),  $P$  is the pressure,  $P_a$  is reference pressure (considered as 1 bar/14.5 psi),  $K$  is the bulk modulus of water (2.2 x 10<sup>6</sup> bars),  $G_{air}$  is the gas constant given by  $T_0 R_0 / M \rho_0^{\gamma-1}$  ( $T_0$  is reference temperature,  $R_0$  is universal gas constant,  $M$  is molecular weight of air),  $\gamma$  is the adiabatic constant and depends on the thermodynamic properties of the gas. The equation was validated using the experimental data from Karplus (1958) for air and water mixture, which showed reasonable agreement. To study the effects of different parameters on pressure gradient, a sensitivity analysis was conducted considering a range of parameters such as void fraction, pressure, and temperature. As shown in **Figure 5.1**, with increase in pressure, the speed of sound increased, which is attributed to the effect of compressibility. Similar trends were observed in isothermal as well as adiabatic cases. At low pressure, with increase in gas void fraction, the speed of sound was found to decrease at low void fraction, reached a minimum value, and then followed an increasing trend as the void fraction was approaching one. However, at high pressures, a monotonically decreasing trend was observed.

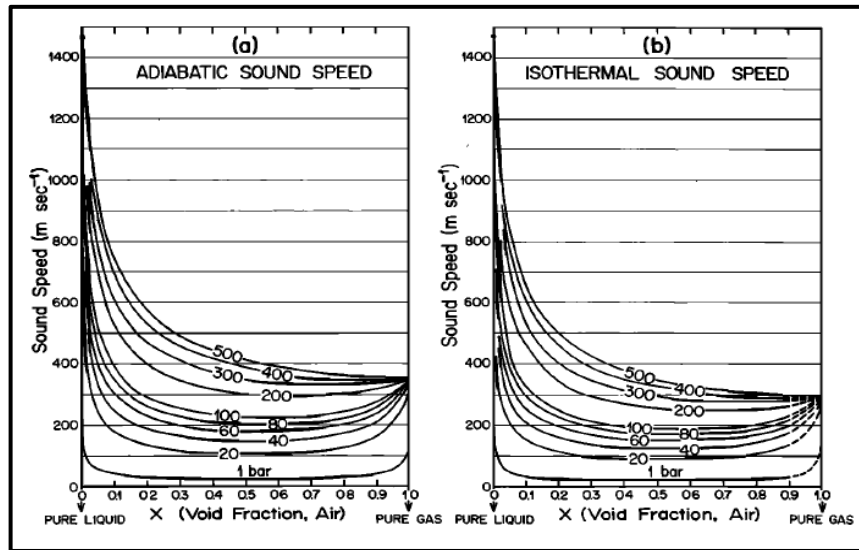


**Figure 5.1** Variation of (a) adiabatic and (b) isothermal speed of sound in air-water mixture with gas void fraction and pressure (Kieffer, 1977)

Every fluid dynamics problem has specific characteristics. In order to understand the intricacies, experimental studies are traditionally conducted. Results of experimental investigations are the

basis of the development of any theoretical model. Keeping this in mind, an extensive survey of past experimental works has been performed. The experimental investigations include two-phase high-velocity flow in tubes and shock waves in tunnels, chokes, and ducts. The next section present reviews of such studies.

## 5.2 Experimental Studies

Most of subsonic and supersonic phenomena for single or two-phase flow occur in the converging-diverging nozzles, chokes, and narrow tunnels in which a high-pressure drop can be attained within a short length (Yazdani et al. 2014; Eddington 1970; Sachdeva et al. 1986; Nakagawa et al. 2008; Guo et al. 2007). A limited number of studies (Luo et al. 2016; Martindale and Smith 1980; Eddington 1970) have been performed to investigate two-phase flow characteristics in small vertical pipes, tubes, nozzles, and ducts at a high velocity in the range of subsonic or supersonic.

Pressure drop and sonic velocity in two-phase flow were investigated by Martindale and Smith (1980). To conduct the test, an air-water mixture was allowed to flow upward in a vertical 32-mm diameter pipe varying gas velocity (12 to 21 m/s) and water flow rate (0 to 34 kg/min). The experiments were performed varying operating pressure (27 to 102 KPa) and temperature (21 to 27°C). A detailed schematic of the test setup is shown in **Figure 5.2**. During the test, the pressure drop was measured using 198 cm apart pressure transducers fitted in the test section. The sonic velocity was determined by measuring the time required for the shock wave to travel between two fixed points (30.5 cm apart) through the test section.

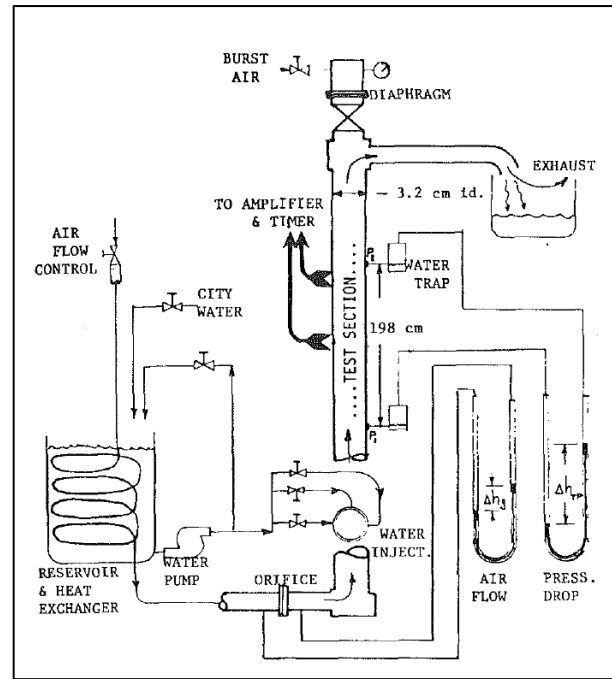


**Figure 5.2 Schematic of experimental setup (Martindale and Smith 1980)**

Shock waves in the tube were generated by rupturing a thin plastic or aluminum diaphragm located in the downstream of the test section.

The experimental observations revealed the occurrence of annular and annular-mist flows. By examining the pressure gradient and sonic velocity measurements, the flow pattern transition (annular to churn froth), was determined (**Figure 5.3**). The actual measurements of two-phase flow tests (pressure drop and sonic velocity) are normalized by the ones obtained from gas flow experiments conducted at the same flow rate. The occurrence of flow pattern transition was detected by sharp reduction in the pressure gradient and discontinuity in the sonic velocity data

at around gas fraction of 0.1. As illustrated in the figure, the sonic velocity remained steady for the different flow regions while quality was varied from 10 to 100%.

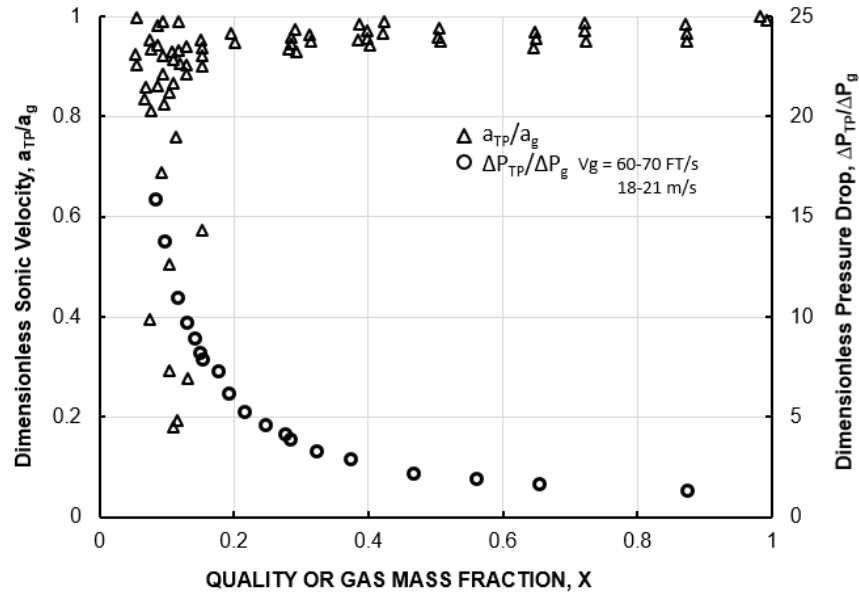


Figure 5.3 Dimensionless sonic velocity and pressure drop versus gas fraction (Martindale and Smith 1980)

Figure 5.4 shows the dimensionless pressure drop versus quality at various superficial gas velocities. The results demonstrate a significant reduction in dimensionless pressure drop with gas mass fraction. At a constant gas mass fraction, increasing gas velocity (gas mass flow rate) reduced the dimensionless pressure drop. In other words, increasing the gas flow rate generated a higher-pressure drop in single gas phase flow than the two-phase flow.

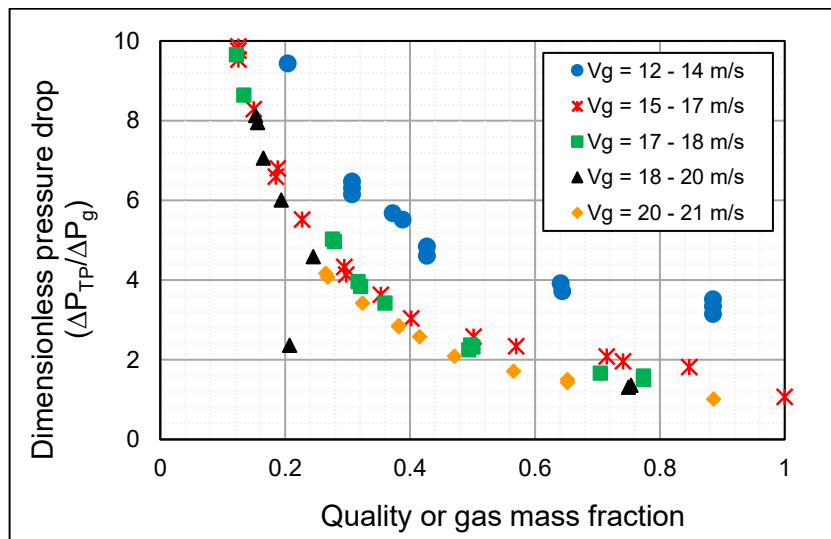
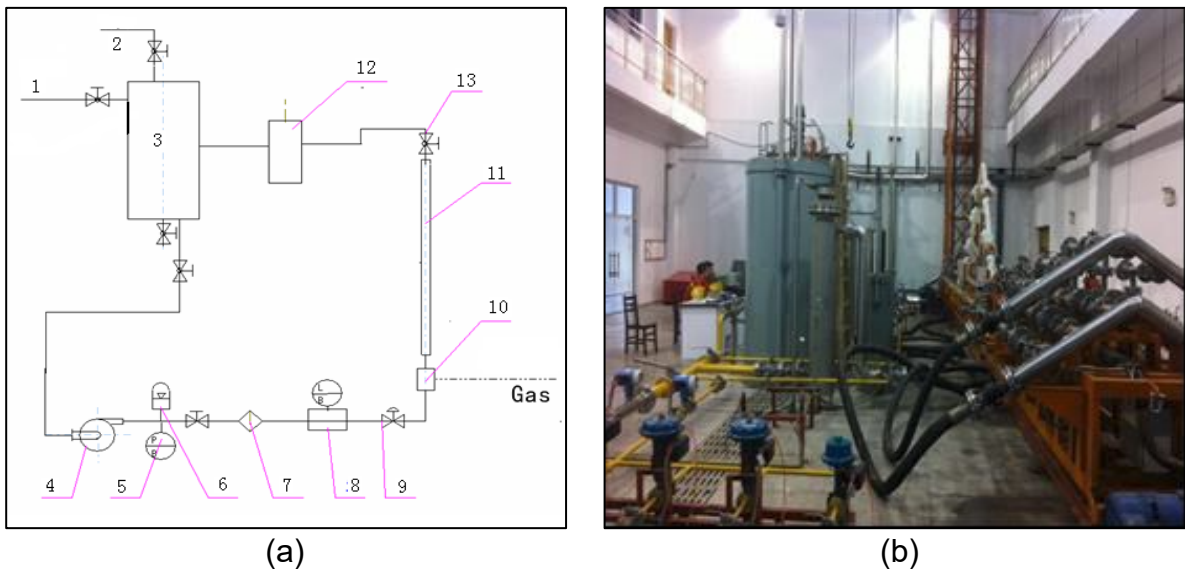


Figure 5.4 Dimensionless pressure drop versus quality at various superficial gas velocities (Martindale and Smith 1980)

More recently, Luo et al. (2016) carried out extensive experiments investigating high-velocity two-phase flows in vertical and inclined pipes. The study also aimed to investigate the impact of inclination angle on two-phase flow characteristics. The inclination angle was varied from 0 to 90° (measured from the horizontal plane). The test setup consisted of a compressor, liquid pump, gas-liquid mixer, gas-liquid separator, flow meters, and 2.5-inch diameter pipe section. The length of the test section is 26.25 ft (8 m). Air and water were used as test fluids. A schematic of test setup and photo of experimental apparatus are presented in **Figure 5.5**. To carry out the experiments, the gas and liquid superficial velocities were varied in the range of 20.47 – 196.5 m/s and 0.205 – 1.965 m/s, respectively. The test was conducted under pressure range of 0 – 1 Mpa. During the experiment, multiphase flow characteristics including flow patterns, pressure drop, temperature and liquid holdups were measured. The flow patterns were evaluated using a high-speed camera and visual observation. Pressure drop and temperature were measured using sensors. The quick closing valve technique was utilized to measure liquid holdup. Under the conditions employed in the study, three flow patterns: slug (at low gas velocity), churn and annular (high gas velocity) were observed.



**Figure 5.5** Experimental facility: a) schematic of test setup, and b) test apparatus (Luo et al. 2016)

Note: In Figure 5.5a – 1 flow entrance of oil, 2 flow entrance of water, 3 oil-water mixer, 4 liquid pump, 5 pressure meter, 6 regulator, 7 moisture content tester, 8 flow meter, 9 adjusting pressure valve, 10 gas-liquid mixer, 11 test tube section, 12 gas-liquid separator, 13 valves.

To present the data in a convenient way, pressure drop and liquid holdup measurements are digitized and re-plotted as a function of superficial gas and liquid velocities (**Figure 5.6**). As depicted in the figure, liquid holdup measurements show a normal and expected trend with gas and liquid velocities. The holdup significantly decreased with gas velocity and slightly increased with liquid velocity. This behavior is found consistent with previous studies (Perez 2008; Zangana 2010; Biria 2013) conducted at low gas superficial velocities. In spite of this, the test

results show abnormal pressure drop increase with gas and liquid flow rates, particularly when gas velocities are less than 80 m/s. This sharp increase in pressure drop implies that total pressure drop in the test section is dominated by the pressure drop due to friction. At high superficial gas velocity (above 80 m/s) and low superficial liquid velocity (less than 1.235 m/s), the measured pressure drop was maintained steady while increasing the gas flow rate.

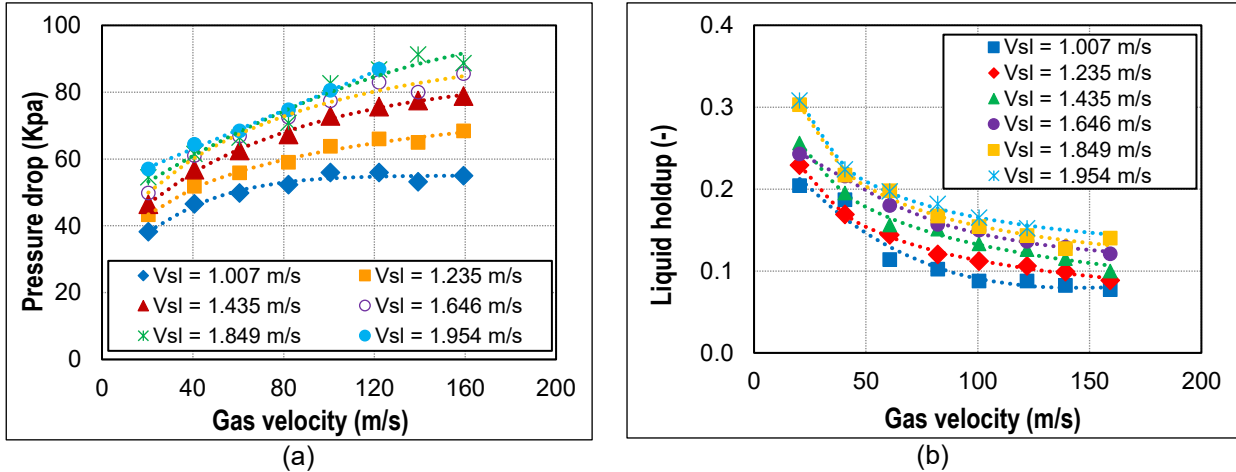
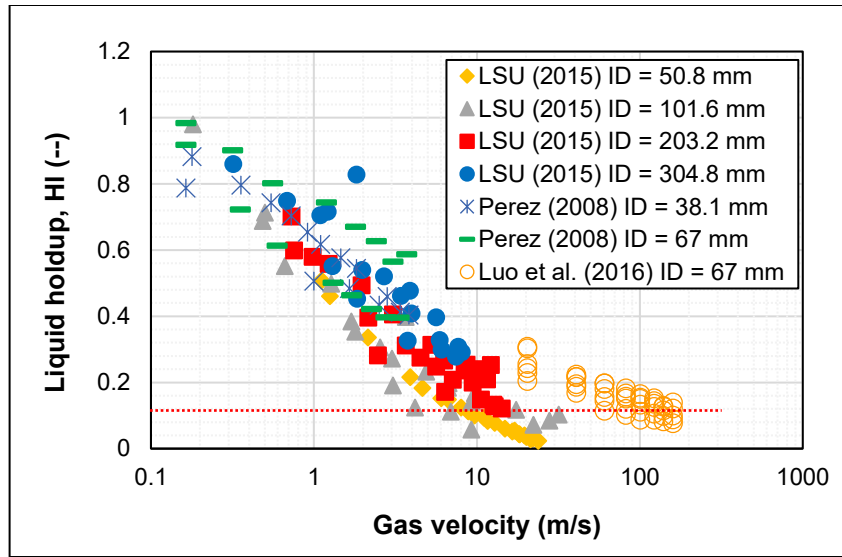


Figure 5.6 Measured two-phase flow characteristics versus gas velocity at various liquid velocities: a) pressure drop, and b) liquid holdup (data from Luo et al., 2016)

After analyzing the test results, the liquid holdup and pressure drop trends have been found consistent with the previous findings. However, to assess the accuracy of the measurements, the liquid holdup is compared to the previous studies (Waltrich et al. 2015, LSU report; Perez, 2008). The data comparison is presented in **Figure 5.7**. The comparative study shows that liquid holdup measurement reported by Luo et al. (2016) is not consistent with the other studies. This deviation could be attributed to the exaggeration of the liquid holdup due to malfunction of quick closing valves. For instance, the liquid accumulated in their test section ( $H_L = 0.1$ ) at very high gas velocity (roughly 159 m/s), as demonstrated by horizontal red line, is equivalent to the one at 10 m/s for approximately similar pipe size, which can be disputed. We believe that the overestimated liquid holdup is due to slow operation of the closing valves used in the experiments. Malfunction of the valves may allow liquid to flow back to the test section and affect the liquid holdup measurement.



**Figure 5.7 Measured liquid holdup versus superficial gas velocity from different previous studies**

Apart from the regular experimental work, some experimental investigations (Zucrow and Hoffmann, 1977) were performed to understand the nature of the shock wave propagations. The innovative works conducted in the past include experiments performed in a tunnel and shock tube. The shock waves are mainly characterized in terms of strength, Mach number, and shock front width. The strength of the shock waves is the ratio of ambient pressure to the change in pressure from the post-shock conditions. The Mach number is the ratio of the wave speed to the speed of sound. The width of shock front is generally in the order of micrometers which is considered negligible for evaluation purpose.

One of the earlier research studies (Eddington 1970) on supersonic phenomena was aimed to investigate normal and oblique shock structure in supersonic two-phase tunnel flows. Two-phase flow parameters such as relative phase velocity, local void ratio, the coefficient of friction and stagnation pressure were investigated. A homogeneous mixture of water and air with 1:1 ratio was used as the test fluid. The tunnel consisted of 1.5 in test section that possesses the capability of attaining a wide range of Mach numbers (5.0 – 100) at a pressure ranging from atmospheric pressure to near the vapor pressure of water at ambient temperature. **Figure 5.8** shows schematic of the two-phase tunnel setup. A water pump with an output capacity of 720 gpm at 1100 psi was employed to inject the liquid phase. In the tunnel design, two-phase injector consisted of 192 small (0.7" I.D.) stainless steel tubes through which the high-pressure water with a velocity exceeding 300 ft/s was introduced. At the exit point of stainless steel tubes, nitrogen gas was injected from upper and lower inlet arrangement to produce high-velocity and low-pressure two-phase mixture in the rectangular mixing duct. The low-velocity boundary layers which were established in the low-pressure mixing section was eliminated by using transparent, flexible sidewall, boundary layer knife assemblies fixed in the test section. The high-velocity boundary layer flow was contained by outer tunnel walls and returned to water tank through a discharge line at the end of the test section. The two-phase tunnel dimensions and operating conditions are

listed in **Table 5.1**. Static pressure was measured through pressure taps drilled along the center line of the opposite plexiglass sidewall. During the experiment, regular and stable shock waves were created in the test section by restricting the flow via a back-pressure valve.

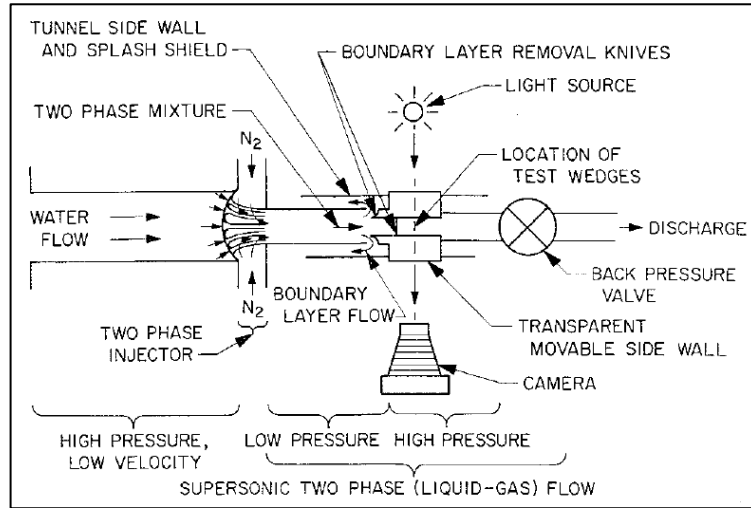


**Figure 5.8 Schematic of two-phase tunnel (Eddington 1970)**

**Table 5.1 Two-phase tunnel dimensions and operating conditions**

Parameter	value
Upstream height (in)	1.956
Upstream width (in)	0.756
Upstream cross section (in <sup>2</sup> )	1.479
Volume ratio ( $r_{vi}$ )	0.77 – 0.96
Test section height (in)	1.600
Test section width (in)	0.381 – 0.756
Test section length (in)	4.00
Water injection pressure (psi)	0 – 1000
Water flow rate ( $m_l$ ) (lb/s)	0 – 100
Gas injection pressure (psi)	0 – 500
Gas flow rate ( $m_g$ ) (lbm/s)	0 – 0.36
Mixture velocity ( $V_1$ ) (fps)	0 – 334
Mach number range ( $M_1$ )	0 – 100
Reynolds number	$2 \times 10^6$
Power density (hp/in <sup>2</sup> )	443

Based on previous investigations of acoustic propagation, Eddington (1970) concluded that a two-phase medium could be treated as an isothermal continuum for the propagation of acoustic waves, if the distance between bubble centers is less than half of the wavelength. This assumption is valid for very small bubbles (radius less than 0.004 in). Based on the isothermal continuum assumption, the Mach number for two-phase flow can be defined as:

$$M = \frac{V}{c} = \frac{V}{(1+r_v)} \left[ \frac{\rho_l r_v (1+r_m)}{P} \right]^{1/2} \quad (5.2)$$

where  $V$  and  $c$  are mixture and sonic velocity, respectively,  $r_v$  and  $r_m$  are gas to liquid volume ratio and gas to liquid mass ratio, respectively,  $\rho_l$  is liquid density, and  $P$  is the static pressure in psi. The relationship between upstream Mach number and mixture velocity at various static pressures for volume ratio of 1.0 is presented in **Figure 5.9**.

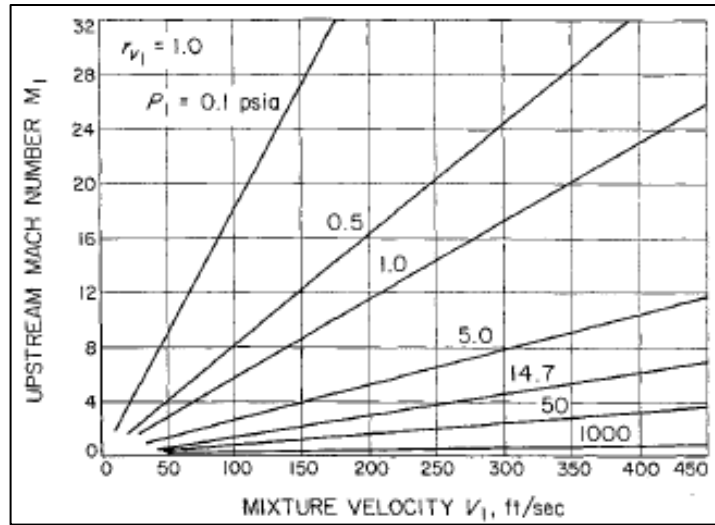


**Figure 5.9** Upstream Mach number versus mixture velocity at various static pressures (Eddington 1970)

Once the shock is developed, the flow conditions (pressure, temperature, fluid density) prior and after the shock becomes considerably different. For a relatively immiscible mixture of air and water, the flow can be considered isothermal through normal shock structure. By applying conservation relations of mass and momentum and the isothermal equation of state, the relation between Mach number and static pressure ratios across the normal shock and upstream can be described as follows:

$$\frac{P_2}{P_1} = M_1^2 \quad (5.3)$$

where  $P_1$  and  $P_2$  represent upstream and downstream pressures, respectively. Similarly, the normal shock analysis can be extended to analyze oblique shock waves with relative simplicity for the isothermal assumption. A comprehensive set of equations including equations of continuity and momentum, mixture density and velocity, the isothermal equation and the geometrical relationships are required to determine flow characteristics of the downstream oblique shock. For oblique shock, the pressure ratio is given as a function of upstream Mach number and shock angle, as follows:

$$\frac{P_2}{P_1} = M_1^2 \sin^2 \beta \quad (5.4)$$

where,  $\beta$  is shock angle. **Figure 5.10** shows pressure ratio ( $P_2/P_1$ ) as a function of upstream Mach number for both normal and oblique shock waves.

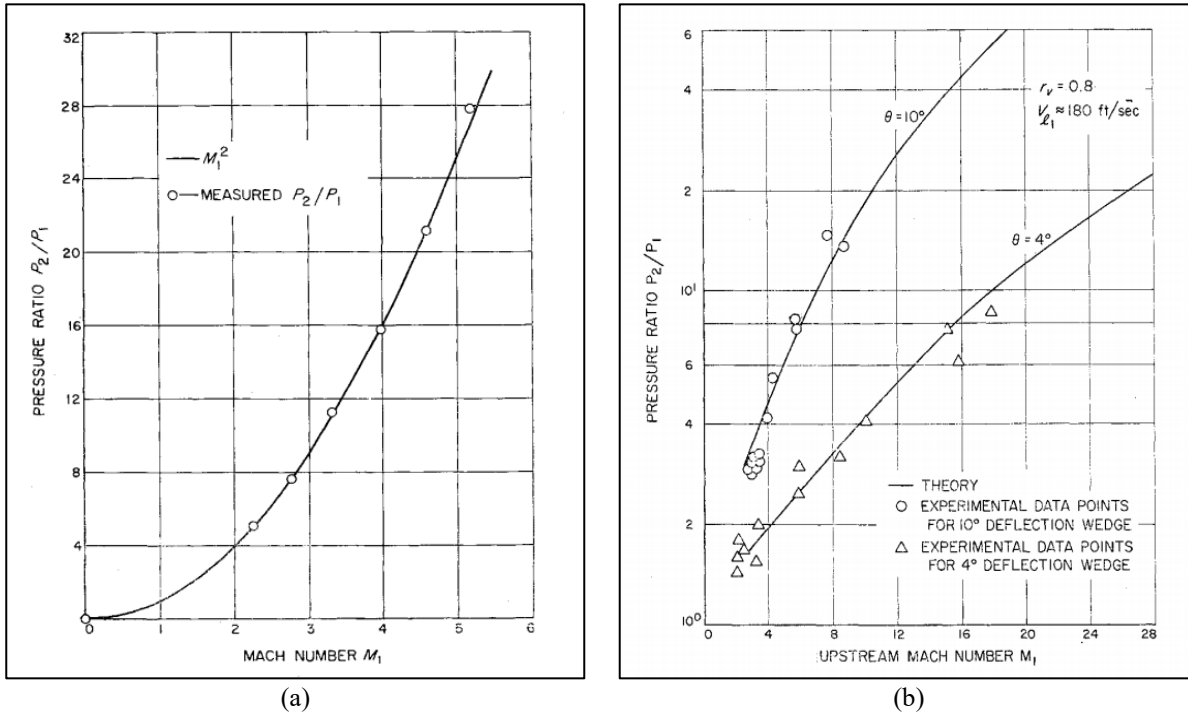


**Figure 5.10 Pressure ratio versus upstream Mach number for two different shocks: a) normal shock, and b) oblique shock (Eddington 1970)**

Chauvin et al. (2012) conducted a study on vertical shock tubes comprised of 0.75 and 3.045 m sections with 0.88 m Plexiglas window. The laboratory setup consisted of a generator for the mono-dispersed cloud of droplets, Photron FastCam SA1, and pressure transducers. The study investigated the influence of the droplet diameters on shock waves under supersonic condition and (Mach number 1.3 and 1.5). The phenomena noticed during the experiment with 250  $\mu\text{m}$  droplet interacting with 1.5 Mach number shock wave, was secondary atomization, fragmentation, momentum transfer, and heat transfer. When the shock waves impacted the droplet cloud, one part of the shock wave was transmitted into the air-water mixture, while the other part was reflected and propagated into the upstream flow. The transmitted wave atomized the droplets into the smaller ones. This fragmentation process was attributed to secondary atomization which was followed by momentum transfer from the shock wave to the cloud. It also led to attenuation process with the heat transfer and atomization phenomenon. Another experiment included fluid comprised of water cloud with droplets of 250  $\mu\text{m}$  and 500  $\mu\text{m}$  diameter having a volume fraction of 0.3% and 1%, respectively and 1.3 Mach number shock waves. During the interaction, similar pressure history was observed till the arrival of the reflected wave by two-phase mixture at pressure transducer placed at the upstream side, as was observed in the absence of two-phase mixture. Increase in the pressure was observed at the downstream side with the transmission of the shock waves, and finally, the equilibrium pressure was established. Overall, it was noted that the cloud with higher droplet diameter has the more

attenuating capacity. In addition, the momentum transfer and heat exchange depend on the exchange surface area.

Dontsov and Nakoryakov (2003) studied the dynamic propagation of pressure waves and bubble mechanism in a vertical shock tube experiment comprised of liquid and distributed gas bubbles in it. The test setup consisted of 1.5 m long steel tubing having an inner diameter of 53 mm fitted with Mylar tube of 37.5 mm ID. The bubble generator was used to induce the gas bubbles in the liquid medium. The liquid phase consisted of 50% solution of glycerin in water by mass and gas phase included Freon 12 and Nitrogen. Pressure waves were generated using the electromagnetic coil implanted at the bottom of the test section. There were several factors observed which impacted the evolution and decay of waves such as heat exchange mechanism, size of the bubbles, inhomogeneity of the mixture, and liquid compressibility. Results suggested that bubbles were redistributed either in the core region or at the cross-section of the tube during the pressure transmission, and the non-uniform distribution of the bubbles had a significant effect on the development of pressure profiles over time and distance. Besides this, the heat transfer between the bubbles and liquid medium was attributed to be the primary mechanism of attenuation rate of pressure waves.

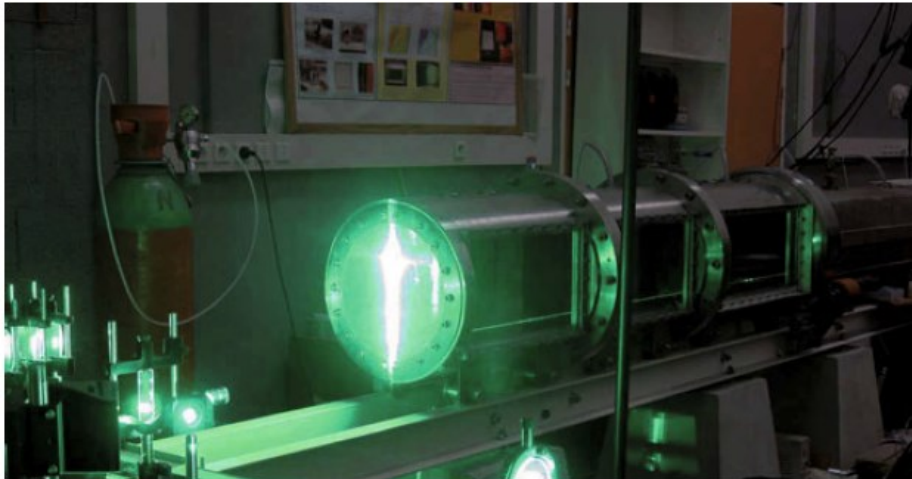


**Figure 5.11 Shock tube experiment for flow instabilities (Mariani et al., 2012)**

Mariani et al. (2012) conducted shock tube experiments in the 1-meter long 20-cm diameter test setup to study the flow instability due to accelerated interface separation of two fluids of different density. The chamber included a piezoelectric dynamic pressure equipment and laser sheet for flow visualization as shown in **Figure 5.11**. The non-linear phase was observed for more extended time considering the extension of the test section of the tube. The evolution of the interface between the phases is studied by tracking the interface with time.

Shock mixing is another critical phenomenon which is observed in the high-velocity multiphase flow. Witte (1969) conducted the theoretical and experimental study of shock mixing during two-phase flow. The mixing phenomenon shows some deviation from planar shock waves. The

temperature change across shock is very small due to the high specific heat of the liquid. The upstream gas phase velocity of the shock may be higher than that of the liquid phase. During the mixing, there is the occurrence of static pressure increase and energy dissipation which leads to change of flow structure from jet flow to froth flow. **Figure 5.12** shows the mixing phenomenon where the gas and liquid phases are introduced in the tube. During the experimental investigation, it was observed that during mixing, a free surface is followed by the entrainment zone where the bubble cloud implodes. After this, a supersonic mixture exists, and compression shock develops. At the exit, the flow will be subsonic in nature. This case might be similar to worst discharge condition where sonic conditions can exist in the wellbore while at the exit subsonic conditions may establish.

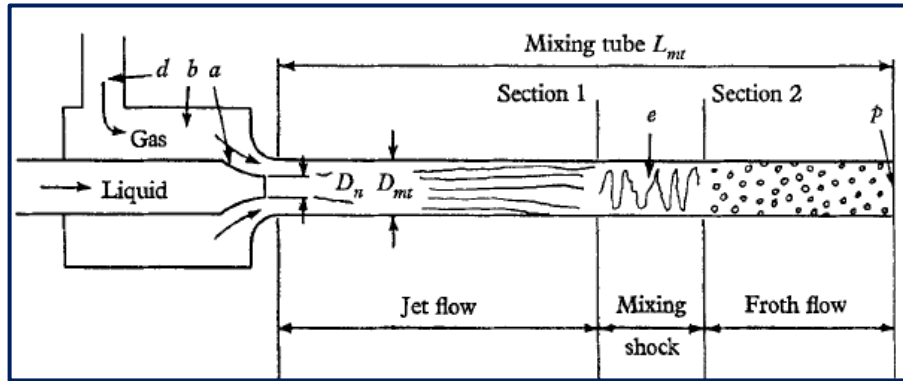


**Figure 5.12** Schematic of experimental set-up for mixing shock (Witte, 1969)

Apart from the regular experimental study of shock waves, tests were conducted to get an insight into the dependency of shock waves on different factors. Fisenko and Sychikov (1977) explored the parameters affecting the resistance coefficient in two-phase one component mixture. The velocity of sound in a two-phase medium with a defined ratio of two phases can be two orders of magnitude smaller than in liquid phase and more than an order of magnitude smaller than the velocity of sound in the gas. Results of the experiments suggest that, at high- gas velocities and high Mach numbers ( $> 0.75$ ), the resistance coefficient decreases with increasing Mach number and approaches 0 as Mach number approaches 1 as shown in **Figure 5.13**. The experiment was conducted using tubes with a constant diameter ranging from 5.8 to 14.2 mm. The pressure at the entrance varied from 145 to 1350 psi, and the mass flux density varied from  $0.567 \times 10^4$  to  $2.983 \times 10^4$  kg/ (m<sup>2</sup>.s).

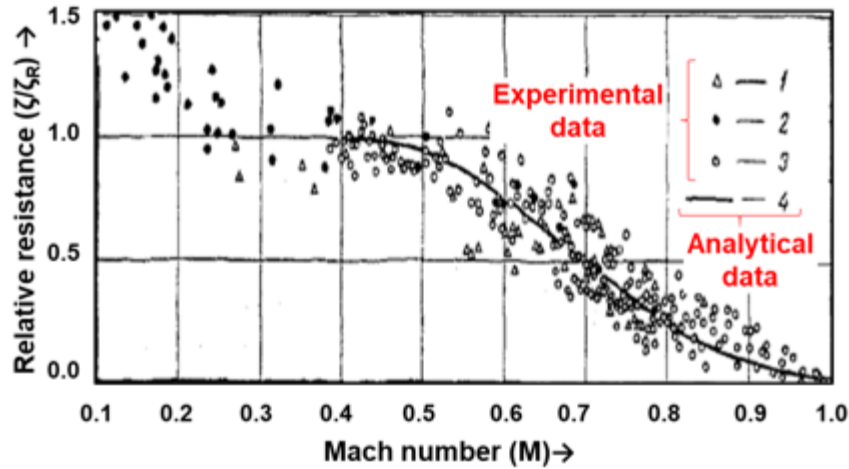


Figure 5.13 Relative resistance coefficient with Mach number (Fisenko and Sychikov 1977)

In addition, the model was using experimental data obtained from steam water flow under adiabatic conditions varying pressure (0.49-14.03 Mpa), diameter (8.06, 2.56, and 1.01 mm), and mass flux ( $0.093 \times 10^4 - 2.52 \times 10^4 \text{ kg/m}^2\text{s}$ ). The experimental results exhibited different characteristics of the resistance coefficient at different Mach numbers. The effect of compressibility was prominent for Mach number above 0.5. Between Mach number 0.3 – 0.5, simultaneous effects of viscous force and compressibility were evident. For Mach number below 0.3, sharp increase in resistance coefficient was observed. At lower velocities, the relative slippage between the phases led to increase in dissipative forces and uniform two-phase flow was less probable. The resistance coefficient for Mach number above 0.4 can be determined by the following relation:

$$\frac{\zeta}{\zeta_r} = \exp[-10M^{0.75}(M - 0.4)^2] \quad (5.5)$$

where  $\zeta$  is the resistance coefficient, and  $\zeta_r$  is the resistance coefficient for flow region similar with respect to Reynolds number. The speed of sound in two-phase flow at thermodynamic equilibrium ( $a_{\text{mix}}$ ) is calculated as:

$$a_{\text{mix}} = v_{\text{mix}} \frac{dP}{dT} \sqrt{\frac{T}{c_{v\text{mix}}}} \quad (5.6)$$

where P is the pressure in the system, T is the temperature,  $c_{v\text{mix}}$  is specific heat of steam-water mixture at constant volume.

There has been consistent effort to apply the concepts of the subsonic and supersonic phenomenon in the industrial setting. Fisenko et al. (2010) illustrated the design of the Fisonic device in which water enters the mixing chamber with velocity in parallel with working stream. The water is introduced through a narrow circumferential annulus surrounding the gas injection

nozzle in a mixing chamber. The mixture is pressurized as it enters into the diffuser. The discharge pressure is higher than the pressure in the system and operates at small compression and high expansion ratios. It had been demonstrated that the sonic speed in multiphase systems is significantly less than the sonic speed in each phase. As shown in **Figure 5.14**, the minimum sonic velocity occurs when the volumetric ratio of the streams is approximately 0.5.

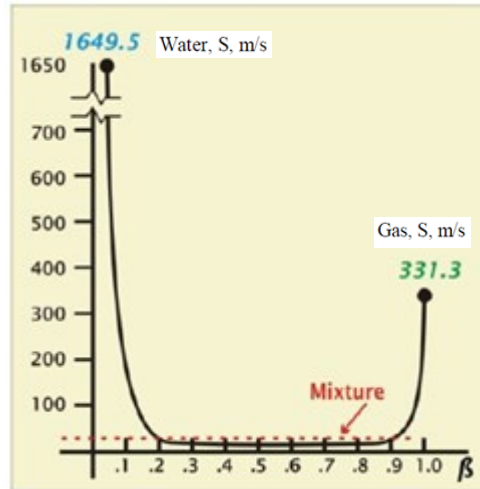


**Figure 5.14** Sonic speed on volumetric ratio of streams (Fisenko et al. 2010)

It was suggested that in the case of uniform multiphase flow, there is momentum exchange between the phases at the point of sudden change. This exchange mechanism is attributed to the elastic interaction of the gas molecules with the uniformly dispersed liquid particles and the sudden change in pressure prevails over the thermal exchange. The temperature of the gas is proportionally lower than the stagnation pressure in the same section. The momentum exchange between the phases depends on the viscous friction forces at the gas-liquid interface. Since heat exchange and friction occurs at the molecular level, the relaxation time will be related to the mean free path of the molecules. Also due to the dependence of momentum exchange on the elastic interaction of gas molecules with dispersed liquid droplets, the relaxation time is proportional to the collision frequency on the order of Avogadro's number. The mixing process accompany with the significant temperature decrease.

Overall, the energy of a system depends on the internal energy of the steam and cold medium simultaneously. In lieu of momentum exchange, sound speed sharply falls, and speed of flow and adiabatic compressibility abruptly increase. Experiments have also been conducted to understand the attenuation phenomenon of shock waves. The attenuation phenomena are based on the dissipation of the energy of the system. Some of the methodologies implemented include the increased roughness and use of baffles on the wall in case of shocks which demonstrates the wall friction effects (Schardin and Reichenbach, 1965; Reichenbach and Kuhl, 1995). Keeran and Neumann (1945) studied the apparent friction coefficient in pipes experimentally at subsonic and supersonic velocities for flow of air. It was observed that Mach number greater than 1 was rarely

maintained for lengths of 50 times diameter. This observation indicates the localized nature of flow characteristics. Also, the coefficient of friction was found to be a function of ratio of length to diameter and Reynolds number. Another strategy comprises of variation of the cross-sectional area to influence the strength of the shock wave (Igra et al., 2001).

### 5.3 Mathematical Modeling

Modeling is the critical and vital component of worst case discharge prediction. After having reviewing subsonic and supersonic flow characteristics, in this section, the relevant modeling concepts of WCD is discussed. The primary limitations of modern WCD models are neglecting the acceleration effects on two-phase flow. Okazaki (1980) developed two-phase flow model which accounts for accelerated flow, phase changes in thermodynamic equilibrium, wall friction, interphase friction and entropy increase in the system. The modeling technique relied on the premise of the density difference between the gas and liquid phase resulting in different acceleration and flowing velocity, and consequently interphase friction. The model used the basic equations comprised of continuity, momentum balance, and energy balance for the system. In addition, the constitutive equations included wall friction, interphase friction, and phase change during the depressurization. The only deviation from the WCD in this model was the use of the concept of evaporation which can be replaced with the concept of gas solubility when dealing with WCD case. The simultaneous differential equations were solved using Runge-Kutta-Gill numerical procedure treating the problem as initial value problem. The limiting condition to estimate the flow variables was obtained by implementing the condition of pressure gradient increasing to infinite at the exit. Accordingly, the mass flux rate was calculated. The model was validated using Ogasawara's experimental results, which provided the reservoir pressure at different discharge rate as shown in **Figure 5.15**.

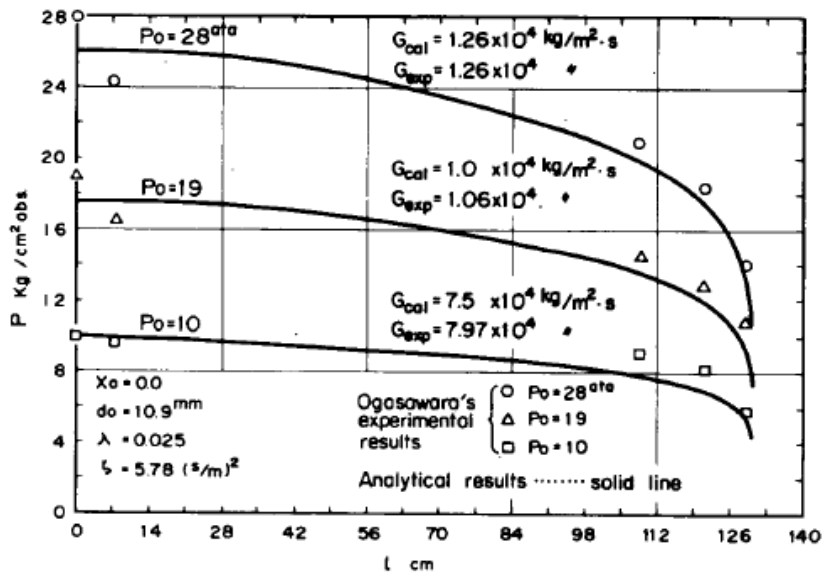


**Figure 5.15** Variation of absolute pressure along the distance from the inlet, G represents the mass flux rate, x is the vapor quality,  $d_0$  is the pipe diameter,  $\lambda$  is the coefficient of wall friction pressure drop,  $\xi$  is the coefficient of interphase frictional pressure drop (Okazaki, 1980).

After the validation of the model, gas and liquid velocity were calculated to get an insight into flow properties, which is depicted in **Figure 5.16**. The results suggested that gas phase was accelerated at the entrance accompanied with deceleration of liquid phase and a decrease in the gas void fraction. At the exit, steep increase in the velocity of gas and liquid phase was observed, which was attributed to a significant contribution from the pressure drop due to acceleration rather than friction. The developed model can be implemented for increased volumetric flow due to depressurization which is a replica of WCD. It was observed that the development of flow along the flow path is essential to analyze critical flow at the exit in case of critical flow (sonic) conditions, where the high-pressure fluid is discharged into the low-pressure domain.

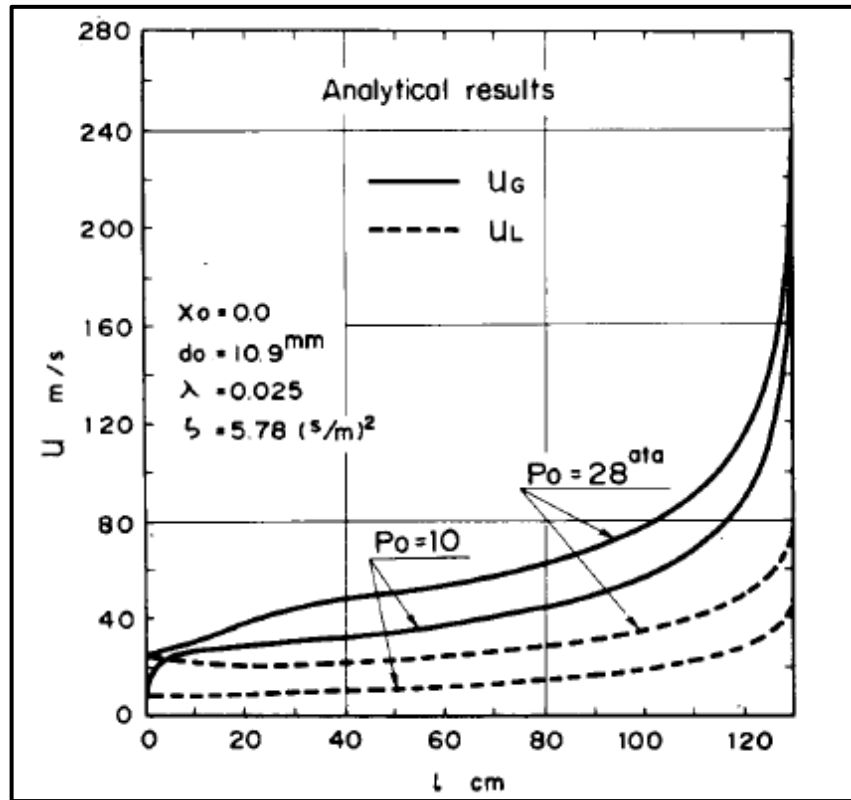


**Figure 5.16** Variation of gas and liquid velocity with the distance from the inlet at different reservoir pressure ( $P_0$ );  $U_G$  represents the gas velocity,  $U_L$  is the velocity of the liquid phase,  $x$  is the vapor quality,  $d_0$  is the pipe diameter,  $\lambda$  is the coefficient of wall friction pressure drop,  $\xi$  is the coefficient of interphase frictional pressure drop (Okazaki, 1980).

Continuing the previous work, Okazaki (1981) validated the model for higher pressure regions for experimental results from Fauske (1965) and Sozzi et al. (1975). The data from these two experiments are shown in **Table 5.2** and **Table 5.3**.

**Table 5.2 Experimental data and calculated results for Fauske’s experiment;  $\lambda$  is the coefficient of wall friction,  $\xi$  is coefficient of interphase friction (Okazaki, 1981)**

Diameter of the pipe (mm)	Initial Conditions		Critical Flow rate (kg/m <sup>2</sup> .s)	
	Upstream Pressure (psi)	Vapor Quality	Experimental results	Calculated results
6.8	310	0.191	4.1 x 10 <sup>3</sup>	4.1 x 10 <sup>3</sup>
6.8	170	0.1388	3.08 x 10 <sup>3</sup>	2.77 x 10 <sup>3</sup>
$\lambda = 0.03, \xi = 0.025$				

**Table 5.3 Experimental data and calculated results for Sozzi et al. (1975) experiment;  $\lambda$  is the coefficient of wall friction,  $\xi$  is coefficient of interphase friction (Okazaki, 1981)**

Pipe length (mm)	Initial Conditions		Critical Flow rate (kg/m <sup>2</sup> .s)	
	Upstream Pressure (psi)	Vapor Quality	Experimental results	Calculated results
12.7	978	0.0035	3.97 x 10 <sup>4</sup>	3.52 x 10 <sup>4</sup>
38.1	974	0.003	3.19 x 10 <sup>4</sup>	3.37 x 10 <sup>4</sup>
63.5	953	0.004	2.9 x 10 <sup>4</sup>	3.21 x 10 <sup>4</sup>
114	971	0.003	2.7 x 10 <sup>4</sup>	3.13 x 10 <sup>4</sup>
228	1005	0.003	2.7 x 10 <sup>4</sup>	2.94 x 10 <sup>4</sup>
318	995	0.003	2.53 x 10 <sup>4</sup>	2.83 x 10 <sup>4</sup>
508	967	0.002	2.29 x 10 <sup>4</sup>	2.52 x 10 <sup>4</sup>
635	960	0.003	2.29 x 10 <sup>4</sup>	2.45 x 10 <sup>4</sup>
1778	910	0.0002	1.88 x 10 <sup>4</sup>	1.92 x 10 <sup>4</sup>
Pipe diameter = 12.7 mm, $\lambda = 0.03, \xi = 0.025$				

Besides the analytical models, numerical models are the backbone for analyzing these types of flows. Recently, computational fluid dynamics algorithms have received growing attention of researchers to investigate multiphase flows. Numerous physical and modeling challenges have been outlined in the context of compressible flow over the years, still strong coupling during acoustic phenomenon is the primary issue. The speed of sound in the individual phase is comparatively higher than in two-phase mixtures. In addition, the compressibility in the flow domain might be limited to local regions, which poses unique situations for numerical schemes. In the past, several levels of modeling such as the Eulerian framework for both phases and Eulerian for carrier phase and Lagrangian for the dispersed phase are identified.

In the Eulerian framework, both phases are treated as a single fluid in the continuity equation, i.e. both phases as an interacting continuum. This type of simulations represent the presence of

all phases with certain volume fraction and no clear interfaces at a particular position in the flow field. In the Eulerian/Lagrangian framework, discrete nature of dispersed phase is considered by tracking the bubbles through the flow domain. The detail of basic CFD algorithms is discussed in Section 3.3.4. Here, the improvement in modeling effort with respect to Mach number  $0.3-1^+$  is reported. The success of CFD model in worst case discharge scenario depends on its ability to capture the compressibility of the flow field efficiently. In the ideal case, the system is assumed to be in equilibrium all the time, while in reality limited residence time and high gas ex-solution lead to substantial deviation from the system equilibrium. As the flow ascends and reaches the bubble point pressure, the thermodynamic equilibrium disrupts and at a certain degree of expansion, a shock like disturbance is generated abruptly. This phenomenon can be related to condensation shock generation in supersonic nozzle where the condensation shock generation leads to instantaneous heat generation that changes the pressure, temperature, and Mach number locally and disrupts the equilibrium of the system.

Federico et al. (2017) developed a customized model within ANSYS Fluent to include phase change and phase interaction models and exploit its capability. The model comprised of mixture model and tested with a well-known steam nozzle test case. The mixture model (single fluid model) consisted of Eulerian approach, where the conservation equations were included based on mixture properties and general Navier-Stokes equation for compressible flow. The mixture properties were quantified in terms of extensive thermodynamic properties such as enthalpy, entropy, and total energy; and intensive properties such as density, temperature, and specific heat capacity using mass weighted averages. In addition, the model used transport equation including conservation of liquid mass and number of droplets which was based on the rate of nucleation of newly generated droplets using classical nucleation theory. The closure equation included flow governing equation based on liquid mass generation rate per unit volume of the mixture. Also, the non-equilibrium phase change of vapor used the fluid properties in a metastable condition which is extrapolated from the generic equation of state. The computations were carried out using  $k-\omega$  SST turbulence model and pressure-based solver. In addition, third order accurate QUICK scheme was used for spatial discretization of transport equation to limit the numerical diffusion scheme ( $k$  refers to the turbulent kinetic energy in J/kg, and  $\omega$  refers to the specific rate of dissipation in 1/s).

Another modeling study (Chang and Bai 2017) on high-velocity compressible flow was conducted to investigate gas well deliquification. The study used supersonic nozzle to atomize liquid by virtue of shear forces generated by the gas jet. Although the study included the verification of nozzle configuration for efficient atomization, it provided insight into the numerical modeling of mist flow regime which occurs at high gas flow rate. The concept of mist flow relies on the suspension properties of the critical droplet diameters which can be given by the equation below.

$$d_{cri} = \frac{3u^2 \xi \rho_g}{4g(\rho_l - \rho_g)} \quad (5.7)$$

where,  $d_{cri}$  is the critical diameter of the droplet,  $u$  is the gas velocity,  $\xi$  is the friction factor,  $\rho_l$  is the liquid density,  $\rho_g$  is the gas density, and  $g$  is acceleration due to gravity.

The numerical model was setup using the continuity, momentum and energy equations. The  $k-\omega$  model was chosen over  $k-\epsilon$  for turbulent flow due to its better accuracy for wall treatment and complex boundary layer flow under extreme pressure gradient ( $\epsilon$  refers to the turbulent dissipation in J/kg-s). However, it is worth mentioning that the feasibility of  $k-\epsilon$  model for fully turbulent flow is high, but it performs poorly for complex flows with a high-pressure gradient, strong streamline curvature, and separation between phases. The results suggested that the low velocity and high-pressure gas flow occurs through the convergent section in subsonic conditions and contracts in the throat, while in the divergent section the high velocity and low-pressure gas expands in the supersonic conditions. The supersonic speed of the gas in the divergent section was attributed to a reduction in the gas density with increase in its volume.

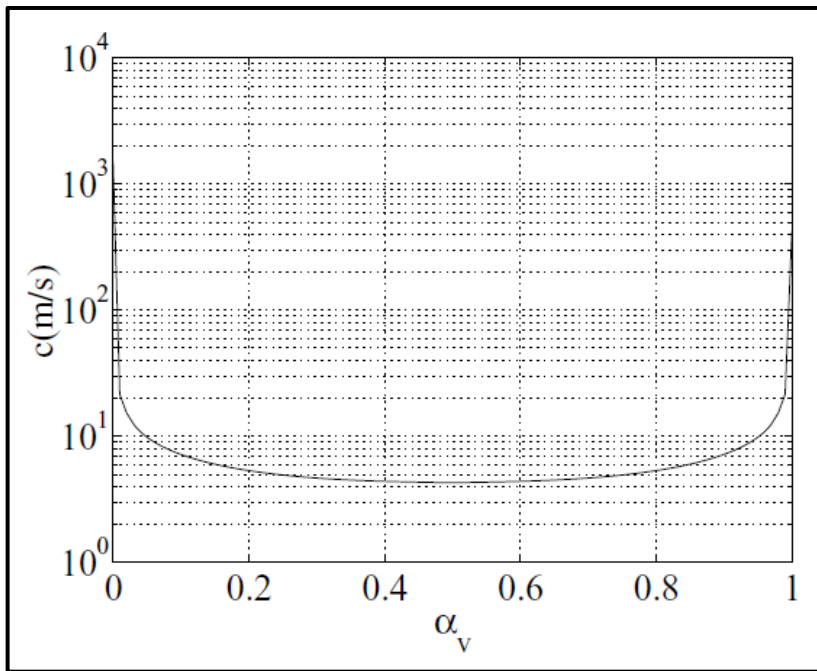


**Figure 5.17** Variation in speed of sound in multiphase mixture flow with void fraction (Venkateswaran et al., 2002)

Venkateswaran et al. (2002) developed a numerical model to study the effects of compressibility in multiphase flow with transonic/supersonic conditions (**Figure 5.17**). It was assumed that the incompressible flow and low Mach number compressible flow exist for pure liquid phase and pure vapor phase, respectively. The primary issue with such mixture flows with compressibility effects are a strong coupling of an acoustic phenomenon which can be resolved by characterizing the local regions. The model used time marching techniques for high-speed compressible flow.

Different numerical techniques such as eigenvalue analysis, perturbation analysis, and preconditioning were employed to solve the equation of motion for volume fraction and mass fraction. The model was validated using the results for standard shock tube problem. It is worthy to notice that in computational fluid dynamics, the numerical models are tested using shock tube problem. The reason for using shock tube problem as a means of validating the numerical scheme is the availability of analytical solution for the shock tube problem.

Another challenge with regards to the numerical modeling is to incorporate the effects of pressure and temperature on solubility of gas. This effect can be addressed using the concept of mass transfer between the phases. In the CFD modeling, it can be addressed using liquid phase mass transfer coefficient, gas-liquid interfacial area, and solubility that depends on in-situ conditions (Nedelchev, 2017; Leonard et al., 2015). There are several correlations which have been developed over past decades to estimate solubility in petroleum fluids. For instance, the Vasquez and Beggs correlation which depends on pressure, temperature, and specific gravity of gas and liquid (Vasquez and Beggs, 1980).

Overall, there is a lack of CFD studies for subsonic and supersonic flows in large diameter pipes. However, supersonic/subsonic conditions have been used in different studies. Based on the past studies, it can be inferred that the effect of gas compressibility, impact of phase transfer in the model will be required to achieve the subsonic/supersonic conditions. High order solver scheme will be needed to resolve the stability issues in localized regions of the model. K- $\omega$  model will be suited for compressible flow. In order to develop the computational tools, the model needs to address the issue of acceleration of the gas phase. At high velocity, this characteristic has a dominant effect on pressure drop calculations.

#### **5.4 Subsonic/Supersonic Discharge Conditions**

In addition to the modeling of two-phase flow in tubes, there are several incidents which have similar discharge characteristics as that of worst case discharge (WCD) during blowouts. Some of these incidents include volcanic eruptions and discharge from the ruptured nuclear vessel through the pipe. In order to understand the nuances of WCD, it is worthwhile to study these case studies having the subsonic and supersonic conditions. One of such scenario is rapid depressurization during rupture of vessel or pipe containing high-pressure fluid which can be modeled using the theoretical concept of critical flow. The basic premise of the non-equilibrium modeling, depends on the characterization of the rapid depressurization because of the absence of thermodynamic equilibrium in the flow field. In such scenarios, the flow field has a finite relaxation time, and two-phase mixture accelerates rapidly. Several models have been developed. However most of these models characterize the thermal and mechanical equilibrium condition at the expense of numerous in-situ information about the flow characteristics such as bubble diameter, interphase friction, and heat transfer characteristics. However, the non-equilibrium models are a rarity in the conventional study for multiphase flow in pipes.

Dobran (1987) developed the non-equilibrium model of two-phase critical flows in tubes to improve the modeling capability and obtain the critical flow conditions at the exit. The model comprises of conservation and constitutive equations for two-phase flow discharging through variable area duct as depicted in **Figure 5.18**. The constitutive equations included the virtual drag coefficient, interfacial area per unit volume, virtual mass coefficient, interfacial heat transfer, and wall friction.

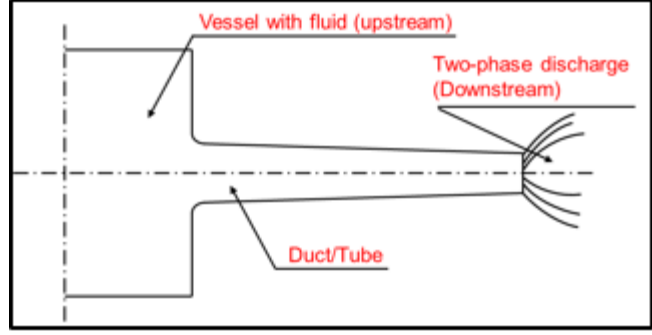


**Figure 5.18** Two-phase flow discharging through a variable duct (Prepared after Dobran, 1987)

The model comprises of conservation and constitutive equations for two-phase flow discharging through variable area duct as depicted in **Figure 5.18**. The constitutive equations included the virtual drag coefficient, interfacial area per unit volume, virtual mass coefficient, interfacial heat transfer, and wall friction.

In the non-equilibrium models, hydrodynamic and thermal non-equilibrium exists. The hydrodynamic non-equilibrium is due to the difference in velocity and pressure difference between the phases while thermal non-equilibrium arises due to the difference in temperature between both phases. The equilibrium model assumes no heat transfer resistance, but in real flow conditions, there is finite heat transfer resistance which implies that the thermal relaxation time is not zero. The temperature of phases at upstream and downstream can vary due to flow disturbance. To achieve the equilibration of temperature through the process of heat transfer between the phases, the process takes finite time. This time is referred as thermal relaxation time. As the two-phase mixture accelerates rapidly, the non-equilibrium model shows deviation from the equilibrium models due to the existence of finite thermal relaxation time. This model is solved considering that the critical flow is dependent on the history of flow up to the critical point. The thermal and mechanical non-equilibrium is defined based on the initial nucleation site density, bubble diameter, interphase friction characteristics, and heat transfer for different flow regimes. The Dobran (1987) models consider the non-equilibrium model. The model assumes that gas phase is in thermal equilibrium and both phases are at the same pressure at any cross-section of the tube. The constitutive equation for modeling of ruptured vessels are given below:

Conservation of mass for gas phase:

$$\rho_G A u_G \frac{d\alpha}{dz} + \alpha A u_G \frac{d\rho_G}{dP} \frac{dP}{dz} + \alpha \rho_G A \frac{du_G}{dz} - M_f \frac{dx_q}{dz} = -\alpha \rho_G u_G \frac{dA}{dz} \quad (5.8)$$

where  $\rho_G$  is the density of the gas phase,  $A$  is cross-sectional area of the tube,  $P$  is the pressure,  $u_G$  is axial velocity of the gas phase in the tube,  $M_f$  is the total mass flow rate,  $x_q$  is the quality,  $z$  is distance from the inlet, and  $\alpha$  is the gas void fraction. Conservation of mass for liquid phase:

$$-\rho_L A u_L \frac{d\alpha}{dz} + (1 - \alpha) A u_L \left( \frac{d\rho_L}{dP} \right)_{h_L} \frac{dP}{dz} + (1 - \alpha) \rho_L A \frac{du_L}{dz} + M_f \frac{dx_q}{dz} + (1 - \alpha) A u_L \left( \frac{d\rho_L}{dh_L} \right)_P \frac{dh_L}{dz} = -(1 - \alpha) \rho_L u_L \frac{dA}{dz} \quad (5.9)$$

where  $\rho_L$  is the density of the liquid phase,  $u_L$  is the axial velocity of the liquid phase in the tube,  $h_L$  is enthalpy of the liquid phase. Conservation of momentum for gas phase:

$$\begin{aligned} & [\rho_G u_G \alpha A + \Delta_{GG} A u_G] \frac{du_G}{dz} + [-\Delta_{GG} A u_L] \frac{du_L}{dz} + [\alpha A] \frac{dP}{dz} - [\eta(u_G - u_L) M_f] \frac{dx_q}{dz} = \\ & -A \xi_{GG} (u_G - u_L) - \rho_G g \alpha A \cos \theta \end{aligned} \quad (5.10)$$

where  $\Delta_{GG}$  is the virtual mass coefficient for relative acceleration between the phases,  $\xi_{GG}$  is the viscous drag coefficient for relative acceleration between the phases,  $\eta$  is the energy redistribution coefficients,  $\theta$  is the angle from the vertical, and  $g$  is acceleration due to gravity. Conservation of momentum for liquid phase:

$$\begin{aligned} & [-\Delta_{GG} A u_G] \frac{du_G}{dz} + [(1 - \alpha) \rho_L A u_L + \Delta_{GG} A u_L] \frac{du_L}{dz} + [(1 - \alpha) A] \frac{dP}{dz} + [(1 - \eta)(u_G - \\ & u_L) M_f] \frac{dx_q}{dz} = A \xi_{GG} (u_G - u_L) - \rho_L g (1 - \alpha) A \cos \theta - F_{wL} A \end{aligned} \quad (5.11)$$

where  $F_{wL}$  is the drag forces per unit volume exerted on the liquid by the wall. Conservation of energy for two-phase flow mixture with adiabatic wall:

$$\begin{aligned} & M_f \left[ h_{LG} + \frac{1}{2} (u_G^2 - u_L^2) \right] \frac{dx_q}{dz} + M_f \left[ x_q M_f \frac{dh_G}{dP} \right] \frac{dP}{dz} + [x_q M_f u_G] \frac{du_G}{dz} + [(1 - \\ & x_q) M_f u_L] \frac{du_L}{dz} + [(1 - x_q) M_f] \frac{dh_L}{dz} + M_f g \cos \theta = 0 \end{aligned} \quad (5.12)$$

where  $M_f$  is the total mass flow rate,  $h_{LG}$  is the difference in enthalpy of gas and liquid,  $h_G$  is enthalpy of the gas phase,  $h_L$  is the enthalpy of the liquid phase. Conservation of energy for liquid phase:

$$M_f \left[ h_{LG} + \frac{1}{2} (u_G^2 - u_L^2) \right] \frac{dx_q}{dz} = \frac{d\dot{Q}_L}{dz} \quad (5.13)$$

where  $\dot{Q}_L$  heat transfer rate.

There are six constitutive equations which are solved to obtain a void fraction ( $\alpha$ ), quality ( $x_q$ ), the velocity of gas ( $u_G$ ), the velocity of liquid ( $u_L$ ), pressure ( $P$ ), and enthalpy of liquid ( $h_L$ ). Other parameters can be determined using the following relations. Viscous Drag Coefficient,  $\xi_{GG}$  can be obtained by using Equation 5.14.

$$\xi_{GG} = \frac{2Cf_i}{D} \sqrt{\alpha} \rho_G (u_G - u_L) \quad (5.14)$$

where the interfacial friction coefficient ( $Cf_i$ ) is given by following equation for different flow regimes. For Bubbly flow:

$$Cf_i = \frac{3}{8} C_{D_{1-\alpha}} (1 - \alpha)^3 \sqrt{\alpha} \frac{\rho_L D}{\rho_G d}; 0 < \alpha \leq \alpha_b \quad (5.15)$$

where  $C_{D_{1-\alpha}}$  is the bubble drag coefficient,  $d$  is the average bubble diameter,  $D$  is tube diameter, and  $\alpha_b$  is generally assumed to 0.3. For the annular flow:

$$Cf_i = 0.079 Re_G^{-0.25} \left[ 1 + 24(1 - \sqrt{\alpha}) \left( \frac{\rho_L}{\rho_G} \right)^{1/3} \right]; \alpha_a \leq \alpha < 1 \quad (5.16)$$

where and  $\alpha_a$  is assumed to 0.8.  $Re_G$  is the Reynolds number for the gas phase and can be calculated using equation 5.17.

$$Re_G = \frac{\rho_G D |u_G - u_L|}{\mu_G} \quad (5.17)$$

where  $\mu_G$  is the viscosity of the gas phase. For the churn and turbulent flow, the interfacial friction coefficient ( $C_{fi}$ ) can be given by Equation 5.18.

$$C_{fi} = C_{fib} + \left( \frac{C_{fib} - C_{fia}}{\alpha_b - \alpha_a} \right) (\alpha - \alpha_b); \alpha_a < \alpha < \alpha_b \quad (5.18)$$

In the Equation 5.15, the bubble drag coefficient  $C_{D_{1-\alpha}}$  can be determined using Equation 5.19.

$$C_{D_{1-\alpha}} = C_D (1 - \alpha)^{-4.7} \quad (5.19)$$

where single bubble drag coefficient is calculated based on Reynolds number.

$$C_D = \frac{24}{Re} (1 + 0.15 Re^{0.687}); Re \leq 1000 \quad (5.20)$$

$$C_D = 0.44; Re > 1000 \quad (5.21)$$

where Reynolds number,  $Re$  is determined using following equation.

$$Re = \frac{\rho_L d (1 - \alpha) |u_G - u_L|}{\mu_L} \quad (5.22)$$

where  $d$  is the average bubble diameter and can be determined by the following equation:

$$d = \frac{6\alpha}{a} \quad (5.23)$$

where interfacial area per unit volume ( $a$ ) can be evaluated by following equations for different flow regimes:

For Bubble flow regime:

$$a = N\pi \left( \frac{6\alpha}{N\pi} \right)^{2/3}; 0 < \alpha \leq \alpha_b \quad (5.24)$$

For annular flow regime:

$$a = \frac{4}{D} \sqrt{\alpha}; \alpha_a \leq \alpha < 1 \quad (5.25)$$

For churn-turbulent flow regime:

$$a = a_b + \left( \frac{a_b - a_a}{\alpha_b - \alpha_a} \right) (\alpha - \alpha_b); \alpha_a < \alpha < \alpha_b \quad (5.26)$$

where  $a_b$  and  $a_a$  are evaluated using Equations 5.24 and 5.25 considering  $\alpha = \alpha_a$  and  $\alpha_b$  respectively. Virtual Mass Coefficient,  $\Delta_{GG}$  is given by the following expression:

$$\Delta_{GG} = \alpha \rho_L C_{VM} \quad (5.27)$$

where the coefficient  $C_{VM}$  is determined by the following equation:

$$C_{VM} = 0.3 \tanh(4\alpha) \quad (5.28)$$

Interfacial Heat Transfer

$$\frac{d\dot{Q}_L}{dz} = \tilde{h}aA(T_L - T_G) \quad (5.29)$$

where  $T_L$  and  $T_G$  are the temperatures of liquid and gas phase, respectively, and interfacial heat transfer coefficient,  $\tilde{h}$  is modeled according to flow regime based on the Nusselt number (Nu). For bubble flow regime:

$$Nu = \frac{\tilde{h}d}{k_L} = 2 + 0.6Re_b^{0.5}Pr_L^{1/3}; 0 < \alpha \leq \alpha_b \quad (5.30)$$

where  $Pr_L$  is the Prandtl number for the liquid phase,  $\tilde{h}$  is the heat transfer coefficient,  $k_L$  is thermal conductivity of the liquid phase,  $Re_b$  is the Reynolds number and can be calculated using Equation 5.31.

$$Re_b = \frac{Re}{1-\alpha} = \frac{\rho_L d |u_G - u_L|}{\mu_L} \quad (5.31)$$

For annular flow regime:

$$Nu = \frac{\tilde{h}D\sqrt{\alpha}}{k_G} = 0.023Re_{Ga}^{0.8}Pr_G^{1/4}; \alpha_a \leq \alpha < 1 \quad (5.32)$$

where  $k_G$  is the thermal conductivity of the gas phase,  $Re_{Ga}$  is Reynolds number for gas phase corresponding to annular flow regime,  $Pr_G$  is the Prandtl number for the gas phase. The Reynolds number  $Re_{Ga}$  can be calculated using Equation 5.33.

$$Re_{Ga} = \frac{\rho_G D \sqrt{\alpha} |u_G - u_L|}{\mu_G} \quad (5.33)$$

For churn-turbulent regime:

$$\tilde{h} = \tilde{h}_b + \left( \frac{\tilde{h}_b - \tilde{h}_a}{\alpha_b - \alpha_a} \right) (\alpha - \alpha_b); \alpha_a < \alpha < \alpha_b \quad (5.34)$$

where  $\tilde{h}_b$  is the heat transfer coefficient and can be calculated using Equation 5.30 with  $\alpha = \alpha_b$  and  $\tilde{h}_a$  is the heat transfer coefficient and can be calculated using Equation 5.32 with  $\alpha = \alpha_a$ . The drag force per unit volume of the mixture can be defined in terms of wall shear stress which can be represented by following equation and represents the wall friction force,  $F_{wL}$ :

$$F_{wL} = \frac{4}{D} \tau_w = - \left( \frac{dP}{dz} \right)_{wall\ friction} \quad (5.35)$$

where  $\tau_w$  is the wall shear stress,  $\left( \frac{dP}{dz} \right)_{wall\ friction}$  is the pressure gradient due to wall friction.

The wall friction force,  $F_{wL}$  is modeled using Chisholm correlation and is defined using the following set of Equations (5.36-5.41).

$$F_{wL} = -\phi_{LO}^2 \left( \frac{dP}{dz} \right)_{FLO} \quad (5.36)$$

where  $\left( \frac{dP}{dz} \right)_{FLO}$  is the pressure gradient due to liquid friction only and is calculated using following relation:

$$\left( \frac{dP}{dz} \right)_{FLO} = \frac{4}{D} f_{LO} \frac{G^2}{2\rho_L} \quad (5.37)$$

where  $f_{LO}$  is single phase frictional coefficient for liquid only, and  $G_1$  is the mass flux.

$$\phi_{LO}^2 = 1 + (Y^2 - 1) \left[ Bx^{(2-n)/2}(1-x)^{(2-n)/2} + x^{2-n} \right] \quad (5.38)$$

where  $n = 0.25$  and the single-phase frictional coefficient,  $f_{LO}$  is given by:

$$f_{LO} = \frac{16}{Re_{LO}}; Re_{LO} = \frac{G_1 D}{\mu_L} \leq 2000 \quad (5.39)$$

$$f_{LO} = 0.079 Re_{LO}^{-0.25}; Re_{LO} = \frac{G_1 D}{\mu_L} > 2000 \quad (5.40)$$

$$Y^2 = \frac{\left( \frac{dP}{dz} \right)_{GO}}{\left( \frac{dP}{dz} \right)_{LO}} = \frac{f_{GO}}{f_{LO}} = \frac{\rho_L}{\rho_G} \quad (5.41)$$

where  $f_{GO}$  is single phase frictional coefficient for gas only which can be calculated using the equations similar to 5.39 and 5.40. The only difference will be that instead of liquid properties, gas properties will be used. Also, the parameter B in Equation 5.38 is determined from the following table:

Y	$G_1$	B
$Y \leq 9.5$	$\leq 500$	4.8
	$500 < G_1 < 1900$	$2400/G_1$
	$\geq 1900$	$55/G_1$
$9.5 < Y < 28$	$\leq 600$	$520/(YG_1^{0.5})$
$Y \geq 2.8$	$> 600$	$21/Y$

The modeling results were primarily validated for critical mass fluxes and pressure distribution using the experimental data from Celata et al. (1983). The model was then extended to study the void fraction, quality, liquid and vapor velocity, and subcooling distribution in the tube. It was observed that the gas and liquid velocities are almost equal except towards the end where gas velocity becomes larger than the liquid velocity (**Figure 5.19**). This phenomenon is attributed to the establishment of mechanical equilibrium while the system is thermally under non-equilibrium conditions. The lack of thermodynamic equilibrium is attributed to the increase in acceleration effects towards the tube end.

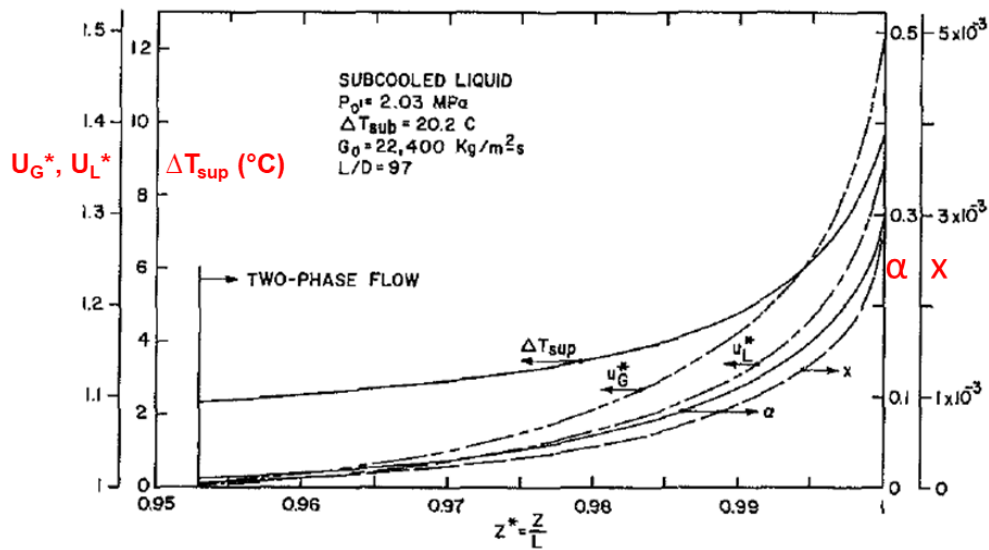
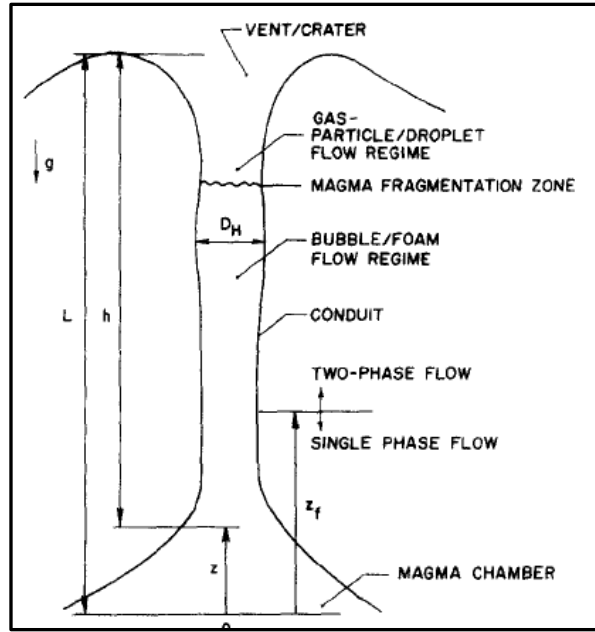


Figure 5.19 Numerical results for flow characteristics and fluid properties,  $U_G^*$  is dimensionless superficial gas velocity,  $U_L^*$  is dimensionless superficial liquid velocity,  $\alpha$  is the volumetric gas fraction,  $x$  is quality (Modified after Dobran, 1987).

Similar to worst case discharge conditions, the volcanic eruptions present the phenomenon of magma discharge through a conduit at subsonic and supersonic conditions. Though the magma flow involves highly viscous fluid, the systemic understanding will assist modeling of WCD. Studies suggest that the magma pressure at the exit is atmospheric. The cross-sectional area assumes a constant shape till the localized two-phase flow velocity becomes sonic. Above this depth, the flow can be supersonic in nature when the area of the conduit increases (Dobran, 1987). It has also been observed that the exit pressures become larger than the atmospheric pressure and the exit flow becomes supersonic, interacting with the localized condition through the system of shocks.

Later, Dobran (1992) presented a steady-state one-dimensional non-equilibrium two-phase flow model to predict the local flow characteristics of volcanic eruptions. The magma flow is considered to be a quasi-steady state flow in which magma accelerates from the static state and releases the dissolved gas (**Figure 5.20**) at a certain height ( $Z_f$ ). Up to this height, the flow was considered to be of single phase in nature in which the mean density and viscosity are assumed to be constant. The single-phase model used the Bernoulli's equation to calculate the height where the dissolved gas starts to come out of the magma. Above this height, the fluid assumes a bubbly flow patterns which can be modeled using the expressions for mass and



**Figure 5.20** Flow regime profile for volcanic eruption (Dobran, 1992)

momentum balance for mixture phase and gas phase. The mixture phase contains liquid and gas bubbles. The forces considered in this phase are interfacial drag forces and frictional effects. The next phase is the fragmentation zone where the continuous gas phase is in contact with the wall and droplets/particles dispersed in gas and dragged along with the expanding gas phase. This zone is more likely a shock generation region in the fluid flow. Similar to the bubbly flow regime, the flow properties of dispersed gas/particle phase was solved using mass balance and momentum equations with a different set of drag coefficients and frictional coefficients. The distinction between the two main flow regimes was made on the basis of void fraction. The bubbly flow regime was assumed for void fraction of 0.75, while the dispersed regime in the range of 0.75-1.

In the fragmented zone, shock generation occurs at the point where the gas phase evolves and separates from the liquid phase. Under this flow condition, the gas and the melt travel with their respective velocity. The frictional pressure loss is calculated using a pipe flow model using liquid viscosity. Also, the slip velocity between droplets and gas phase is calculated considering the flow as a dynamic equilibrium of dilute gas dispersions. In the Dobran (1992) model, the exit condition is assumed sonic. Also, a non-equilibrium flow scenario is considered for bubbly and gas-particle/droplet regimes. The length of fragmentation zone is estimated using the upper boundary condition of the bubbly flow and lower boundary condition of the gas/droplet regime. This consideration implies that the level at which difference between pressure gradients of bubbly and pure liquid flows exceeds a critical value is the lower boundary for generation of shock waves. The upper boundary is represented by the gas velocity at which particles are supported by the upward gas flow.

The non-equilibrium model for volcanic eruption considers two flow regimes: single-phase and two-phase flow regime. The single-phase flow regime is described by assuming that flow of magma is in quasi-steady state condition in which at a particular height, gas starts evolving from the solution and two-phase flow develops. The governing equations are given below:

**Single phase flow regime:**

In this model, the length of single-phase regime ( $z_f$ ) is calculated on the basis of Bernoulli equation and can be given by the following equation:

$$z_f = \frac{D_H}{4f} \left[ \frac{2\rho_L(P_o - P_f)}{G^2} - 1 + K_1 \right] \times \frac{1}{1 + \frac{2\rho_L g D_H}{G^2 4f}} \quad (5.42)$$

where  $P_o$  is magma chamber pressure in stagnation state,  $P_f$  is the pressure of single-phase region,  $\rho_L$  is the effective density of liquid which is magma,  $G$  is the mass flux,  $f$  is the friction loss coefficient,  $D_H$  is the hydraulic diameter,  $K_1$  is the entrance loss coefficient ( $K_1 = 0.03-0.05$  for smooth entrance and  $K_1 = 0.4-0.5$  for sharp edged entrances. The friction coefficient,  $f$  is given by following equation:

$$f = \frac{B_1}{Re} + B_2 \quad (5.43)$$

where  $Re$  is Reynolds number and is calculated using Equation 5.44:

$$Re = \frac{GD_H}{\mu_L} \quad (5.44)$$

where  $\mu_L$  is magma viscosity,  $Re$  is Reynolds number. For circular conduit,  $B_1=16$  and  $B_2 = 0.01-0.05$ . The minimum velocity of magma through the conduit is given by the following equation:

$$u_{fmin} = \frac{B_1 \mu_L}{B_2 \rho_L 2 D_H} \left\{ \left( 1 + \frac{4B_2 \rho_L (\rho_c - \rho_L) 8g D_H^3}{(4B_1)^2 \mu_L^2} \right)^{1/2} - 1 \right\} \quad (5.45)$$

**Two-phase flow regime:**

Mass balance for gas phase:

$$M_G = \rho_G \alpha A u_G = X M_f \quad (5.46)$$

where  $M_G$  is the mass flow rate of the gas,  $M_f$  is the total mass flow rate,  $X$  is the evolved fraction of gas,  $A$  is cross-sectional area,  $u_G$  is the velocity of the gas phase,  $\alpha$  is the gas volumetric fraction. Mass balance for liquid phase:

$$M_L = \rho_{Lm} (1 - \alpha) A u_L = (1 - X) M_f \quad (5.47)$$

where  $M_L$  is the mass flow rate of the liquid phase,  $\rho_{Lm}$  is the mean magma density,  $u_L$  is velocity of the liquid phase. The mean magma density,  $\rho_{Lm}$  having gas mass fraction  $Y$  is given by following Equations 5.48 and 5.49:

$$\frac{1}{\rho_{Lm}} = \frac{Y}{\rho_G} + \frac{1-Y}{\rho_L} \quad (5.48)$$

where  $Y$  is gas mass fraction and is calculated using the constitutive equation for solubility as shown below:

$$Y = S_c P^m \quad (5.49)$$

where  $S_c$  is the solubility constant and  $m$  is an exponent of solubility law. Momentum balance for gas phase:

$$\rho_G u_G A \alpha \frac{du_G}{dz} = -\alpha A \frac{dP}{dz} - F_{LG} A - F_{wG} A - \rho_G g A \alpha \quad (5.50)$$

where  $\rho_G$  is the density of the gas phase,  $z$  is depth,  $P$  is the pressure,  $F_{LG}$  is interfacial drag forces between the phases,  $F_{wG}$  is friction force between wall and gas phase,  $F_{wL}$  is the frictional force between wall and liquid phase,  $g$  is acceleration due to gravity. Momentum balance for liquid phase:

$$\rho_{Lm} u_L A (1 - \alpha) \frac{du_L}{dz} = -(1 - \alpha) A \frac{dP}{dz} + F_{LG} A - F_{wL} A - \rho_{Lm} g A (1 - \alpha) \quad (5.51)$$

The drag forces can be calculated using following relations:

$$F_{LG} = \xi_{GG} (u_G - u_L) \quad (5.52)$$

where  $\xi_{GG}$  is the viscous drag coefficient for relative acceleration between the phases.

$$F_{wL} \neq 0; \text{ in bubbly flow region and } = 0; \text{ in gas/droplet flow regime} \quad (5.53)$$

$$F_{wG} = 0; \text{ in bubbly flow region and } \neq 0; \text{ in gas/droplet flow regime} \quad (5.54)$$

The evolved gas fraction,  $X$  is given by the following equation:

$$X = \frac{X_f + Y_f(1 - X_f) - Y}{1 - Y} \quad (5.55)$$

where  $X_f$  is the maximum evolved gas fraction,  $Y_f$  is the maximum dissolved gas mass fraction in the magma and can be calculated using Equation 5.49. The constitutive equations for bubbly or gas/particle regimes can be given by following equations

$$\xi_{GG} = \frac{2Cf_1}{D_H} \sqrt{\alpha} \rho_G (u_G - u_L) \quad (5.56)$$

where  $Cf_1$  is the interfacial friction coefficient.

$$F_{wL}, F_{wG} = \frac{2f_{TP}G^2}{D_H \rho_m} \quad (5.57)$$

where  $f_{TP}$  is the two-phase friction factor and can be calculated from Equation 5.58.

$$f_{TP} = \frac{B_1}{Re} + B_2 \quad (5.58)$$

where  $Re$  is Reynolds number which can be calculated using following relation:

$$Re = \frac{GD_H}{\mu_m} \quad (5.59)$$

where  $\mu_m$  is the viscosity of mixture phase.

$$\rho_m = \alpha\rho_G + (1 - \alpha)\rho_{Lm} \quad (5.60)$$

where  $\rho_m$  is the density of the mixture.

**For bubble regime:**

The range of gas volumetric fraction is assumed to be between 0 and 0.75 ( $0 \leq \alpha \leq 0.75$ ).

$$C_D = \frac{24}{Re_b} (1 + 0.15Re_b^{0.687}); Re_b \leq 1000 \quad (5.61)$$

$$C_D = 0.44; Re_b > 1000 \quad (5.62)$$

where  $C_D$  is the drag coefficient which depends on the Reynolds number. The Reynolds number for bubble flow regime,  $Re_b$  is given by the Equation 5.63:

$$Re_b = \frac{\rho_L d_b (1 - \alpha) |u_G - u_L|}{\mu_m} \quad (5.63)$$

where  $d_b$  is the bubble diameter.

$$d_b = \left( \frac{6\alpha}{\pi N} \right)^{1/3} \quad (5.64)$$

where  $N$  is bubble nucleation density. For steam water systems  $N = 10^{11} \text{ m}^{-1}$ .

$$\mu_m = \mu_L (1 - \alpha)^{-2.5(\mu_G + 0.4\mu_L)} / (\mu_G + \mu_L) \quad (5.65)$$

where  $\mu_L$  is the viscosity of liquid phase and  $\mu_g$  is the viscosity of gas phase. The interfacial friction coefficient,  $Cf_1$  is given by equation 5.66.

$$Cf_1 = \frac{3}{8} C_{D_{1-\alpha}} (1 - \alpha)^3 (\alpha)^{1/2} \frac{\rho_L D_H}{\rho_G d_b} \quad (5.66)$$

$$C_{D_{1-\alpha}} = C_D (1 - \alpha)^{-4.7} \quad (5.67)$$

where  $C_{D_{1-\alpha}}$  is bubble drag coefficient. The friction between wall and gas phase,  $F_{wG}$  for bubble regime is considered to be 0.

$$F_{wG} = 0 \quad (5.68)$$

**For Gas-particle/droplet regime:**

The range of void fraction is assumed to be between 0.75 and 1 ( $0.75 \leq \alpha \leq 1$ ). The drag coefficient,  $C_D$  is given by following relations defined in Equations 5.69-5.72.

For  $r_d^* < 34.65$

$$C_D = \frac{24}{Re_b} (1 + 0.1Re_b^{0.75}) \quad (5.69)$$

$$r_d^* = \frac{d_d}{z} \left( \frac{\rho_G g (\rho_L - \rho_G)}{\mu_G^2} \right)^{1/3} \quad (5.70)$$

where  $d_d$  is the particle/droplet diameter.

$$C_D = 0.45 \left( \frac{1+17.67[f(1-\alpha)]^{6.7}}{18.67[f(1-\alpha)]} \right)^2 \quad (5.71)$$

For  $r_d^* \geq 34.65$

where  $f(1 - \alpha)$  is a constant and can be determined using following relation:

$$f(1 - \alpha) = \alpha^{0.5} \frac{\mu_G}{\mu_m} \quad (5.72)$$

For particle/droplet regime, the coefficient of interfacial friction,  $Cf_1$  is described by following equation.

$$Cf_1 = \frac{3}{8} \frac{1-\alpha}{\alpha^{0.5}} \frac{D_H}{d_d} C_D \quad (5.73)$$

where  $C_D$  is the drag coefficient and can be determined by relations defined by Equations 5.69-5.72. Also,  $d_d$  is the particle/droplet diameter and is given by Equation 5.74.

$$d_d = \frac{4\sigma}{(\sigma g (\rho_L - \rho_G))^{0.5}} \quad (5.74)$$

where  $\sigma$  is the surface tension. The Reynolds number for particle droplet regime,  $Re_d$  is defined by the equation given below:

$$Re_d = \frac{\rho_G d_d |u_G - u_L|}{\mu_m} \quad (5.75)$$

$$\mu_m = \mu_L \left( 1 - \frac{1-\alpha}{\alpha_{dm}} \right)^{-2.5\alpha_{dm}(\mu_G + 0.4\mu_L)} / (\mu_G + \mu_L) \quad (5.76)$$

where maximum particle density,  $\alpha_{dm} = 0.62$ . The friction between wall and liquid phase,  $F_{wL}$  in this regime is considered to be 0.

$$F_{wL} = 0 \quad (5.77)$$

The modeling results were compared with the homogeneous model, and a significant deviation was observed (**Figure 5.21**). The model also exhibited a drastic upsurge in velocity towards the exit of the conduit, which can replicate the sonic conditions.

Melnik (2000) studied the ascent of gas saturated magma using non-equilibrium two-phase model under steady and unsteady state conditions. The model was established based on three flow regimes during the upward flow (**Figure 5.22**) similar to Dobran (1992). At the bottom of the conduit, bubbly liquid exists and changes into the gas-particle flow in the upper section, when a critical overpressure condition is encountered. The transition zone between bubbly flow and dispersed gas flow is described in terms of discontinuity elucidated by fragmentation wave.

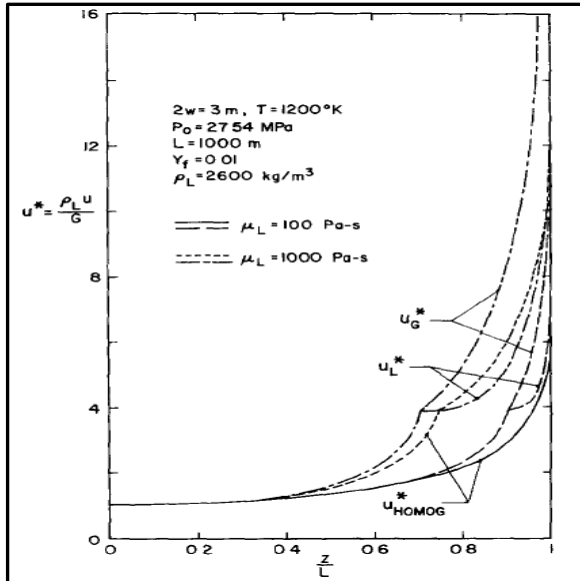


Figure 5.21 Velocity distribution along the height for homogeneous and non-homogeneous model ( $u^*$  is dimensional velocity parameter) (Dobran, 1992)

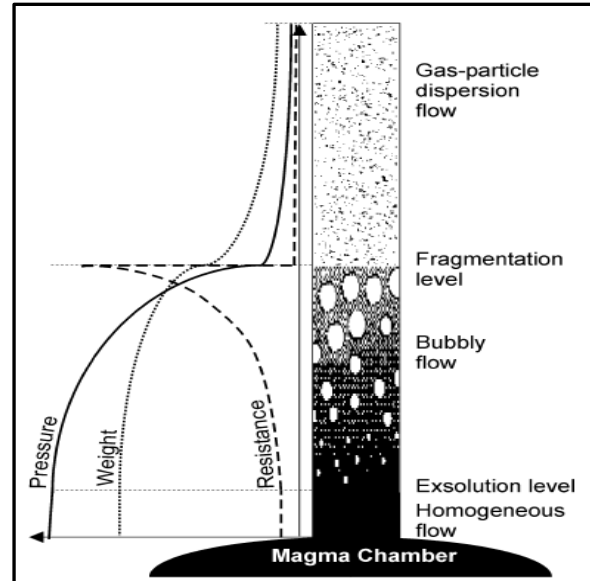


Figure 5.22 Multiphase flow during Volcanic Eruptions (Melnik, 1999)

In the bubbly flow model, the velocity of both gas and liquid phases is considered to be the same while temperature variations between the phases are assumed negligible. Moreover, bubble nucleation is assumed to be instantaneous, and mass transfer between dissolved gas and bubbles maintain the equilibrium condition of the flow domain. The system of equations included continuity, momentum, Rayleigh-Lamb equation for bubble growth and other fluid properties. For the dispersed gas flow, the main assumptions outlined is the isothermal flow in the conduit. In addition, gas released from particles formed during fragmentation is neglected. In this regime; the continuity, momentum, interaction force between particles and gas, and equation of state for the gas are used. To distinguish the fragmentation zone, critical threshold pressure and gas velocity are accounted. The lower boundary for the fragmentation zone is used to determine pressure difference between growing bubbles and the liquid from the threshold value, while the upper boundary is defined by gas velocity capable of supporting the particles in the upward flow. The critical value is dependent on the melt viscosity and increases with vertical acceleration. For the unsteady case, the outlet pressure is assigned to be at atmospheric for subsonic conditions. The previous two models (Dobran, 1987 and 1992) are based on the steady-state formulation of equations where the flow characteristics do not change with time. In the unsteady model, the flow characteristics are dependent on time, and time-dependent terms are incorporated in the governing equations. The steady-state considers that the magma chamber pressure variation is independent of time. It assumes that the velocity at the outlet is corresponding to the pressure equal to atmospheric. In the steady state case, the solution is obtained numerically. In the numerical method, a set of differential equations are solved using Runge-Kutta fourth order method with step correction at each step of the iteration. For a given flow rate, the conduit length is calculated and compared with the actual conduit length. Depending on the error, a new flow rate is chosen, and steps are repeated until a solution is obtained.

In the unsteady state model, chamber pressure variation with time is considered, and a purely implicit compact difference method is applied (Melnik, 2000). To use this method, a uniform mesh is created, and conservation equations are solved at four points in the neighborhood of disintegration wave, and the velocity of fragmentation waves is determined. The moving boundary of fragmentation wave complicates the solution which is handled using the four points around discontinuity (two in bubble regime and two in gas-droplet dispersion regime). The accuracy is controlled by using a norm function which depends on the increment of dependent variables.

*Difference between non-equilibrium models and mechanistic/analytical models:*

The basic governing equations are similar to the equation applied in the derivation of mechanistic models. However, the treatment of the governing equations is different. The mass transfer between the phases is not considered during the derivation of mechanistic and analytical models. In addition, the density is treated as constant, while in volcano eruptions and nuclear vessel rupture models, the density varies with temperature, pressure and other flow properties. Another major difference observed is the way viscosity is calculated. The viscosity in volcano eruption model is considered to be dependent on the dissolved gas content.

## 6. Conclusions and Recommendations

A thorough study of existing work on the multiphase flow is conducted to facilitate the understanding of the concepts and its application in worst case discharge (WCD). WCD generally occurs during blowout events. In Section 2, an effort has been made to understand the WCD during blowouts. Then, a brief review of different problems including the challenges in experimental and theoretical work in the context of WCD is presented.

It is worth mentioning that effect of geometry, setting up of basic and constitutive equations, an approach for solving these equations pose a severe challenge for tackling the WCD modeling problem. Most of the errors reported in the past literature study are around 10% percent for empirical correlations, considering the nearest in-situ condition of WCD. However, these models are frequently used in the industry. Analytical models have been developed using several simplifications, and therefore, the validity of these models is still questionable for WCD. Mechanistic models are more sophisticated than empirical and analytical models, but those models are problem specific and need considerable improvement for WCD case. Numerical models are the rigorous models that have potential to address this multiphase problem. However, these models are computationally costly; hence, it is mostly used to facilitate model development and validation.

Experimental studies have been reviewed extensive. A holistic comparative study of several previous experimental works including Waltrich et al. (2015), Perez (2008), Biria (2013), and Shen et al., (2010) is presented in Section 4. LSU data show good agreement with measurements of other studies obtained under similar conditions. Studies suggest a significant change in axial pressure profile at high velocities. In addition, multiphase flow characteristics in annular flow exhibit considerable deviation from pipe flow. However, this conclusion is only limited to very low superficial gas and liquid velocities. More investigation is needed high velocities.

Subsonic and supersonic multiphase flow are addressed in Section 5. An extensive literature review has been conducted to understand the worst-case discharge from subsonic and supersonic perspective. The presence of shock waves in the system during these conditions is highly likely; however, it has not been examined exhaustive. Hence, a thorough investigation is needed to better understand shock waves, their generation, the strength of shock waves, and their evolution process in two-phase flow. The challenges and limitations of existing models have been identified, and the possible avenues for modeling efforts have been explored. In addition, relevant studies in other engineering applications closely related with worst case discharge phenomena are covered the literature survey.

## 6.1 Conclusions

The main points of this literature survey can be summarized into following points:

- At high superficial velocities, annular and mist flow regimes establish in gas-liquid vertical flows. Most of the empirical correlations cannot model the annular flow regime. Mechanistic models are best suited for annular flow regime. These models are the semi-empirical type and have shown greater accuracy in comparison to the empirical or analytical models. In addition, in-situ geometry has a significant effect on the annular flow pattern. This can be attributed to the difference in film thickness at the tubing and casing walls.
- Our analysis shows good agreement between LSU data and other available measurements. In general, the pressure drop increases with liquid superficial velocity.
- One of the most vital aspects of multiphase flow in the context of worst case discharge is subsonic and supersonic condition during the flow. The available models have not been validated under these conditions. The total pressure drop obtained using the available models is dominated by the contribution of frictional pressure loss. However, past studies suggest that the impact of pressure drop due to acceleration is the dominant component of total pressure drop during subsonic and supersonic conditions.
- The worst-case discharge conditions show substantial similarity to the discharges during volcanic eruptions and during the rupture of high-pressure vessels. Studies suggest that the generation of shock waves in the control volume during the flow leads to a decoupling of pressure transmission, which means the presence of discontinuity in the flow system. In all the wellbore models, the concept of discontinuity is missing, and hence a thorough investigation is required to develop reliable models for such circumstances.
- In addition, the concept of the existence of non-equilibrium conditions is not considered in the current models. The existence of the non-equilibrium condition under subsonic and supersonic conditions requires different treatment of the constitutive and basic equations.

## 6.2 Recommendations

- The existing models need to be improved to provide reliable predictions for subsonic and supersonic conditions.
- The experimental investigation is required to better understand the phenomena shock wave formation and WCD conditions.
- The CFD investigation is needed to investigate two-phase flow characteristics in large diameter pipes and at high superficial gas and liquid velocities.

## References

- Aggour, M. A., & Al-Yousef, H. Y. 1996. Vertical Multiphase Flow Correlations for High Production Rates and Large Tubulars. (1996, February 1). Society of Petroleum Engineers. doi:10.2118/28465-PA.
- Asheim, H. 1986. MONA, An Accurate Two-Phase Well Flow Model Based on Phase Slippage, SPEPE (May 1986) 221-30,
- Ali, S. F. 2009. Two Phase Flow in Large Diameter Vertical Riser. PhD Dissertation. Cranfield University, School of Engineering Department of Process and Systems Engineering.
- Ansari, A. M., Sylvester, N. D., Sarica, C., Shoham, O., & Brill, J. P. (1994, May 1). A Comprehensive Mechanistic Model for Upward Two-Phase Flow in Wellbores. Society of Petroleum Engineers. doi:10.2118/20630-PA.
- Awad, M. M., & Muzychka, Y. S. 2010. Two-phase Flow Modeling in Microchannels and Minichannels. *Heat Transfer Engineering*, 31(13), pp.1023-1033.
- Awad, M.M. 2012 Two-Phase Flow. INTECH.
- Aziz, K., Govier, G. W., & Fogarasi., M. (1972, July 1). Pressure Drop in Wells Producing Oil and Gas. Petroleum Society of Canada. doi:10.2118/72-03-04.
- Baxendell, P. B., & Thomas, R. (1961, October 1). The Calculation of Pressure Gradients in High-Rate Flowing Wells. Society of Petroleum Engineers. doi:10.2118/2-PA.
- Bhagwat, S.M. and Ghajar, A.J., 2014. A flow pattern independent drift flux model based void fraction correlation for a wide range of gas–liquid two phase flow. *International Journal of Multiphase Flow*, 59, pp.186-205.
- Bourgoyne, A. T., Rocha, L., Bender, C. V., & Bourgoyne, D. 1995. Analysis of Platform Vulnerability to Cratering Induced by a Shallow Gas Flow.
- Bowman, S. (2012, September 1). Altering an Existing Well Design to Meet New BOEMRE Worst-Case Discharge Criteria. Society of Petroleum Engineers. doi:10.2118/161929-PA.
- Beggs, D. H., & Brill, J. P. (1973, May 1). A Study of Two-Phase Flow in Inclined Pipes. Society of Petroleum Engineers. doi:10.2118/4007-PA.
- Bijleveld, A. F., Koper, M., & Saponja, J. (1998, January 1). Development and Application of an Underbalanced Drilling Simulator. Society of Petroleum Engineers. doi:10.2118/39303-MS.

- Biria, S. 2013. Prediction of pressure drop in vertical air/water flow in the presence/absence of sodium dodecyl sulfate as a surfactant. M.S. Thesis, University of Dayton, Dayton, Ohio.
- Brown, K. E., & Lea, J. F. (1985, October 1). Nodal Systems Analysis of Oil and Gas Wells. Society of Petroleum Engineers. doi:10.2118/14714-PA
- Caetano, E. F. 1985. Upward vertical two-phase flow through an annulus. Ph.D. dissertation, The University of Tulsa, Tulsa, Oklahoma.
- Caetano, E. F., Shoham, O. O., & Brill, J. P. 1992a. Upward Vertical Two-Phase Flow Through an Annulus—Part I: Single-Phase Friction Factor, Taylor Bubble Rise Velocity, and Flow Pattern Prediction. *ASME. J. Energy Resour. Technol.* 1992; 114(1):1-13. doi:10.1115/1.2905917.
- Caetano, E. F., Shoham, O. O., & Brill, J. P. 1992b. Upward Vertical Two-Phase Flow through an Annulus—Part II: Modeling Bubble, Slug, and Annular Flow. *ASME. J. Energy Resour. Technol.* 1992; 114(1):14-30. doi:10.1115/1.2905916.
- Celata, G.P., Cumo, M., Fraello, G.E. & Incalcaterra, P.C. 1983. Critical flow of subcooled liquid and jet forces (No. CONF-830702-). ENEA-Dipartimento Reactori Termici Rome.
- Chang, P., & Bai, B., 2017. An improved method of gas well deliquification using supersonic nozzle. *International Journal of Heat and Mass Transfer*, 108, pp.2262-2272.
- Chauvin, A., Jourdan, G., Daniel, E., Houas, L., & Tosello, R., 2012. Study of the interaction between a shock wave and a cloud of droplets. In 28th International Symposium on Shock Waves (pp. 39-44). Springer, Berlin, Heidelberg.
- Committee, T. R. (2015, March 10). Calculation of Worst-Case Discharge (WCD). Society of Petroleum Engineers. doi:NULL
- CSB Report, 2014. Explosion and Fire at the Macondo Well. Investigation Report Overview, Volume 2, U.S. Chemical Safety and Hazard Investigation Board. Report No. 2010-10-I-OS
- CSB Report, 2016. Explosion and Fire at the Macondo Well. Investigation Report Overview, Volume 3, U.S. Chemical Safety and Hazard Investigation Board. Report No. 2010-10-I-OS
- Darcy, H. (1857). *Recherches Experimentales Relatives Au Mouvement De L'eau Dans Les Tuyaux* (Engl. Transl.: "Experimental Research Relating to the Movement of Water in Pipes"). Mallet–Bachelier: Paris, 2.

- Das, R., Rat, R., & Mukerjee, R. K., 1993, January. Oil Spill and the Environmental Damage from Blownout Oil/Gas Wells: An Integrated Approach. In The Third International Offshore and Polar Engineering Conference. International Society of Offshore and Polar Engineers.
- Damir, G. 2012. Multiphase flow in large diameter pipes. M.S. Thesis, University of Nottingham. London, United Kingdom.
- Dobran, F. 1987. Nonequilibrium modeling of two-phase critical flows in tubes. *J. Heat Transfer*, 109, pp.731-738.
- Dobran, F. 1992. Nonequilibrium flow in volcanic conduits and application to the eruptions of Mt. St. Helens on May 18, 1980, and Vesuvius in AD 79. *Journal of Volcanology and Geothermal Research*, 49(3-4), pp.285-311.
- Dontsov, V. E., & Nakoryakov, V. E., 2003. Pressure Waves in a Gas–Liquid Medium with a Stratified Liquid–Bubbly Mixture Structure. *Journal of applied mechanics and technical physics*, 44(4), pp.538-542.
- Duns, H., & Ros, N. C. J. (1963, January 1). Vertical flow of gas and liquid mixtures in wells. World Petroleum Congress.
- Dukler, A.E., Wicks, M., & Cleveland, R.G. (1964). Frictional Pressure Drop in Two-Phase Flow: A. A Comparison of Existing Correlations for Pressure Loss and Holdup. *AIChE Journal*, 10(1): p. 38-43.
- Eaton, B. A., Knowles, C. R., & Silberbrg, I. H. (1967, June 1). The Prediction of Flow Patterns, Liquid Holdup and Pressure Losses Occurring During Continuous Two-Phase Flow in Horizontal Pipelines. Society of Petroleum Engineers. doi:10.2118/1525-PA
- Eddington, R. 1970. Investigation of Supersonic Phenomena in a Two-Phase (Liquid-Gas) Tunnel, *A IAA J.* 8:1.
- Fauske, H.K., 1965, June. Two-phase two-and one-component critical flow. In Proc. of Symp. on Two-phase Flow (Vol. 1, pp. G101-114).
- Federico, M., Francesco, G., & Adriano, M., 2017. CFD modelling of the condensation inside a Supersonic Nozzle: implementing customized wet-steam model in commercial codes. *Energy Procedia*, 126, pp.34-41.
- Fetkovich, M. J. (1973, January 1). The Isochronal Testing of Oil Wells. Society of Petroleum Engineers. doi:10.2118/4529-MS.

- Fernandes, R. C., Semiat, R., and Dukler, A. E. 1983. Hydrodynamic Model for Gas-Liquid Slug Flow in Vertical Tubes, *AIChE Jour*, VoL 9, 6, 981-989.
- Fisenko, V., R. Kremer, & I. Olikier. (2010). "INDUSTRIAL APPLICATIONS OF FISONIC™ DEVICES." January 2010. Accessed November 6, 2017. [https://www.allbeton.ru/upload/mediawiki/7e2/industrial-applications-of-fisonicdevices-\\_fisenko\\_.pdf](https://www.allbeton.ru/upload/mediawiki/7e2/industrial-applications-of-fisonicdevices-_fisenko_.pdf).
- Fisenko, V. V. & Sychikov, V. I. (1977). Effect of Compressibility on the Hydrodynamics of Two-phase Flows. *Journal of Engineering Physics*. 1977, June 01, 32-6, pp. 686--688, ISSN 1573-871X, DOI: 10.1007/BF00862574
- Fluent, A.N.S.Y.S., 2014. Ansys Inc. USA. <https://www.ansys.com>.
- Griffith, P. & Wallis, G. B. (1961). Two-Phase Slug Flow. *Journal of Heat Transfer*, 1961. 83(3): p. 307-318.
- Gilbert, W. E. 1954. Flowing and gas lift well performance. *Drill. Prod. Pract.*, : 126–143.
- Gomez, L. E., Shoham, O., Schmidt, Z., Chokshi, R. N., & Northug, T. (2000, September 1). Unified Mechanistic Model for Steady-State Two-Phase Flow: Horizontal to Vertical Upward Flow. *Society of Petroleum Engineers*. doi:10.2118/65705-PA.
- Guo B., Lyons W.C. & Ghalambor A. (2007). *Petroleum production engineering: A computer-assisted approach*. Elsevier Science & Technology Books.
- Hagedorn, A. R., & Brown, K. E. (1965, April 1). Experimental Study of Pressure Gradients Occurring During Continuous Two-Phase Flow in Small-Diameter Vertical Conduits. *Society of Petroleum Engineers*. doi:10.2118/940-PA.
- Hasan, A. R., & Kabir, C. S. (1988, May 1). A Study of Multiphase Flow Behavior in Vertical Wells. *Society of Petroleum Engineers*. doi:10.2118/15138-PA
- Hasan, A.R. and Kabir, CS. 1990. Performance of a Two-Phase Gas/Liquid Flow Model in Vertical Wells, *Journal of Petroleum Science and Engineering*, 4: 273-289
- Hasan, A.R. & Kabir, C.S. (1992). Two-phase Flow in Vertical and Inclined Annuli. *International Journal of Multiphase Flow*, 18(2), pp.279-293.
- Hasan, A. R., Kabir, C. S., & Wang, X. (1998, June 1). Wellbore Two-Phase Flow and Heat Transfer during Transient Testing. *Society of Petroleum Engineers*. doi:10.2118/38946-PA

- Hasan, A. R., & Kabir, C. S. (2007, May 1). A Simple Model for Annular Two-Phase Flow in Wellbores. Society of Petroleum Engineers. doi:10.2118/95523-PA
- Hasan, A. R., & Kabir, C. S., Sayarpour, M. (2007, January 1). A Basic Approach to Wellbore Two-Phase Flow Modeling. Society of Petroleum Engineers. doi:10.2118/109868-MS
- Hewitt, G.F., & Roberts, D.N. A. (1969). Studies of Two-Phase Flow Patterns by Simultaneous X-Ray and Flash Photography. United Kingdom Atomic Energy, G. Research, E. Atomic Energy Research, and D. Chemical Energy. Harwell, England; [London]: Chemical Engineering Division, Atomic Energy Research Establishment; Available from H.M. Stationery Office.
- Hewitt, G., Hall Taylor, N., 1970. Annular Two-Phase Flow. Pergamon Press, UK.
- Hopper, A. R. (2015). National Notice to Lessees and Operators of Federal Oil and Gas Leases and Holders of Rights-of-Use and Easements on the Outer Continental Shelf (OCS). US DOI, BOEM, NTL No. 2015-N01, 2015, January 14.
- Hibiki, T., & Ishii, M. (2003). One-dimensional drift-flux model and constitutive equations for relative motion between phases in various two-phase flow regimes. *International Journal of Heat and Mass Transfer*, 46(25), pp.4935-4948.
- Hsu, Y.-Y., 1972. Review of critical Flow Rate, Propagation of Pressure Pulse, and Sonic Velocity in Two-Phase Media: NASA-Lewis Research Center.
- Ishii, M., & Hibiki, T., 2010. Thermo-fluid dynamics of two-phase flow. Springer Science & Business Media.
- Igra, O., Wu, X., Falcovitz, J., Meguro, T., Takayama, K., & Heilig, W., 2001. Experimental and theoretical study of shock wave propagation through double-bend ducts. *Journal of Fluid Mechanics*, 437, pp. 255-282.
- Kabir, C.S., & Hasan A.R. (1990). Performance of a Two-phase Gas/Liquid Flow Model in Vertical Wells, In *Journal of Petroleum Science and Engineering*, Volume 4, Issue 3, 1990, Pages 273-289, ISSN 0920-4105, [https://doi.org/10.1016/0920-4105\(90\)90016-V](https://doi.org/10.1016/0920-4105(90)90016-V).
- Karplus, H.B. 1958. The Velocity of Sound in a Liquid Containing Gas Bubbles, Armour Research Foundation; Project No. A-097. Atomic Energy Commission Contract No. AF (11-1)-528, United States Atomic Energy Commission.
- Kawanishi, K., Hirao, Y. and Tsuge, A., 1990. An experimental study on drift flux parameters for two-phase flow in vertical round tubes. *Nuclear engineering and design*, 120(2-3), pp.447-458.

- Kelessidis, V. C , and Dukler, A. E. 1989, Modelling Flow Pattern Transitions for Upward Gas-Liquid Flow in Vertical Concentric and Eccentric Annuli, *International Journal of Multiphase Flow*, 15: 173-191.
- Keeran J. H., and Neumann, E. P. (1945). Friction in Pipes at Supersonic and Subsonic Velocities. Technical Note No. 963 National Advisory Committee for Aeronautics.
- Kieffer, S.W. 1977. Sound speed in liquid-gas mixtures: Water-air and water-steam. *Journal of Geophysical research*, 82(20), pp.2895-2904.
- Krehl, P.E.T.E.R. 2000. History of shock waves. *Handbook of Shock Waves* (Edited by G. Bendor, O. Igra, and T. Elperin), 1, pp.1-142.
- Lockhart, R.W., & Martinelli, R.C., 1949. Proposed Correlation of Data for Isothermal Two-phase, Two-component Flow in Pipes. *Chem. Eng. Prog*, 45(1), pp.39-48.
- Liu, H., Vandu, C.O., & Krishna, R. (2005). Hydrodynamics of Taylor Flow in Vertical Capillaries: Flow Regimes, Bubble Rise Velocity, Liquid Slug Length, and Pressure Drop. *Industrial & Engineering Chemistry Research*, 44(14): p. 4884-4897.
- Liu, R., A.R. Hasan, and S. 2014. Mannan, Flow Rate and Total Discharge Estimations in Gas-Well Blowouts, Society of Petroleum Engineers.
- Lage, A. C. V. M., & Time, R. W. (2000, January 1). Mechanistic Model for Upward Two-Phase Flow in Annuli. Society of Petroleum Engineers. doi:10.2118/63127-MS
- Luo, W., Li Y., Qinghua, W., Li J., Liao, R., & Liu, Z. 2016. Experimental Study of Gas-Liquid Two-Phase Flow for High Velocity in Inclined Medium Size Tube and Verification of Pressure Calculation Methods, *international journal of heat and technology*, 34, (3): 455-464.
- Lain, S., Broder D., & Sommerfeld, M. (2000). "Numerical Modeling of the Hydrodynamics in a Bubble Column Using the Euler Lagrange Approach ", Universitat Halle-Wittenberg, D O6099 Halle (Saale). Germany.
- Leonard, C., Ferrasse, J.H., Boutin, O., Lefevre, S., & Viand, A. 2015. Bubble column reactors for high pressures and high temperatures operation. *Chemical Engineering Research and Design*, 100, pp.391-421.
- LedaFlow Software 2016; Available from: <http://www.kongsberg.com/en/kogt/products%20and%20services/flow%20assurance/ledaflo-w%20software/> .

- Mariani, C., Biamino, L., Jourdan, G., Houas, L., Vandenboomgaerde, M. & Souffland, D. 2012. Long Time Observation of the Richtmyer-Meshkov Instability. In 28th International Symposium on Shock Waves (pp. 371-376). Springer, Berlin, Heidelberg.
- Martindale W. R., & Smith, R. V. 1980. Pressure-drop and sonic Velocity in separated two-phase flow, *J. of Fluids Eng. ASME*, 102/113.
- Mcquillan, K.W., & Whalley, P. B. (1985). Flow Patterns in Vertical Two-Phase Flow. *International Journal of Multiphase Flow*, 11(2): p. 161-175.
- Martinelli, R.T. & D. Nelson 1948. Prediction of Pressure Drop During Forced-Circulation Boiling of Water. *Trans. ASME*, 1948. 70(6): p. 695-702.
- Melnik, O. 2000. Dynamics of two-phase conduit flow of high-viscosity gas-saturated magma: large variations of sustained explosive eruption intensity. *Bulletin of volcanology*, 62(3), pp.153-170.
- Moyer, M. C., Lewis, S. B., Cotton, M. T., & Peroyea, M. (2012, January 1). Challenges Associated with Drilling a Deepwater, Subsalt Exploration Well in the Gulf of Mexico: Hadrian Prospect. *Society of Petroleum Engineers*. doi:10.2118/154928-MS
- Mukherjee, H. & Brill, J. P. (1985). Pressure drop correlations for inclined two-phase flow. *Journal of energy resources technology*, 107(4), pp.549-554. doi:10.1115/1.3231233.
- Muzychka, Y. S., & Awad, M. M., 2010. Asymptotic Generalizations of the Lockhart–Martinelli Method for Two Phase Flows. *Journal of Fluids Engineering*, 132(3), p.031302.
- Nakagawa, M., Berena, M. S., & Harada, A. 2008. Shock Waves in Supersonic Two-Phase Flow of CO<sub>2</sub> in Converging-Diverging Nozzles, in *International Refrigeration and Air Conditioning Conference*, Purdue.
- Nedeltchev, S., 2017. Theoretical prediction of mass transfer coefficients in both gas–liquid and slurry bubble columns. *Chemical Engineering Science*, 157, pp.169-181.
- Nguyen, D.L., E.R.F. Winter, and M. Greiner, Sonic Velocity in Two-Phase Systems. *International Journal of Multiphase Flow*, 1981. 7(3): p. 311-320.
- Okazaki, M., 1980. Theoretical Study for Accelerated Two-Phase Flow: (1), Constant-area Flow. *Bulletin of JSME*, 23(178), pp.536-544.
- Okazaki, M., 1981. Theoretical Analysis for Accelerated Two-Phase Flow: Vol. 2, Two-Phase Critical Flow Condition and the Flow Variables. *Bulletin of JSME*, 24(191), pp.823-833.

- Omebere-Iyari, N. K., Azzopardi, B. J. and Ladam, Y. (2007), Two-phase flow patterns in large diameter vertical pipes at high pressures. *AIChE J.*, 53: 2493–2504. doi:10.1002/aic.11288.
- Orkiszewski, J. (1967, June 1). Predicting Two-Phase Pressure Drops in Vertical Pipe. Society of Petroleum Engineers. doi:10.2118/1546-PA.
- Osman, E.S.A., & Aggour, M.A. (2002). Artificial Neural Network Model for Accurate Prediction of Pressure Drop in Horizontal and Near-horizontal-multiphase Flow. *Petroleum Science and Technology*, 20(1-2), pp.1-15.
- Oudemans, P., Baaijens, M. N., & Avest, D. ter. (1993, January 1). Modelling Blowout Control by Means of Downhole Kill Fluid Injection. Society of Petroleum Engineers. doi:10.2118/26732-MS
- Oudemans, P. (2010, September 1). Validation of Blowout-Rate Calculations for Subsea Wells. Society of Petroleum Engineers. doi:10.2118/115019-PA
- Ohnuki, A. & Akimoto, H., 1996, An experimental study on developing air-water two-phase flow along a large vertical pipe: effect of air injection method. *Int. J. Multiphase Flow*, Vol. 22, No. 6, 1996, pp. 1143-1154.
- Ohnuki, A. & Akimoto, H., 2000, Experimental study on transition of flow pattern and phase distribution in upward air-water two-phase flow along a large vertical pipe. *Int. J. Multiphase Flow*, Vol. 26, 2000, pp. 367-386.
- Ozar, B., Jeong, J. J., Dixit, A., Juliá, J. E., Hibiki, T., & Ishii M. 2008. Flow Structure of Gas-Liquid Two-Phase Flow in an Annulus. *Chem. Eng. Sci.* 63: 3998–4011.
- Oudemans, P., & Kerem, M., 2006. Transient Behavior of Annular Pressure Buildup in HP/HT Wells. *SPE Drill. Complet.* 21 (4), 234-241. <http://dx.doi.org/10.2118/88735-PA>.
- OLGA Dynamic Multiphase Flow Simulator. 2016; Available from: <https://www.software.slb.com/products/olga> .
- Pagan, E., Williams, W. C., Kam, S., & Waltrich, P. J. (2016, December 28). Modeling vertical flows in churn and annular flow regimes in small- and large-diameter pipes. BHR Group.
- Pai, S.I. 2013. *Two-phase Flows (Vol. 3)*. Springer-Verlag.
- Poettman, F. H., & Carpenter, P. G. (1952, January 1). The Multiphase Flow of Gas, Oil, and Water through Vertical Flow Strings with Application to the Design of Gas-lift Installations. American Petroleum Institute.

- Per Holland. (2017). Loss of Well Control Occurrence and Size Estimators, Phase I and II. BSEE Report no. ES201471/2.
- Perez V. H. 2008. Gas-liquid two-phase flow in inclined pipes. PhD Thesis, University of Nottingham. London, United Kingdom.
- Perez-Tellez, C., Smith, J. R., & Edwards, J. K. (2003, September 1). A New Comprehensive, Mechanistic Model for Underbalanced Drilling Improves Wellbore Pressure Prediction. Society of Petroleum Engineers. doi:10.2118/85110-PA
- Prasser, H-M., Boettger, A., Beyer, M., Carl, H., Lucas, D., Schaffrath, A., Schütz, P., Weiss, F. P., and Zschau, J. (2002) "TOPFLOW tests on the structure of the gas-liquid Interface in a large vertical pipe". Forschungszentrum Rossendorf Annual Report-2002, FZR-380.
- Putcha, V. B., & Ertekin, T. (2017, October 9). A Fast and Robust Compositional, Multi-Phase, Non-Isothermal Wellbore Hydraulics Model for Vertical Wells. Society of Petroleum Engineers. doi:10.2118/187072-MS
- Reichenbach, H. & Kuhl, A.L. 1995. Shock-induced turbulent flow in baffle systems. In *Shock Waves @ Marseille IV* (pp. 69-74). Springer, Berlin, Heidelberg.
- Replogle, D.R. (2009). BP: Regional Oil Spill Response Plan - Gulf of Mexico: Appendix H- Worst Case Discharge. 2009.
- Rouhani, S.Z., & Axelsson, E. 1970. Calculation of Void Volume Fraction in the Subcooled and Quality Boiling Regions. *International Journal of Heat and Mass Transfer*, 13(2), pp.383-393.
- Rozenblit, R., Gurevich, M., Lengel, Y., & Hetsroni, G., 2006. Flow Patterns and Heat Transfer in Vertical Upward Air–water Flow with Surfactant. *International Journal of Multiphase Flow*, 32(8), pp.889-901.
- Sachdeva, A., Schmidt, Z., Brill, J.P., & Blais, A.M. 1986. Two-phase Flow through chokes, Paper SPE 15657 presented at the 61st SPE Annual Technical Conference and Exhibition, New Orleans.
- Sawai, T., Kaji, M., Kasugai, T., Nakashima, H., & Mori, T. 2004. Gas–liquid interfacial structure and pressure drop characteristics of churn flow. *Experimental Thermal and Fluid Science*, Vol. 28, 597-606.
- Schardin, H. & Reichenbach, H., 1965. The behavior of shock waves in ducts and when entering entrance structures. In *Proceedings of Symposium Protective Structures for Civilian Populations*, National Research Council (USA) Washington, DC, USA (pp. 193-206).

- Schlegel, J., Hibiki, T. and Ishii, M., 2010. Development of a comprehensive set of drift-flux constitutive models for pipes of various hydraulic diameters. *Progress in Nuclear Energy*, 52(7), pp.666-677.
- Schlegel, J.P., Miwa, S., Chen, S., Hibiki, T., Ishii, M., 2012, Experimental study of two-phase flow structure in large diameter pipes. *Experimental Thermal and Fluid Science*, Vol. 41, 2012, pp. 12-22.
- Schoppa, W., Zabararas, G. J., Menon, R., & Wicks, M. (2013, May 6). Gaps and Advancements for Deepwater Production and Remote Processing: Large Diameter Riser Laboratory Gas-Lift Tests. *Offshore Technology Conference*. doi:10.4043/23968-MS
- Selli, M.F., & Seleglim, P., 2007, January. On-line Identification of Horizontal Two-phase Flow Regimes through Gabor Transform and Neural Network Processing. In 2006 International Pipeline Conference (pp. 813-820). American Society of Mechanical Engineers.
- Shen, X., R. Matsui, K. Mishima, & H. Nakamura (2010), Distribution parameter and drift velocity for two-phase flow in a large diameter pipe, *Nucl. Eng. Des.*, 240, 3991–4000.
- Shen, X., Mishima, K., & Nakamura, H., 2005. Two-phase phase distribution in a vertical large diameter pipe. *Int. J. Heat Mass Transfer* 48, 211–225.
- Shen, X., Saito, Y., Mishima, K., Nakamura, H., 2006. A study on the characteristics of upward air–water two-phase flow in a large diameter pipe.” *Experimental Thermal and Fluid Science*, Vol. 31. 21-36.
- Shi, H., Holmes, J.A., Durlinsky, L.J., Aziz, K., Diaz, L.R., Alkaya, B. and Oddie, G., 2005, January. Drift-flux modeling of multiphase flow in wellbores. In *SPE Annual Technical Conference and Exhibition*. Society of Petroleum Engineers.
- Shiple, D.G., 1984. Two phase flow in large diameter pipes., *Shorter Communications, Chemical Engineering Science*, Vol. 39, No.1, 1984, pp. 163-165.
- Shippen, M., & Bailey, W.J. (2012). *Steady-State Multiphase Flow Past, Present, and Future, with a Perspective on Flow Assurance*. *Energy & Fuels*, 26(7), pp.4145-4157.
- Shirdel, M., & Sepehrnoori, K. (2011, January 1). Development of a Transient Mechanistic Two-Phase Flow Model for Wellbores. *Society of Petroleum Engineers*. doi:10.2118/142224-MS
- Shoham O. (2005). *Mechanistic modeling of gas-liquid two - phase flow in pipes*. Tulsa. The Society of Petroleum Engineers (SPE).

- Sultan K. M. 1999. The propagation of pressure waves in two-phase gas/liquid flows, M.Sc., The University of Western Ontario, London, Ontario.
- Taha T., & Cui, Z.F. (2006). CFD Modelling of Slug Flow in Vertical Tubes, In *Chemical Engineering Science*, Volume 61, Issue 2, 2006, Pages 676-687, ISSN 0009-2509, <https://doi.org/10.1016/j.ces.2005.07.022>.
- Taitel, Y., Bornea, D. & Dukler, A.E. (1980). Modelling Flow Pattern Transitions for Steady Upward Gas-liquid Flow in Vertical Tubes. *AIChE Journal*, 26(3), pp.345-354.
- Tang C. C., Tiwari S., Ghajar A. J. 2013. Effect of Void Fraction on Pressure Drop in Upward Vertical Two-Phase Gas-Liquid Pipe Flow. *J. Eng. Gas Turb. Power* 135 (2): 0229011-0229017.
- Turner, J.C.R. (1966). On Bubble Flow in Liquids and Fluidised Beds. *Chemical Engineering Science*, 21(11), pp.971-974.
- Vasquez, M., & Beggs, H. D. (1980, June 1). Correlations for Fluid Physical Property Prediction. Society of Petroleum Engineers. doi:10.2118/6719-PA
- Venkateswaran, S., Lindau, J.W., Kunz, R.F. & Merkle, C.L., 2002. Computation of multiphase mixture flows with compressibility effects. *Journal of Computational Physics*, 180(1), pp.54-77.
- Vogel, J. V. (1968, January 1). Inflow Performance Relationships for Solution-Gas Drive Wells. Society of Petroleum Engineers. doi:10.2118/1476-PA
- Vuong, D. H., Sarica, C., Pereyra, E., & Al-Sarkhi, A. (2017, October 9). Pressure Effects on Pressure Gradient and Liquid Holdup in Two-Phase Oil-Gas Low-Liquid-Loading Flow in Horizontal Pipes. Society of Petroleum Engineers. doi:10.2118/187229-MS
- Waltrich, P. J., Capovilla, M. S., Lee, W., Zulqarnain, M., Hughes, R., Tyagi, M., & Griffith, C. (2017, April 18). Experimental Evaluation of Wellbore Flow Models Applied to Worst-Case-Discharge Calculations. Society of Petroleum Engineers. doi:10.2118/184444-MS
- Waltrich, P. J., Hughes R., Tyagi M., Kam S., Williams W., Cavalcanti de Sousa P. Zulqarnain M., Lee W., & Capovilla S. M. (2015). Experimental Investigation of Two-Phase Flows in Large-Diameter Pipes and Evaluation of Flow Models Applied to Worst-Case-Discharge Calculations, BOEM Report M15PC00007, Craft & Hawkins Department of Petroleum Engineering, Louisiana State University, Baton Rouge.

- Waltrich, P. J., Falcone, G., & Barbosa Jr, J.R. (2013). Axial Development of Annular, Churn and Slug Flows in a Long Vertical Tube. *Int J Multiphase Flow* 57: 38–48. <http://dx.doi.org/10.1016/j.ijmultiphaseflow.2013.06.008>.
- Wallis, G.B. 1980. Critical Two-Phase Flow. *International Journal of Multiphase Flow*. 6(1): p. 97-112.
- Wallis, G.B. 1969. *One-Dimensional Two-Phase Flow*, McGraw-Hill Book Co. Inc., New York City.
- Weisman, J., Duncan, D., Gibson, J., & Crawford, T. (1979). Effects of Fluid Properties and Pipe Diameter on Two-phase Flow Patterns in Horizontal Lines. *International Journal of Multiphase Flow*, 5(6), pp.437-462.
- Witte, J.H., 1969. Mixing shocks in two-phase flow. *Journal of Fluid Mechanics*, 36(4), pp.639-655.
- Worst Case Discharge 2016; Available from: <http://geminisi.com/?q=consulting/worst-case-discharge>.
- Yuan, K., & Bello, O. (2014, April 1). Use of Computational Fluid Dynamics Model for Evaluating Performance of High Pressure High Temperature Wells. *Society of Petroleum Engineers*. doi:10.2118/167896-M
- Yuan, Z., Hashemian, Y. & Morrell, D., 2015. Ultra-deepwater blowout well control analysis under worst case blowout scenario. *Journal of Natural Gas Science and Engineering*, 27, pp.122-129.
- Yazdani M, Alahyari AA, Radcliff TD. 2014. Numerical modeling and validation of supersonic two-phase flow of CO<sub>2</sub> in converging-diverging nozzles. *J Fluids Eng Trans ASME* 2014:136.
- Zangana M., Van der Meulen, G. P., Azzopardi B.J. 2010. The Effect of Gas and Liquid Velocities on Frictional Pressure Drop in Two Phase Flow for Large Diameter Vertical Pipe. 7th International Conference on Multiphase Flow ICMF, Tampa, FL USA, May 30-June 4.
- Zuber, N. & Findlay J. A. (1965). Average Volumetric Concentration in Two-Phase Flow Systems. *Journal of Heat Transfer*. 87(4): p. 453-468.